

UNIVERSITY OF MISKOLC  
FACULTY OF MECHANICAL ENGINEERING AND INFORMATICS



**MODELLING AND TESTING OF ADVANCED INTAKE AND  
EXHAUST SYSTEM COMPONENTS FOR RACE CAR ENGINES**  
PHD THESES

Prepared by

**Barhm Abdullah Mohamad**  
Fuel and Energy Engineering (BTech),  
Mechanical Engineering Powertrain (MTech)

**ISTVÁN SÁLYI DOCTORAL SCHOOL OF MECHANICAL ENGINEERING SCIENCES**  
**TOPIC FIELD OF MECHANICAL ENGINEERING SCIENCES**  
**TOPIC GROUP OF DESIGN OF MACHINES AND ELEMENTS**

Head of Doctoral School

**Dr. Gabriella Bognár**  
DSc, Full Professor

Head of Topic Group

**Dr. Gabriella Bognár**  
DSc, Full Professor

Scientific Supervisor

**Dr. Károly Jálics**  
PhD, Associate Professor

**Miskolc**  
**2021**

**CONTENTS**

<b>CONTENTS.....</b>	<b>I</b>
<b>SUPERVISOR’S RECOMMENDATIONS.....</b>	<b>III</b>
<b>LIST OF SYMBOLS AND ABBREVIATIONS.....</b>	<b>IV</b>
<b>1. INTRODUCTION .....</b>	<b>11</b>
1.1. Motivation .....	11
1.2. Objectives.....	11
1.3. Research relevance .....	12
<b>2. GENERAL DESCRIPTION OF AUTOMOTIVE INTAKE AND EXHAUST SYSTEMS .....</b>	<b>13</b>
2.1. Possible system layouts .....	13
2.2. The Plenum .....	13
2.2.1. General description .....	13
2.2.2. Formula race car powertrain specification .....	15
2.2.3. Engine limitation.....	15
2.3. Turbocharger .....	16
2.4. Gasoline particle filter (GPF).....	17
2.5. Catalytic converters (CAT) and modelling technique .....	17
2.6. Intercooler.....	19
2.7. Exhaust gas recirculation (EGR) .....	19
<b>3. INTRODUCTION TO INTAKE- AND EXHAUST ACOUSTICS.....</b>	<b>22</b>
3.1. Basics of acoustics .....	22
3.2. Acoustic Parameters of Components Related to Intake- and Exhaust Systems.....	22
3.2.1. Transmission loss.....	22
3.2.2. Attenuation.....	23
3.2.3. Noise reduction index .....	23
3.2.4. Insertion loss.....	23
3.2.5. Transfer function.....	24
3.3. Time domain methods .....	24
3.3.1. CFD, 1D acoustics (Fluent, Boost, GT Power, etc.).....	24
3.4. Frequency domain methods .....	24
3.4.1. Transfer matrices .....	24
3.4.2. Linear acoustics.....	27
3.5. Linear acoustic models of turbochargers, CAT, PM, EGR, etc. ....	28
3.5.1. Turbocharger acoustics and measurement techniques .....	28
3.5.2. Linear acoustic modelling of catalytic converters and intercoolers .....	29
3.5.3. Linear acoustic modelling of particle filters .....	30
3.5.4. Exhaust gas recirculation: Design and analysis.....	33
3.6. Active intake-and exhaust systems: Active noise control (ANC) .....	33
3.7. Noise contribution of intake and exhaust noise to pass-by and to interior noise .....	35
<b>4. ANALYSIS OF RACE CAR ENGINE INTAKE SYSTEM.....</b>	<b>39</b>
4.1. Air intake system: Location and function.....	39

---

4.2. Model description.....	40
4.2.1. Wave ram cylinder overcharging.....	44
4.2.2. Variable intake system .....	46
4.3. Numerical analysis.....	47
4.3.1. Overview .....	47
4.3.2. Geometrical model.....	48
4.3.3. Software .....	49
4.3.4. Computational methods .....	51
4.4. Calculation Results .....	55
4.4.1. Design of Simulations .....	55
4.4.2. Velocity distribution.....	56
4.4.3. Pressure loss .....	60
4.4.4. Sound pressure level for the intake system .....	61
4.4.5. Temperature at restrictor.....	62
4.5. Experimental results of the engine power output.....	63
<b>5. ANALYSIS OF RACE CAR ENGINE EXHAUST SYSTEM .....</b>	<b>65</b>
5.1. Structural design of formula race car exhaust system .....	65
5.2. Model description.....	66
5.2.1. Exhaust manifold .....	67
5.2.2. Exhaust muffler.....	70
5.3. Calculation results .....	76
5.3.1. Velocity and pressure distribution in muffler.....	76
5.3.2. Exhaust gas flow distribution.....	79
5.3.3. Pulsating and flow acoustic .....	80
5.3.4. Thermodynamic analysis .....	80
5.3.5. Engine combustion.....	81
5.3.6. Fuel type and their effects on exhaust gas properties .....	81
5.3.7. The surface roughness and chemical composition of stainless steel alloy.....	86
5.3.8. Johnson–Champoux–Allard model (JCA).....	86
5.3.9. Design of Simulations .....	88
5.3.10. Effect of muffler design on the engine characteristic.....	90
<b>6. THESES – NEW SCIENTIFIC RESULTS.....</b>	<b>103</b>
<b>7. SUMMARY .....</b>	<b>104</b>
<b>ACKNOWLEDGEMENTS.....</b>	<b>105</b>
<b>REFERENCE.....</b>	<b>106</b>
<b>LIST OF PUBLICATIONS RELATED TO THE TOPIC OF THE RESEARCH FIELD.....</b>	<b>111</b>
<b>APPENDICES .....</b>	<b>113</b>

## SUPERVISOR'S RECOMMENDATIONS

PhD candidate Barhm Mohamad Abdullah was under my supervision for the past 3 years. From September 2016 till August 2020 he was a full-time PhD student in the framework of "Stipendium Hungaricum Scholarship Programme" at István Sályi Doctoral School of Mechanical Engineering Sciences; his affiliated organisation is Institute of Machine and Product Design / Faculty of Mechanical Engineering and Informatics. 2018 the change of the scientific supervisor was needed, since the direction of his scientific work turned into the field of acoustics and powertrain, which research field domiciled at the Institute of Machine and Product Design.

The chosen topic about the acoustics of ICE intake and exhaust system is in general an active research field in the automotive industry, not only by the commercial passenger vehicles, but also by the racing cars. The intake and exhaust noise are dominant in the vehicle pass-by noise, and the regulations demand decreasingly lower noise levels. Not only lower levels are important, but the sound design of an engine (through exhaust and intake system) is an important research field. The sound design defines the characteristics of sport car, a race car and a commercial car passenger car. Overall the noise abatement of exhaust and intake systems is and will be a attractive and important topic for a phd thesis.

The candidate worked often independently and showed initiative, e.g. the cooperation with the formula student team of the University of Miskolc was his own idea and he managed the first contact and later the cooperation with the team.

The course of the research work was planned together. We set up the scientific tasks and defined a time plan for the completion. The research plan was regularly checked and updated by the regular meetings.

In the second phase of the Phd studies, after his complex exam the publication activity was increased since the amount and quality of the results went up continuously. The results of candidate's research work was published or presented in scientific journals, in doctoral seminars, doctoral forums, and international conferences, and in conference proceedings.

The scientific results themselves and of course the earned know-how and competences during the research work will open new possibilities for Barhm Abdullah Mohamad in his future work.

Miskolc. 23.08.2021

Jálics Károly PhD.

**LIST OF SYMBOLS AND ABBREVIATIONS**

**GREEK LETTERS**

$\theta$	Absolute temperature	
$\theta_t$	Valve degree	
$\lambda_a$	The volumetric efficiency	
$\lambda_w$	The cylinder wall thickness	$m$
$\rho_m$	The density of the material	$kg.m^{-3}$
$\rho_o$	Air density	$kg.m^{-3}$
$\rho_t$	The aparent density of the material	
$\rho_g$	Gas density	$kg.m^{-3}$
$\delta_{ij}$	The Kronecker symbol	
$\omega$	The angular frequency	$rad.s^{-1}$
$\mu$	Dynamic viscosity	$Pa.s$
$\alpha_\infty$	Tortuosity	
$\alpha_{m,p}$	The measured and predicted absorpion coefficients, respectively	$m^{-1}$
$\nu$	The flow velocity	$m.s^{-1}$
$\nu_c$	The cavity volume	$m^3$
$\tau_{ij}$	The averaged Reynolds stress for components ij	
$Z$	The turbulence model	
$\partial$	Partial derivative	
$\Lambda$	Viscous characteristic length	$\mu m$
$\varphi$	The porosity	

**LATIN LETTERS**

*ICE* Internal Combustion Engine

LIST OF SYMBOLS AND ABBREVIATIONS

---

<i>0D</i>	Zero-Dimensional	
<i>1D</i>	One-Dimensional	
<i>3D</i>	Three-Dimensional	
<i>FS</i>	Formula Student	
<i>CFD</i>	Computational Fluid Dynamics	
<i>A<sub>em</sub></i>	Area of exhaust manifold apertures	$m^2$
<i>A<sub>ipt</sub></i>	The area of the throat at intake valves	$m^2$
<i>A<sub>ept</sub></i>	The area of the throat at exhaust valves	$m^2$
<i>C<sub>emp</sub></i>	The ratio of port area to exhaust manifold pipes	
<i>A<sub>im</sub></i>	Area of intake manifold apertures	$m^2$
<i>A<sub>i</sub></i>	The instantaneous value of combustion chamber area depends on actual piston , location	$m^2$
<i>C<sub>imp</sub></i>	The ratio of port area to intake manifold pipes	
<i>n<sub>iv</sub></i>	The number of intake valves	
<i>n<sub>ev</sub></i>	The number of exhaust valves	
<i>D</i>	Cylinder bore	$m$
<i>D<sub>m</sub></i>	The manifold diameter	$m$
<i>GPF</i>	Gasoline Particulate Filter	
<i>PPT</i>	Petrol Particulate Filter	
<i>OPF</i>	Otto Particle Filter	
<i>DPF</i>	Diesel Particulate Filter	
<i>PM</i>	Particulate Matter	
<i>CAT</i>	Catalytic Converters	
<i>EGR</i>	Exhaust Gas Recirculation	
<i>NO<sub>x</sub></i>	Nitrogen oxide	
<i>CO<sub>2</sub></i>	Carbon dioxide	
<i><math>\dot{m}</math></i>	Mass flowrate of gas	$kg.s^{-1}$
<i>SR</i>	Short-Route system	
<i>LR</i>	Long-Route system	
<i>S<sub>1, 2, 3</sub></i>	The cross-sectional areas atpoints 1, 2, 3 of the transition	$m^2$

LIST OF SYMBOLS AND ABBREVIATIONS

---

<i>OEM</i>	The original equipment manufacturer	
<i>CAE</i>	Computer-Aided Engineering	
<i>NVH</i>	Noise, Vibration and Harshness	
<i>ATF</i>	Acoustic transfer function	
<i>HVAC</i>	Heating, ventilation, and air conditioning	
<i>COG</i>	Centre of Gravity	
<i>BDC</i>	Bottom Dead Center	
<i>TDC</i>	Top Dead Center	
<i>EIC</i>	The effective inlet valve closing point	
$m_g$	The mass of air that is trapped in cylinder	<i>kg</i>
$m_{th}$	The theoretical mass of air that can be trapped in cylinder	<i>kg</i>
$V_M$	The material volume	$m^3$
$V_{th}$	The volume of cylinder	$m^3$
$V_t$	The total (bulk) volume	$m^3$
$V_g$	The Volume of gas trapped in cylinder	$m^3$
$V_v$	The void (air) volume	$m^3$
$\rho_{th}$	The theoretical density of air in cylinder	$kg.m^{-3}$
$\rho_g$	Gas density	$kg.m^{-3}$
<i>CP</i>	The specific heat of the gas at constant pressure	$J.kg^{-1}.K^{-1}$
<i>CV</i>	The specific heat of the gas at constant volume	$J.kg^{-1}.K^{-1}$
<i>d/dt</i>	The substantial derivative	
<i>SB</i>	System boundary	
<i>RI</i>	Restrictor	
<i>PL</i>	Plenum	
<i>C</i>	Cylinder	
<i>MP</i>	Measuring point	
<i>TL</i>	Transmission loss	<i>dB</i>
<i>IL</i>	Insertion loss	<i>dB</i>
<i>NR</i>	Noise Reduction Index	<i>dB</i>
<i>dB</i>	Decibels	

LIST OF SYMBOLS AND ABBREVIATIONS

$P_i$	The power of incident wave coming towards	$W$
$P_t$	The power of transmitted wave going away	$W$
$P_s$	The signal power at the transmitting end (source)	$W$
$P_d$	The signal power at the receiving end (destination)	$W$
$A_p$	The power attenuation	$dB$
$P_{RMS}$	The rms sound pressure measured after the muffler	$Pa$
$P_A$	The sound power received by the load after insertion	$W$
$P_B$	The sound power measured before the insertion	$W$
$T_F$	Transfer function	
$T_{in, out}$	Transfer functions of import and export sections of DPF	
$T_I, T_{II}$	The transfer functions model the short ducts at the inlet and outlet to the catalytic channels with lengths corresponding to the plug length	
$SID$	Sound Inside Duct	
$u$	Mass velocity	$m.s^{-1}$
$u_i$	Particle velocity at location of element	$m.s^{-1}$
$u_I$	The inlet velocity	$m.s^{-1}$
$c$	The speed of sound	$m.s^{-1}$
$L_i$	Mean density of gas	$kg.m^{-3}$
$\bar{V}$	Mean velocity	$m.s^{-1}$
$Y$	The distance from the pipe wall	$m$
$Y_i$	The rate of the speed of sound per cross section of element	
$Y_o$	The characteristic impedance of the tube	
$A, B$	Amplitudes of right- and left-bound fields	
$k$	The adiabatic index of air	
$k_c$	Frictional energy loss along straight pipe segments	
$k_p$	Pressure loss coefficient	
$K_{cond}$	Thermal conductivity	$W.m^{-1}.K^{-1}$
$T_{ij}$	Element of transmission matrix	
$C_1$	The coefficient of the progressive wave	
$C_2$	The coefficient of the reflective wave	



LIST OF SYMBOLS AND ABBREVIATIONS

$L_2$	Length of extended inlet /outlet pipe	$m^3$
$p$	Acoustic pressure	$Pa$
$P^+$	Acoustic pressure waves propagating in positive direction	$Pa$
$P^-$	Acoustic pressure waves propagating in negative direction	$Pa$
$a$	The inlet of the two-port	
$b$	The outlet of the two-port	
$s$	The specific entropy	$kJ.kg^{-1}.K^{-1}$
$S_h$	The volumetric heat sources	$J.K^{-1}.m^{-3}$
$S_f$	The friction slope	
$H_e$	The transfer function taken between the microphone signal and a reference signal	
$G_{mn}$	The pressure cross-spectrums between a pair of pressure transducers	$Pa$
$h$	The specific enthalpy	$kJ.kg^{-1}$
$h_{conv}$	The convective heat transfer coefficient	$W.K^{-1}.m^{-2}$
$ANC$	The active noise control system	
$A_n$	The neck cross section area	$m^2$
$L_n$	The neck length	$m$
$L_m$	Length of the muffler	$m$
$Dm_{in}$	Influence of diameter	$m$
$Dm_{out}$	Diameter out of muffler shell	$m$
$Dm_{hole}$	Diameter of hole of perforated inner pipe	$m$
$SPL$	Sound pressure level	$dB$
$A_i, B_i, C_i, D_i$	The four-pole parameters of matrix $T_i$	
$T_i$	The acoustic transfer matrix of element	
$N$	The number of spectra	
$n$	Engine speed	$s^{-1}$
$E_f$	The specific exergy	$J/kg$
$\dot{E}_f$	The total exergy	$j/s$
$o$	The reference state	
$q$	The heat transfer in the radial direction from the gas to the manifold	$W$

LIST OF SYMBOLS AND ABBREVIATIONS

$q_w$	The heat transfer through the duct wall	$W$
$T_w$	The temperature of the pipe inner wall	$K$
$T_g$	The temperature of gas	$K$
$T_s$	Mean temperature in the intake system	$K$
$R$	Gas constant	$J. kg^{-1}.K^{-1}$
$L_{rez}$	The length of the ram wave intake runner	$m$
$FEM$	Finite Element Method	
$FVM$	Finite Volume Method	
$BC$	Boundary condition	
$t$	Time vector	
$j$	The imaginary unit	
$S_{in}$	The total cross-sectional areas of the inlet particulate filter ducts	$m^2$
$g$	Gravitational acceleration	$m.s^{-2}$
$Q_m$	The mass flow	$kg.s^{-1}$
$C_D$	The orifice discharge coefficient	
$PPiP$	Perforated Pipe inside Pipe	
$AM$	Absorptive Material	
$M$	Mach number	
$W_{bjk}$	The projections of velocity vector	$m.s^{-1}$
$G_i$	The projection of the density vector of the volume forces	
$O_{xi}$	Axis of a rectangular Cartesian coordinate system	
$S_z$	Single – zone model	
$AISI$	Austenitic stainless-steel alloy	
$JCA$	Johnson–Champoux–Allard model	
$N_{pr}$	Prandtl number	
$Z$	The impedance of surface acoustic	$dB$
$Z_c$	The characteristic impedance	$dB$
$BSFC$	Break Specific Fuel Consumption	$g. kw^{-1}.h^{-1}$
$F_c$	Cut-off frequency	$Hz$
$A, B$	Loudspeaker references	

## LIST OF SYMBOLS AND ABBREVIATIONS

---

$r$	Pipe radius	$m$
$\dot{R}$	The reflection coefficient of sound pressure	
$H$	The total specific energy	$J.kg^{-1}$
$i_{jk}$	The unit vectors	
$x, y, z$	The direction of vectors	
$RON$	Research Octane Number	
$dQ_B$	The heat released from fuel	$J.deg^{-1}$
$H_u$	The calorific value of fuel	$kJ.kg^{-1}$
$dm_b$	The amount of burned fuel	$kg$

### SUBSCRIPTS

$rpm$	Revolutions per minute	
$G_{++}$	The strength of acoustic modes	
$TMM$	Transfer Matrix Method	
$CSD$	Transfer matrices for cross-sectional discontinuities	
$IM$	Intake manifold	
$EM$	Exhaust manifold	
$F1$	Formula 1	
$Re$	Reynolds number	
$Mod$	Modification	
$Min$	Minimum	
$Max$	Maximum	

## 1. INTRODUCTION

### 1.1. Motivation

In a race car powered by an internal combustion engine, the quintessential element defining the character of the race car is the engine. The common intake and exhaust system of the engine have improved significantly over the years; therefore, the issue now is more about the quality of the sound of the engine than its noisiness. The identification and the features of sound power emitted by engine components are an important challenge for the race car industrials. Noise generated in interior and exterior parts of the race car grew together with racetrack requiring better noise absorbing technology (Krebber et al. 2002; García and Faus, 1991).

The noise generated in the intake system as a result of the high velocity of air streaming into the engine combustion chamber increased to the point that rules were needed to prevent the negative impacts of race car noise pollution. Recently, they have been amended to apply a tougher restriction, and the European Union's Environment Action Programme to 2020 proposed a large reduction in noise pollution, almost reaching the World Health Organization's recommended noise levels (Juraga et al. 2015). One of the pieces of equipment used to reduce noise in the circumstances mentioned above is the vehicle's intake and exhaust plenum. Positioned at the upstream and downstream of an internal combustion engine (*ICE*) such as intake manifold and exhaust system include filters, exhaust manifold, intercooler, catalyst convertor and mufflers are an engineering solution to control engine noise levels and combustion emissions. Increasingly sophisticated modelling methods assist acoustic research and upgrade work on intake and exhaust systems. Such techniques include *1D* gas dynamic simulation codes with the choice to model some components in *3D*. These can provide accurate outputs within a reasonable calculation period.

### 1.2. Objectives

i. The objective of this research work is the selection, tuning and development of the intake manifold for a Formula Student race car in accordance with the Formula Student regulations. For this purpose, a four-cylinder Honda motorbike engine was chosen by the "Engine Team". Therefore, the first task was to enhance the air flow, resp. to provide sufficient amount of air to the combustion inside the cylinder at higher rpm and reduce the shock waves which may lead to higher sound pressure.

ii. There are secondary injectors on the intake manifold in the original engine, which work as nitro or fuel booster to the air to create rich air to fuel mixture at high engine speed (over *8000 rpm*) and providing only *1 hp* according to the dynamometer. The task is to remove these secondary injectors and rebuild the entire intake manifold. This may compensate the power loss due to removing secondary injectors.

- iii. Design a proper exhaust system (exhaust manifold, muffler, junctions) for the current formula race car to sustain the critical operation condition.
- iv. Simulation and analysing the fluctuation and the uniformity of the flow along the system.
- v. Prediction of the emitted noise, generated by the pulsating flow from the intake and exhaust of the system ducts, by using *CFD* (Computational Fluid Dynamics) techniques.
- vi. Energy losses troubleshooting by diagnose the heat losses from entire engine block systems.

### **1.3. Research relevance**

Formula Student Car (*FS*) is an international race car design competition for students at technical universities and universities of applied sciences. The winning team is the one that obtains the greatest overall score in design and racing performance, rather than the one who builds the fastest racing car. The arrangement of inner components for example, predicting aerodynamics of the air intake system is crucial to maximizing car performance as speed varies. The air intake system consists of an inlet nozzle, throttle, restrictor, air box and cylinder suction pipes (runners) (Mohamad et al. 2020). The exhaust system of an engine is just as important as the intake when it comes to power and efficiency, especially at the header and exhaust port. The team, on the other hand, had a lot of options this year for improving the system's flow. The exhaust system was driven by packaging and material restrictions, with some adjustment accessible throughout the length of the runner. This research work examines the use of *CFD* numerical simulations in conjunction with the experiment approach during component design and optimization.

## 2. GENERAL DESCRIPTION OF AUTOMOTIVE INTAKE AND EXHAUST SYSTEMS

### 2.1. Possible system layouts

Motorsport is a global pioneer in the development and application of revolutionary automotive engineering concepts and technology. It is a place where parts are put to the test to their limits, and the eventually bad design comes out earlier. Mistakes could easily mean the termination of the race due to early engine fault. The racing car as a whole must function flawlessly, and engineers are working hard to fine-tune each component to its greatest potential. One of the most essential automotive design groups is the engine. Commercial and racing engines have a lot of differences.

Naturally aspirated racing engines have lower combustion pressure and charging efficiency in general, however this only applies to restricted engine speeds due to resonance manifold adjustment. The higher charging pressure is one of the major distinctions between supercharged and normally aspirated engines. This is due to the charging efficiency of the turbocharger or compressor being employed. In professional motor sport classes new engines are developed with high expertise, such engines like in *FI*, specifically for extreme loads and situations. Non-professional, or amateur racing classes cannot afford enough money, infrastructure, and time for development, so they rather buy something from the manufacturer, and try to tune and improve it, as far as they can.

Basic factors leading to the successful engine tuning include improving the intake and exhaust manifolds, tuning the resonance manifold, improving the flow through intake ports and valve seats etc. As a result, engineers use simulation software to determine the effects of engine component changes on overall engine performance.

The time it takes to optimize and tune an engine is reduced when simulation software is used, but the results and data produced this way must be confirmed experimentally.

### 2.2. The Plenum

#### 2.2.1. General description

The role of the plenum (airbox) in a racing automobile differs slightly from that of a commercial engine. The plenum or airbox of a racing car is frequently used as a resonator and is connected to the resonant runners. It's located in the front of the engine compartment to provide for easier access to cold air, which is fed to the plenum via huge intake cutouts. The main advantage of the race car plenum is to prevent the engine from overcharging when the throttle valve is fully

open, while the car is approaching the corner/curve exit or this happens when the car is entering the corner. It must reduce its speed (throttle valve closure) due to the physical constraints. At this moment the throttle valve is closed but the air is still rushing into the plenum (airbox) causing blast overcharging of the plenum. Therefore, the throttle valve is opened again on the corner/curve exit, the surplus pressure from the plenum (airbox) overcharges the cylinders.

The throttle valves must be situated between the engine and the plenum for this to operate. While the engine is in the intake stroke, the plenum's task is to reflect pressure waves elicited by the transient flow. In addition, the racing plenum evenly distributes air to the various cylinders.

There are intake and exhaust poppet valves in the basic geometry of the cylinder or the cylinder head of a four-stroke engine that connect the cylinder to its manifolding. This is seen in the figure below showing the number of intake and exhaust valves, respectively,  $n_{iv}$  and  $n_{ev}$  (Adámek, 2011).

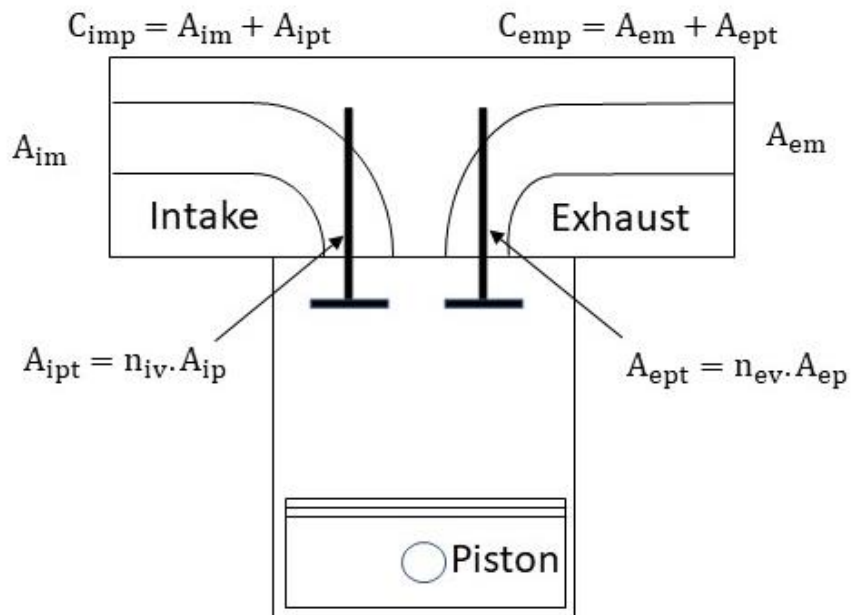


Figure 1 The pipe to port area ratios for a 4-stroke engine .

The throat area at each of these valves is  $A_{ip}$  and  $A_{ep}$ , respectively. The valves are connected to intake and exhaust manifold apertures of area  $A_{im}$  and  $A_{em}$ , respectively. This gives rise to the concept of pipe (manifold) to port area ratios  $C_{mp}$ , which are defined as follows:

$$C_{imp} \frac{A_{im}}{n_{iv} \cdot A_{ip}} \tag{1}$$

$$C_{emp} \frac{A_{em}}{n_{ev} \cdot A_{ep}}$$

The intake manifold to port area ratios of these top engines are approximately  $0.90$  and  $1.00$ , as indicated in table 1, making these values an useful starting point for determining intake port design criteria.

Table 1 Measured manifold-port area ratio (Blair, 1998).

Engine	Exhaust $C_{emp}$	Intake $C_{imp}$
2.0L 14 4v F2	1.26	0.84
3.5L V12 4v F1	1.60	0.90
0.6L 14 4v SRM	1.40	1.00
3.0L V10 4v F1	1.40	0.90
3.5L V8 4v F1	1.60	0.90
4.5L V8 4v SRC	1.40	1.10
2.0L 14 4v ITC	1.20	1.00
8.2L V8 2v OPB	1.55	1.05

Another critical component is the cross section area of the intake valve. It should be around  $0.6 D$ , where  $D$  is the diameter of the cylinder . The valve should likewise be short to keep the weight down, but the intake port's sharp angle must be maintained. The valve seat angle should be around  $45$  degrees in order to ensure proper cylinder sealing. Radius shaping valve seats are also used in racing engines to provide greater air flow. Sharp edges can promote flow separation, resulting in a reduction in mass air flow through the valve seat.

### 2.2.2. Formula race car powertrain specification

This chapter provides an overview of the SAE formula regulations for the powertrain, exhaust system, and noise control. The engine speed that corresponds to an average piston speed of  $15.25 m/s$  will be the maximum sound level test speed for a certain engine. The computed speed will be rounded up to the nearest  $500 rpm$ , therefore, up to this computed speed, the maximum permissible sound level is  $110 dB$ . The team will determine the idle test speed for each engine based on their calibrated idle speed. If the idle speed varies , the vehicle will be evaluated over a range of idle speeds that the team has determined. The maximum permissible sound level at idle is  $103 dB$ . The rules are available at sources (Formula SAE rules 2019).

### 2.2.3. Engine limitation

“The car's engine(s) must be piston engines with a four-stroke primary heat cycle and a displacement of not more than  $610 cm^3$  per cycle. Hybrid powertrains , such as those that use electric motors to generate electricity from stored energy, are not allowed.” (Formula SAE rules 2019).



### 2.3. Turbocharger

A turbocharger is a type of forced intake system used in internal combustion engine, in almost every section of the transport industry (e.g. trains, ships, airplanes). The idea of implementing the unexploited enthalpy of hot exhaust gases for driving the inlet charger dates from early 20<sup>th</sup> century aviation where the decrease of air density at high altitudes resulted in loss of the IC engine power output. Devices based on such a principle are referred to as turbochargers (figure 2). The turbocharger always consists of a compressor which is normally driven by an exhaust turbine. While the turbine transforms recovered enthalpy into mechanical energy, the centrifugal compressor utilizes this energy to provide high pressure charge air. Nowadays in the ICE industry, turbochargers are used for efficiency reasons, and thus they carry a key role in the engine downsizing concept.

To determine the sound radiation from a turbocharger, it is necessary to comprehend how diverse components interact with sound waves. The low frequency engine pulsations in the gas exchange system are influenced by both the turbine and the compressor. This is referred to as the turbocharger's passive acoustic feature (Ricardo et al. 2017).

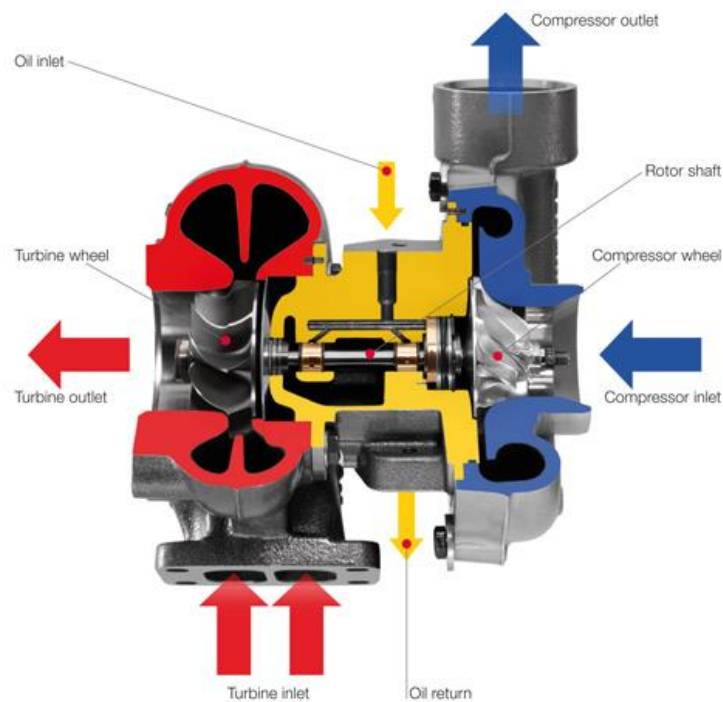


Figure 2 A modern automotive turbocharger cutaway (MAHLE, 2017).

The active and passive parts of the acoustics of any fluid machine, such as a turbocharger, can be separated. The passive aspects (reflection and transmission) refer to acoustic wave scattering, whereas the active aspects refer to the machine's sound source. Variations in geometry (area changes), as well as changes in temperature (sound speed) and density, will change the reflection and transmission of sound in a fluid machine. Flow-related losses will also cause acoustics losses. Two-Port method is recommended to measure acoustic level and more information will be illustrated in chapter 3.

## 2.4. Gasoline particle filter (GPF)

Particle filters, often referred to as soot trap from gasoline engine emission and other heavy fuel operating engines. The technology is also referred to as diesel or petrol particulate filter (*DPF*, *PPF*) and, in some German literatures, as Otto particle filter, abbreviated *OPF*. The *GPF* consists of honeycomb structure, usually made from synthetic ceramic. The porosity of the honeycomb in *PM* is the main factor for selection it for the engines. To prevent issues, that requires a constant monitoring of the soot load in the filter. More details were found in figure 3.

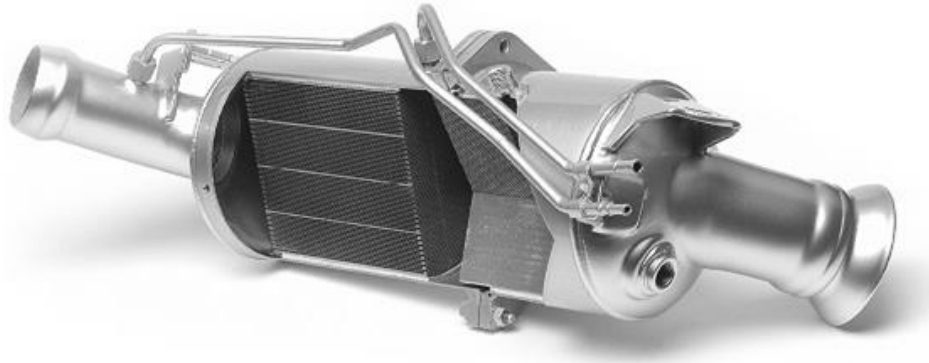


Figure 3 Gasoline particulate filters (*GPF*) for passenger cars.

As particulates accumulate in the filter, backpressure builds-in upstream the filter. This will result an increase in the fuel consumption due to losses by gas exchange and could even lead to an engine failure. This must be absolutely avoided thus regeneration (cleaning) of the *PF* is needed. Regeneration consists in oxidizing the accumulated soot in the filter (Martyr and Rogers, 2021).

The aftertreatment devices such as *PF* can be modelled using absorptive material theory to describe the flow and other physical properties like wall impedances when calculating the targeted wave number. It is necessary to solve the fluid-dynamics governing equations also across to the porous wall. An example of such a model can be found in previous work by (Montenegro et al. 2011), in which a Darcy-Forchheimer law has been adopted for predicting the pressure drop across the *PF* wall and the narrow tubes inside.

## 2.5. Catalytic converters (CAT) and modelling technique

The catalytic converter is a mechanical device. It reduces the harmful emissions created in the exhaust system of an engine through chemical reactions. It is an important device as it works with the harmful gases, which the engine creates during combustion process. A catalytic converter's primary function is to convert carbon monoxide into carbon dioxide, as well as hydrocarbons into carbon dioxide and water. It also recycles nitrogen oxides, converting them back into nitrogen and oxygen. It consists of three stage elements coated onto a ceramic honeycomb or ceramic beads that are housed before the muffler part. Figure 4 shows the components of the intake/exhaust ducts of a turbocharged IC-engine.

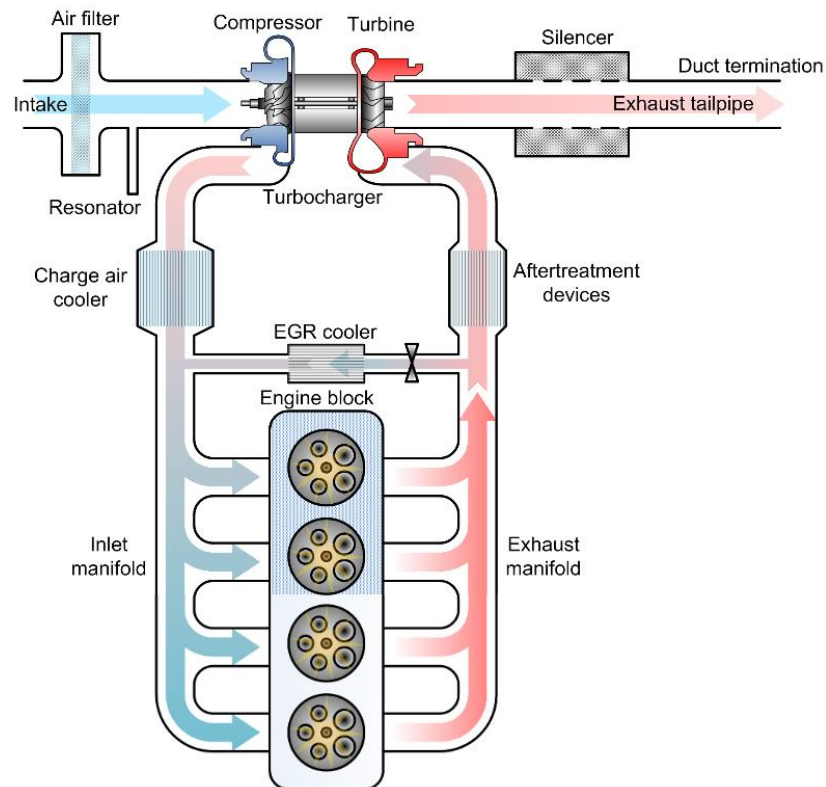


Figure 4 Components of a typical intake/exhaust duct in a turbocharged *IC*-engine (Tiikoja et al. 2011).

Honeycomb shapes with many small, parallel channels running axially through the portion are called monolithic catalyst substrates. When a catalyst is exposed to a gas flow stream, it causes a flow resistance in the gas stream, resulting in a pressure drop. This resistance is mainly due to two different contributions: (i) gas-wall friction inside the tiny channels (distributed pressure loss); (ii) sudden contraction and sudden expansion at the inlet and at the outlet of the monolith respectively. They also improve the acoustic performance of exhaust systems (Tiikoja et al. 2011). The model of the catalyst requires to accomplish both accuracy and computational runtime constraints. In fact, the modelling of all the substrate channels would imply the resolution of the smallest channel edge leading to an unacceptable computational burden. Therefore, the approach adopted consists of discretizing the monolith in a certain number of macro-cells, having the same mesh size of the fluid cells in the inlet and outlet cones as shown in figure 5. Each macro-cell models a group of tiny channels, whose total number is given by the cell frontal area and substrate density (Montenegro et al. 2012).

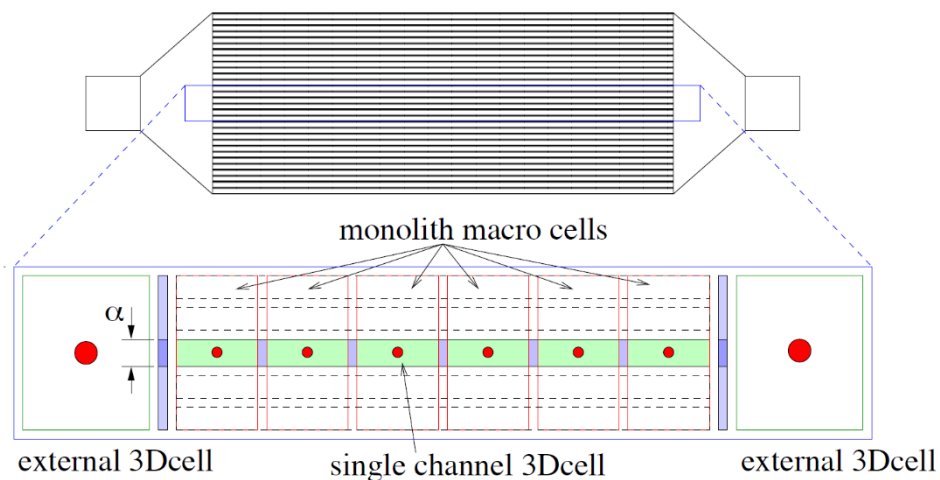


Figure 5 Decomposition domain into macro-cells for the modelling of the catalyst substrate (Montenegro et al. 2012).

The conservation equations are solved for a single channel before being extended to all additional channels in the same macro-cell.

## 2.6. Intercooler

Heat exchangers are inanimate mechanical pieces that facilitate the transfer of heat energy from one medium to another without mixing. They use the air that is flowing through the intercooler to cool the charged exhaust gas inside the intercooler. As show in figure 4. They're essentially a radiator that cools the hot exhaust gas rather than the coolant within the engine. The majority of intercoolers are air-to-air, however in rare circumstances, engine coolant is employed as a second medium to form a water-to-air configuration. Because air is extremely hot when compressed by a turbocharger or supercharger, lowering the temperature of the air from the intercooler increases density, allowing more mass to flow into the engine. Intercoolers consist mainly of three components: a tube bundle, in which heat is removed from the air flow, and two collectors that connect the heat exchanger to the inlet and outlet pipes. The approach followed for the modelling of the tube bundle is, in terms of equations involved, similar to the one adopted for the catalyst. However, in this case it is no longer necessary to resort to the definition of the macro-cells since the tubes of the intercoolers have sizes comparable to the usual mesh size adopted for the discretization. The location and function of the intercooler is up to the duty of turbocharger or supercharger, reducing its temperature and thereby increasing the density of the air supplied to the engine (Eric et al. 2011).

## 2.7. Exhaust gas recirculation (EGR)

The exhaust gas recirculation (*EGR*) valve contributes in the reduction of exhaust emissions from the vehicle (gases from the tailpipe). It recirculates a part of the exhaust fumes from the engine by returning it to the intake manifold, where the engine may burn it again, lowering emissions. The types of *EGR* were described in table 2. In the engine compartment, you'll find the

EGR valve (underneath the hood ). To meet emissions standards , most engines require exhaust gas recirculation. The automobile will not pass emissions if the *EGR* valve has failed. It is also feasible to avoid the production of emissions during combustion rather than utilizing aftertreatment devices to comply with exhaust emission laws. Because the raw emissions are decreased, no aftertreatment is required. It is common practice nowadays, to use *EGR* to reduce the formation of  $NO_x$  emissions. The exhaust gases are recirculated into the combustion chambers in part. This can be accomplished either internally through appropriate valve timing or externally through pipes, figure 4 shows this schematically.

In addition, the energy is used to heat up a bigger part of the gas than would be the case without *EGR*. The mass of a gas fraction having the required amount of oxygen increases as air is diluted by exhaust gas. Another effect is the change in heat capacity (Simon, 2010). Due to the increased degree of freedom of the  $CO_2$ -molecule, exhaust gas has a higher specific heat capacity than air, hence a gas mass incorporating *EGR* will have a lower temperature than pure air for the same amount of combustion energy. Since this rate of  $NO_x$  release is strongly temperature dependent, a lower combustion temperature immediately lowers  $NO_x$  formation , figure 6.

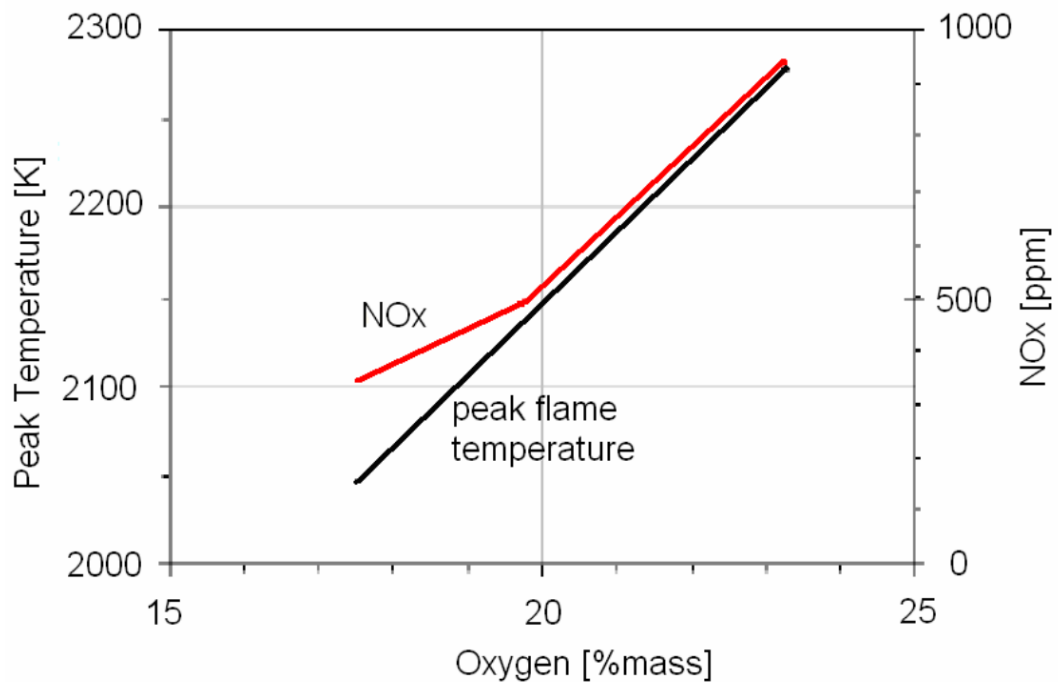


Figure 6 The production of  $NO_x$  is temperature dependent (DieselNet, 2006).

The mass-percentage of oxygen is shown on the X-axis. This is a metric for expressing how much *EGR* is recirculated. A reduced oxygen concentration is caused by increased amount of *EGR* in intake air and increase the pressure drop in the exhaust system. Another way to express the amount of *EGR* is the *EGR*-rate, which is defined as follows:

$$EGR[\%] = \frac{\dot{m}_{Exhaust, Intake}}{\dot{m}_{Exhaust, Intake} + \dot{m}_{Air, Intake}} \quad (2)$$

Where  $\dot{m}$  indicates the mass flow rate of gas.

Table 2 The *EGR*- in different path (Münz, 2008).

Type of EGR	Location	Advantage	Disadvantage
Short-Route System ( <i>SR</i> )	Upstream	Its ease of use and quick reaction to <i>EGR</i> demands.	Fouling because of amount soot in <i>SR</i>
Long-Route System ( <i>LR</i> )	Downstream	High amount of gas flow	Corrosion and clogging risk in <i>LR</i>
Hybrid EGR System	Combines	Best engine efficiency gain	High cost

Entire intake and exhaust system parts modelling technique will be illustrated in chapter 4.

### 3. INTRODUCTION TO INTAKE- AND EXHAUST ACOUSTICS

#### 3.1. Basics of acoustics

The sound can be radiated in only a fluid and it can only propagate in wave form. The frequency range of technical interest extends beyond the range that can be heard by the human ear, often known as the hearing range. The hearing range starts at about  $20\text{ Hz}$  and ranges up to  $20000\text{ Hz}$  (or  $20\text{ kHz}$ ). For the young and pure ear-health person it can be said to range could up to  $20\text{ kHz}$  (Mustafa et al. 2018). There are many unwanted sounds that are coming from vehicles, machines and industrial applications. The unwanted noise level can lead to very dangerous diseases and permanent hearing loss on the person's body. The sound can be affected by some external influences like pressure, temperature and the density of the medium. Mufflers play a crucial part in decreasing exhaust and intake system noise, and as a result, a lot of research goes into making these systems as effective as possible. The propulsion noise comprises of combustion, mechanical noise and the noise radiated from the open terminations of the intake and exhaust systems which is caused by:

- The pressure pulses produced by the charging and discharging process on a regular basis, which propagates to the open ends of the duct system (Pulse noise).
- The mean flow in the duct system, which generates significant turbulence and vortex shedding at geometrical discontinuities (Flow generated noise).

#### 3.2. Acoustic Parameters of Components Related to Intake- and Exhaust Systems

The acoustic performance of a muffler and/or its related pipework is described by various characteristics. These include the noise reduction index ( $NR$ ), the insertion loss ( $IL$ ), and the transmission loss ( $TL$ ).

##### 3.2.1. Transmission loss

The transmission loss in  $dBs$  is the difference in the sound power between the incident wave entering and the transmitted wave exiting the muffler when the muffler termination is anechoic; the  $TL$  is a property of the muffler only and is also depending on that sound power level. The muffler  $TL$  may be calculated from models but is difficult to measure. This part will focus on measuring the muffler  $TL$ . The  $TL$  can be measured using the decomposition method (Tao and Seybert, 2003). More details for the calculations and methods will be illustrated in next chapter.

$$TL = 10\text{Log}_{10} \left[ \frac{P_i}{P_t} \right] \quad (3)$$

here  $P_i$  is the power of incident wave coming towards a defined area in Watts,  $P_t$  is the power of transmitted wave going away from the defined area in Watts.

### 3.2.2. Attenuation

Attenuation is a general term that refers to any reduction in the strength of a signal. Attenuation occurs with any type of signal, whether digital or analogue. Sometimes it is called loss. Attenuation is a natural consequence of signal transmission over long distances. The extent of attenuation is usually expressed in units called decibels ( $dBs$ ) (Mohamad et al. 2019).

Attenuation is a property dependent on the muffler and also the termination, therefore attenuation predicts the actual behavior of the muffler after it is installed in a system. In addition to the transmission loss, attenuation helps to verify the acoustic length of the muffler.

If  $P_s$  is the signal power at the transmitting end (source) of a communications circuit and  $P_d$  is the signal power at the receiving end (destination), then  $P_s > P_d$ . The power attenuation  $A_p$  in decibels is given by the formula [Linda Rosencrance, 2019]:

$$A_p = 10\log_{10} \left[ \frac{P_s}{P_d} \right] \quad (4)$$

### 3.2.3. Noise reduction index

The noise reduction measured in  $dBs$  defined as The sound pressure level differential over the muffler. Though the  $NR$  can be easily measured, it is not particularly helpful for muffler design.

$$NR = 20\log_{10} \frac{p_{RMS,before}}{p_{RMS,after}} \quad (5)$$

where  $p_{RMS,before}$  is the rms sound pressure measured before the muffler and  $p_{RMS,after}$  is the rms sound pressure measured after the muffler.

### 3.2.4. Insertion loss

The insertion loss measured in  $dBs$  is defined as the sound pressure level difference at a point, usually outside the system, without and with the muffler present. Though the  $IL$  is extremely important to industry, it is difficult to calculate since it is dependent on only on the muffler shape but also on the source and radiation impedances.

$$IL = 10\text{Log}_{10} \left[ \frac{P_B}{P_A} \right] \quad (6)$$



Where  $P_B$  is the sound power measured before the insertion at the load,  $P_A$  is the sound power received by the load after insertion.

### 3.2.5. Transfer function

Transfer function ( $T_F$ ) is defined as the relationship between a sound pressure of a source, and the sound pressure at some remote point known as the receiver. A practical example of a sound source on a vehicle might be the engine, an exhaust tailpipe orifice or an individual component such as a steering pump. The receiver in this context is often simply the driver's ear or passengers' ear (AVA, 2018).

## 3.3. Time domain methods

### 3.3.1. CFD, 1D acoustics (Fluent, Boost, GT Power, etc.)

There are some general methods for calculating fluid flow through engine manifolds with those it is possible to predict the acoustical and performance behaviour. The following outline is mainly taken from (Ferziger, 2002). The finite difference method is the oldest method for numerical solution of partial differential equations, it has been introduced by Euler.

It is the easiest method for simple geometries but that is also its main disadvantage. Usually, this method has been used to create structured grids where it is very simple and effective. The finite volume method is the most used method in *CFD* codes (computational fluid dynamics) which is proposed modelling on the perforated intersection between *3D* cells is based on it. In contrary to the previous method, it can handle any type of grid, so also complex geometries are possible. The finite element method which uses an unstructured grid that makes it more difficult to find efficient solution methods. The distinguishing feature of finite element methods is that the equations are multiplied by a weight function before they are integrated over the entire domain (AVL BOOST, 2017). The ability to handle complex geometries is more advanced compared to other methods. A combination of finite volume and finite element method would be a hybrid method, the so-called control volume based finite element method. AVL BOOST is a *1D*- gas dynamic tool which predicts engine cycle and gas exchange simulation of the entire engine. It also incorporates the linear acoustic prediction tool SID (Sound In Ducts), so it is possible to simulate both the non-linear and linear acoustic behavior of the system.

## 3.4. Frequency domain methods

### 3.4.1. Transfer matrices

As a technique for simulating the acoustic transfer characteristic, the transfer matrix method, which defines the principle of impedance, is applied. This approach, which is widely used for acoustic systems because of its computational simplicity, makes design simple because each element is modelled separately.

Considering acoustic pressure,  $p$ , and mass velocity,  $u$ , as the two state variables in the transfer matrix method, the results from the four-pole parameters from the conditions of both sides, which can be described as Equation (7), where  $(p_r, u_r)^T$  is called the state vector at the upstream point,  $r$  and  $(p_{r-1}, u_{r-1})^T$  is called the state vector at the downstream point  $r-1$  (Hyoun-Jin Sim et al. 2008):

$$\begin{bmatrix} p_r \\ u_r \end{bmatrix} = \begin{bmatrix} \text{Transfer matrix} \\ 2 \times 2 \end{bmatrix} \begin{bmatrix} p_{r-1} \\ u_{r-1} \end{bmatrix} \quad (7)$$

The transmission loss is independent of the source and presumes an anechoic termination at the downstream end. It is defined as the difference between the power incident on the acoustic element and that transmitted downstream into an anechoic termination. As a result, it simplifies the process of evaluating and predicting to leave the reflected pressure due to emission impedance out of consideration. The transmission loss is an energy loss of acoustic elements, so the ratio of sound pressure between the inlet and outlet of acoustic elements can be expressed in  $dB$  scale.

For pipe with uniform cross section the acoustical pressure and mass velocity fields  $p, \rho_0 S u$  in a pipe with uniform cross section  $S$  and the flow velocity  $v$  in the acoustic field are given by:

$$P(x) = (Ae^{-jkcx} + Be^{jkcx})e^{j(Mkcx + \omega t)} \quad (8-a)$$

$$\rho_0 S u(x) = (Ae^{-jkcx} - Be^{jkcx}) \frac{e^{j(Mkcx + \omega t)}}{Y_i} \quad (8-b)$$

Where  $S$  is cross section of the pipe;  $p_i$  is acoustical pressure at  $i$ th location of element;  $u_i$  is particle velocity at  $i$ th location of element;  $\rho_0$  is mean density of gas;  $c$  is the speed of sound and equal to  $331 \sqrt{\frac{\theta}{273}}$ ;  $\theta$  is absolute temperature,  $K = ^\circ C + 273$ ;  $S_i$  is cross section of element at  $i$ th location;  $l_i$  is the length of element  $i$ ;  $Y_i$  is the rate of the speed of sound per cross section of element and its equal to  $\frac{c}{S_i}$ ;  $A, B$  is amplitudes of right and left bound fields;  $K_c = \frac{k_0}{(1-M^2)}$  assuming negligible frictional energy loss along straight pipe segments;  $K_o = \frac{\omega}{c} = 2\pi \frac{f}{c}$ ;  $\omega = 2\pi f$ ;  $f$  is represent frequency;  $M$  is Mach number and its equal to  $\frac{V}{c}$ ;  $v$  is the flow velocity through  $S$  and  $T_{ij}$  is  $(ij)$ th element of transmission matrix of symbols without subscripts, such as  $v, c$ , and  $M$ , describe quantities associated with the reference duct.

In equations (8-a and 8-b) above can be evaluated at  $x = 0$  and  $x = l$ , to obtain corresponding fields  $p_2, \rho_0 S u_2$  and  $p_1, \rho_0 S u_1$ , respectively. Upon the elimination of constants  $A$  and  $B$ , one obtains:

$$\begin{bmatrix} p_2 \\ \rho_0 S u_2 \end{bmatrix} = \begin{bmatrix} T_{11} & T_{12} \\ T_{21} & T_{22} \end{bmatrix} \begin{bmatrix} p_1 \\ \rho_0 S u_1 \end{bmatrix} \quad (9)$$

Where the transfer matrix  $T_{pipe}$  is given by:

$$T_{Pipe} = \begin{bmatrix} T_{11} & T_{12} \\ T_{21} & T_{22} \end{bmatrix}_{Pipe} = e^{-Mkct} \begin{bmatrix} \cos kc l & j Y_o \sin kc l \\ \frac{j}{Y_i} \sin kc l & \cos kc l \end{bmatrix} \quad (10)$$

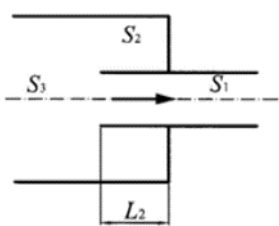
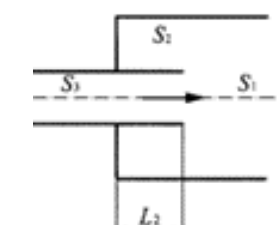
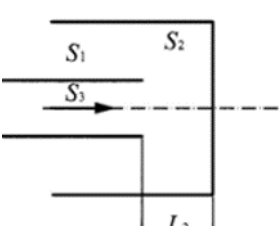
In the transfer matrix of equation (10), The friction between the gas and the rigid wall is neglected , as is the turbulence that causes acoustic energy dissipation, these effects, which would result in a slightly different matrix, may be noticeable in very long exhaust system but they are negligible for most intake and exhaust part applications.

For cross-sectional discontinues the transition elements used to modelling the cross-sectional discontinuities are shown in the Table 3. Using decreasing element subscript values with distance from the noise source , the cross-sectional areas upstream, at, and downstream of the transition ( $S_3$ ,  $S_2$ , and  $S_1$ ) are related through (Munjal, 1987).

$$C_1 S_1 + C_2 S_2 + S_3 = 0 \quad (11)$$

Where the constants  $C_1$  and  $C_2$  are selected to satisfy the compatibility of the cross-sectional areas across the transition, more details in Table 3. For each configuration the table also shows pressure loss coefficient ( $K$ ), which account of some mean-flow energy and acoustical field energy to heat at discontinues .

Table 3 Parameter value of transition elements.

Element type	$C_1$	$C_2$	$K$
	-1	-1	$\frac{1 - \frac{S_1}{S_3}}{2}$
	-1	1	$\left(\frac{S_1}{S_3} - 1\right)^2$
	1	-1	$\left(\frac{S_1}{S_3}\right)^2$

	1	-1	0.5
--	---	----	-----

Transfer matrices for cross-sectional discontinuities (*csd*) in the presence of mean-flow that include terms proportional up to the fourth power ( $M^4$ ) of the Mach number are presented in (Munjal, 1987). This simplification reduces the matrix  $T_{csd}$ , which relates the upstream and downstream acoustical fields  $p_3, \rho_0 S_3 u_3$  and  $p_1, \rho_0 S_1 u_1$  through:

$$\begin{bmatrix} p_3 \\ \rho_0 S_3 u_3 \end{bmatrix}_{Upstream} = T_{csd} \begin{bmatrix} p_1 \\ \rho_0 S_1 u_1 \end{bmatrix}_{Downstream} \quad (12)$$

to

$$T_{csd} = \begin{bmatrix} 1 & KM_1 Y_1 \\ \frac{c_2 S_2}{c_1 S_2 Z_2 + S_2 M_3 Y_3} & \frac{c_2 S_2 Z_2 - M_1 Y_1 (c_1 S_1 + S_3 k)}{c_2 S_2 Z_2 + S_3 M_3 Y_3} \end{bmatrix} \quad (13)$$

where

$$Z_2 = -j \left( \frac{c}{S_2} \right) \cot k_o l_2 \quad (14)$$

$l_2$ : Length of extended inlet /outlet pipe, m .

Letting length  $l_2$  tend to zero (as in case of sudden expansion and contraction, the yields the transfer matrix:

$$\begin{bmatrix} 1 & KM_1 Y_1 \\ 0 & 1 \end{bmatrix} \quad (15)$$

### 3.4.2. Linear acoustics

Noise from the intake and exhaust systems contributes significantly to the interior and exterior noise of cars. Institutions and industry have created a range of linear acoustic tools to estimate the acoustic characteristics of intake and exhaust systems (Mohamad et al. 2019). The concept of minor pressure disturbances within the ducts is used in linear acoustic models. Linear acoustic models are frequency domain approaches that, for example, compute the transmission loss of mufflers using the four-pole transfer matrix method. Although this method is faster, the projected findings may be inaccurate since the propagating pressure disturbances in an exhaust system usually have a limited amplitude (Kumar, 2007). The standard techniques will be discussed in detail in next chapter.

### 3.5. Linear acoustic modells of turbo chargers, CAT, PM, EGR, etc.

#### 3.5.1. Turbocharger acoustics and measurement techniques

The acoustics of turbomachines A turbocharger, for particular, can be divided into active and passive parts. The theory for the measurement technique is presented in the remainder of this section. In many applications , the passive properties of the turbocharger may be used to derive plane wave acoustic scattering characteristics as a function of frequency. Two-Port method technique was selected to study automotive turbochargers.

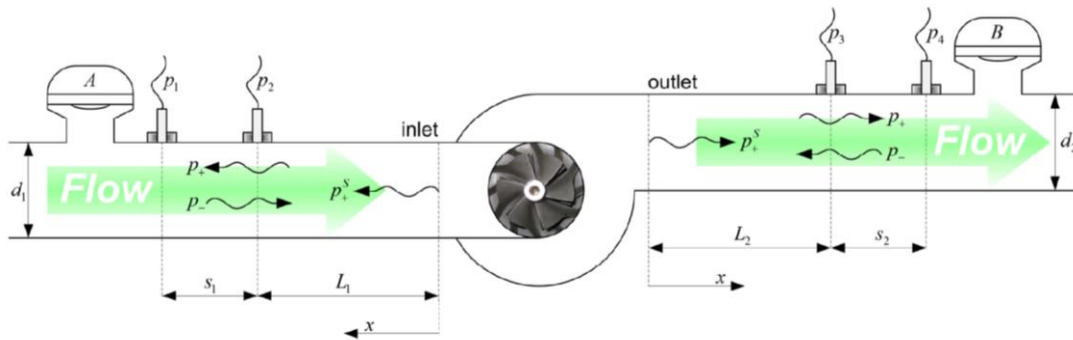


Figure 7 Diagram of a turbocharger represented and evaluated as an acoustic two-port. The acoustic pressure ( $p$ ) is recorded at four locations, with A and B being external sources (loudspeakers) utilized to stimulate the system from the upstream and downstream sides, respectively (Heiki, 2012).

The four complicated quantities in the plane wave acoustic two-port describe how incoming acoustic waves are reflected and transmitted through the acoustic element in the passive section at each frequency. The two-port also has an active portion that describes sound source. Decompose acoustic pressure waves travelling in both the positive ( $p+$ ) and negative ( $p-$ ) directions. To determine experimentally these unknowns at least two microphones in the inlet and outlet side must be used to. So the two-port can be represented as:

$$\underbrace{\begin{bmatrix} P_{a+} \\ P_{b+} \end{bmatrix}}_{P+} = \underbrace{\begin{bmatrix} S_{11} & S_{12} \\ S_{21} & S_{22} \end{bmatrix}}_S \underbrace{\begin{bmatrix} P_{a-} \\ P_{b-} \end{bmatrix}}_{P-} + \underbrace{\begin{bmatrix} P_{a+}^S \\ P_{b+}^S \end{bmatrix}}_{P+^S} \quad (16)$$

where ( $a$ ) represents to the inlet and ( $b$ ) represents the outlet side of the two-port, the superscript ( $S$ ) represents to source strength in the active section, the plus and minus signs represents propagation outwards and into the two-port respectively,  $S_{11}$ ,  $S_{22}$  and  $S_{12}$ ,  $S_{21}$  explain the incoming waves' reflection and transmission, respectively .

To obtain the  $S$  matrix elements for two independent test cases, the acoustic state variables on the inlet and exit sides must be measured. By conducting the two different test cases, we can express equation 16 in measurable quantities as:

$$\begin{bmatrix} H_{ea+}^I & H_{ea+}^{II} \\ H_{eb+}^I & H_{eb+}^{II} \end{bmatrix} = \begin{bmatrix} S_{11} & S_{12} \\ S_{21} & S_{22} \end{bmatrix} \begin{bmatrix} H_{ea-}^I & H_{ea-}^{II} \\ H_{eb-}^I & H_{eb-}^{II} \end{bmatrix} \quad (17)$$

where ( $H_e$ ) is the transfer function taken between the microphone signal and a reference signal, e.g. loudspeaker voltage, and the superscript indicates the loudspeaker signal used (I – loudspeaker A used as a reference, II – loudspeaker B used as a reference). The transmission loss ( $TL$ ) is directly related to the transmission part of the ( $S$ ) matrix elements and can be calculated as follows:

$$TL = 10 \log_{10} \left( \frac{W_{in}}{W_{tr}} \right) = 10 \log \begin{cases} \frac{(1+M_b)^2 A_b \rho_b c_a}{(1+M_a)^2 A_a \rho_b c_b |S_{12}|^2}, & \text{upstream} \\ \frac{(1+M_a)^2 A_a \rho_a c_b}{(1+M_b)^2 A_b \rho_b c_a |S_{21}|^2}, & \text{downstream} \end{cases} \quad (18)$$

where  $\rho$  is the air density,  $M$  is the Mach number,  $A$  is the cross-sectional area of the pipe,  $c$  is the speed of sound and in  $W_{in}$ ,  $W_{tr}$  are the incident and transmitted acoustic powers respectively.

Active properties of the turbocharger along with attenuating sound or damping a turbocharger is also act as sound generator, generating high frequency narrow band sound linked to the rotational speed of the impeller. Lavrentjev et al. 1995 described the following procedure of the source strength part of the two-part. Here another method was selected to capture the source strength beyond the plane wave range, in case the reflections in the test rig terminations are small or can be suppressed by spatial averaging, it is suggested that the strength of acoustic modes  $G_{++}$  propagating in the duct away from the source can be estimated as:

$$G_{++} = Re \left[ \sum_{m \rightarrow n} \frac{G_{mn}}{N} \right] \quad (19)$$

where

$G_{mn}$ : is the pressure cross-spectrums between a two of pressure transducers;  
 $N$ : is the number of spectra.

### 3.5.2. Linear acoustic modelling of catalytic converters and intercoolers

Most of the researchers use acoustic two-port method to describe acoustic level. In Dokumaci, 2014 a scattering matrix formulation was utilized, which may be easily changed to a transfer matrix formulation. The pressure and acoustic velocity have a Fourier transfer form and it can be written as:

$$\hat{P}(x) = A \exp(iKk_o x) \text{ and } \hat{q}(x) = X(r) \hat{P}(x) \quad (20)$$

where  $K$  has two roots, and  $H(r)$  is functions of tube radius  $r$ , air density  $\rho_o$ , and  $T_o$  is air temperature. The acoustic two-port for a single tube with length ( $L$ ) can be written as:

$$\begin{pmatrix} \hat{P}(0) & \hat{P}(L) \\ H(r_1) \hat{P}(0) & H(r_2) \hat{P}(L) \end{pmatrix} = T \begin{pmatrix} \hat{P}(L_1) & \hat{P}(L_2) \\ H(r_1) \hat{P}(L_1) & H(r_2) \hat{P}(L_2) \end{pmatrix} \quad (21)$$

therefore, the transfer matrix  $T$  is:

$$T = \begin{pmatrix} 1 & 1 \\ H(r_1) & H(r_2) \end{pmatrix} \begin{pmatrix} \exp(ik_o K_1 L) & \exp(ik_o K_2 L) \\ H(r_1) \exp(ik_o K_1 L) & H(r_2) \exp(ik_o K_2 L) \end{pmatrix} \quad (22)$$

This is for one narrow tube. The matrix transfer of a whole catalyst converter or intercooler with  $N$  tubes is:

$$\hat{T} = \begin{pmatrix} T_{11} & \frac{T_{12}}{N} \\ NT_{21} & T_{22} \end{pmatrix} \quad (23)$$

### 3.5.3. Linear acoustic modelling of particle filters

In particulate filters the channels are blocked at the end. Therefore, the model for a *PF* should be modified somewhat compared to the model for catalytic converters. The pressure will be varied for channel in-flow and out-flow, since the flow must pass through the filter components. While *GPF* and *DPF* are closely related, so most of *NVH* literatures utilized *DPF* in matters of acoustics. Allam and Åbom, 2005 presented a first attempt to perform *DPF* acoustically by a two-port model, and the filter was considered as an equivalent acoustic resistance since the model ignored wave propagation. The transmission loss of the model agreed within 1 dB with measured data on a typical filter by one-dimensional approach. Hou et al. 2017 represent mathematical calculation model for measuring transmission loss in *DPF* using transfer matrix theory (*TMM*).

Four-terminal grid transfer matrix or four-pole transfer matrix According to the plane wave assumption, the acoustic condition on any segment of the pipeline system can be characterized by two state parameters that were the pressure  $p$  and the volume velocity  $u$ .

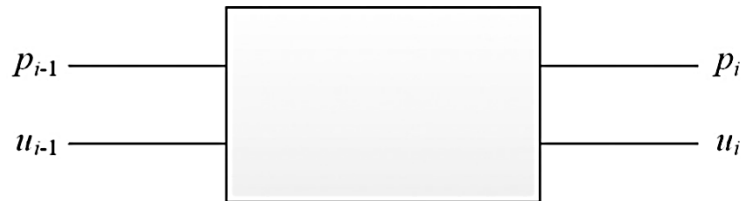


Figure 8 Acoustic units of four-pole method.

The sound pressure and velocity have a functional relationship, in which expressed as:

$$P_i = A_i P_{i-1} + B_i u_{i-1} \quad (24)$$

$$u_i = C P_i + D u_2 \quad (25)$$

$$\begin{bmatrix} P_i \\ u_i \end{bmatrix} = \begin{bmatrix} A_i & B_i \\ C_i & D_i \end{bmatrix} \begin{bmatrix} P_{i-1} \\ u_{i-1} \end{bmatrix} = |T_i| \begin{bmatrix} P_{i-1} \\ u_{i-1} \end{bmatrix} \quad (26)$$

where  $[T_i]$  is the transfer matrix of acoustic units;  $A_i$ ,  $B_i$ ,  $C_i$ , and  $D_i$  were the four-pole parameters of matrix  $[T_i]$ , respectively, related to the unit structure, and can be obtained from equation:

$$\begin{aligned}
 A_i &= \frac{P_i}{P_{i-1}} \Big|_{v_{i-1}=0, v_i=1} \\
 B_i &= \frac{P_i}{-v_{i-1}} \Big|_{P_{i-1}=0, v_i=1} \\
 C_i &= \frac{v_i}{P_{i-1}} \Big|_{v_{i-1}=0, v_i=1} \\
 D_i &= \frac{v_i}{-v_{i-1}} \Big|_{P_{i-1}=0, v_i=1}
 \end{aligned} \tag{27}$$

Based on the acoustic transfer matrix, the pressure and velocity at one end of the unit can be calculated by the pressure and velocity at the other end. On both sides of the transfer matrix, there were two input and two output parameters, related by the transfer matrix. If a system contains ( $N$ ) acoustic elements with the transfer matrix of each element having obtained, then the transfer matrix for the whole system can be written as:

$$[T] = [T_N] \dots [T_i][T_{i-1}] \dots [T_0] \tag{28}$$

where  $[T]$  and  $[T_i]$  were system transfer functions and the acoustic element transfer matrix, respectively. The acoustic element transfer matrix's multiplication sequence corresponded to the acoustic element's location in the system. The transfer matrix can be used to calculate the plenum, chambers and mufflers characteristics of the intake and exhaust system components. Mathematical calculation model of transmission loss of the *DPF*. The particulate filter was divided into  $T_{IN}$ ,  $T_I$ ,  $T_{II}$ ,  $T_{III}$ , and  $T_{OUT}$  as shown in figure 9.

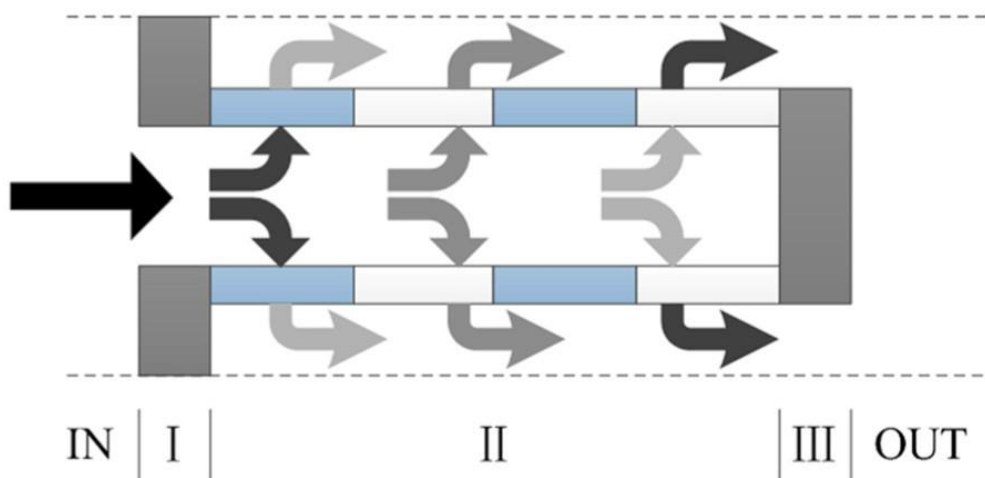


Figure 9 Transfer matrix diagram of diesel particulate filter (*DPF*).



The transfer matrix of the  $DPF$  can be written as:

$$T_{DPF} = \begin{bmatrix} T_{11}^{DPF} & T_{12}^{DPF} \\ T_{21}^{DPF} & T_{22}^{DPF} \end{bmatrix} = T_{in}T_I T_{II} T_{III} T_{out} \quad (29)$$

where  $T_{in}$  and  $T_{out}$  were transfer functions of import and export sections of  $DPF$ , which were obtained by applying the principle of energy and momentum conservation. The two portions indicate the coupling of two ports, which were necessary because pressure and velocity were not constant when the flow region changed abruptly. The flow in the catalytic converter portion is assumed to have a low Mach number.,  $T_{in}$  and  $T_{out}$  were expressed as:

$$T_{in} = \begin{bmatrix} 1 & 1.5 \frac{\rho_o c_o M}{S_{in}} \left( \frac{1}{M^2} - 1 \right) + j \frac{\rho_o \omega l}{S} \\ 0 & 1 \end{bmatrix} \quad (30)$$

$$T_{out} = \begin{bmatrix} 1 & 2 \frac{\rho_o c_o M}{S_{out}} \left( 1 - \frac{1}{M} \right) + j \frac{\rho_o \omega l}{S} \\ 0 & 1 \end{bmatrix} \quad (31)$$

where  $M$  is Mach number,  $c_o$  is the speed of sound in  $m/s$ ,  $m$  is the open area ratio,  $S_{in}$  is the total cross-sectional areas of the inlet particulate filter ducts in  $m^2$ ,  $S_{out}$  is the total cross-sectional areas of the outlet particulate filter ducts in  $m^2$ .

$T_I$  and  $T_{III}$  were the transfer functions of the model, the short ducts at the inlet and outlet to the catalytic channels with lengths corresponding to the plug length, respectively. It was assumed that, compared to the acoustic wavelength, the lengths of  $I$  and  $III$  was tiny. Then,  $T_I$  and  $T_{III}$  can be expressed as equation :

$$T_I = T_{III} = \begin{bmatrix} 1 & j\rho_o \omega l/S \\ 0 & 1 \end{bmatrix} \quad (32)$$

where  $\rho_o$  is the air density in  $kg/m^3$ ,  $\omega$  is the angular frequency in  $rad/s$ ,  $S$  is the cross-sectional area of the channel of particulate filter in  $m^2$ ,  $J$ : is the imaginary unit,  $T_{II}$ : is the core component of particulate filter. Transfer matrix  $T_{II}$  can be calculated by:

$$T_{II} = \begin{bmatrix} \left( \frac{A}{C} \right) & \left( \frac{B - \frac{AD}{C}}{S} \right) \\ \left( \frac{1}{C} \right) S & \left( -\frac{D}{C} \right) \end{bmatrix} \quad (33)$$

The acoustic transmission loss [ $TL$ ] for the whole particulate filter could be calculated by:

$$TL = 20 \text{Log}_{10} \left[ \frac{1}{2} \left( T_{11}^{DPF} + \frac{T_{21}^{DPF} S}{\rho_o c_o} + \frac{\rho_o c_o T_{21}^{DPF}}{S} + T_{22}^{DPF} \right) \right] \quad (34)$$

### 3.5.4. Exhaust gas recirculation: Design and analysis

The principle of *EGR* was illustrated in chapter 2. In this section the latest approach will be presented through reviewing of literatures. The efficiency of the *EGR*-system can be analysed by measuring the exergy of system. The amount of work that can be extracted from a gas flow in a particular environment is known as exergy, unlike energy, can be destroyed. Exergy analysis is used to indicate how different system components might be improved. Exergy analysis as a tool is introduced and contrasted to energy analysis of a system at the same time. Simon, 2014 uses exergy analysis methodologies to examine the full gas exchange system, including *EGR*. In *1D* and *3D* calculations, the mixing of air and *EGR*, as well as the influence of pulses in the *EGR* stream on the cylinder-to-cylinder distribution of *EGR*, were studied. The author proved that the main exergy losses on the analyzed engine are the exergy loss in the *EGR*-cooler and the exergy that leaves the system at the exhaust, on the present light-duty engine, the *EGR*-cooler of the high-pressure system smashing up to 30% of the exergy from the exhaust gas by cooling it and dismissing the heat to the environment. In the low-pressure system the corresponding exergy destruction is only in the order of 20%. The exergy that leaves the system lies in the order of 30 to 45% of the available exergy at the exhaust valves.

The specific exergy in [J/kg] of a gas flow is expressed as:

$$E_f = (h_1 - h_o) - T_o(s_1 - s_o) + \frac{1}{2}u_1^2 \quad (35)$$

The total exergy in [J/s] contained in a mass flow then becomes:

$$\dot{E}_f = \dot{m} \left( (h_1 - h_o) - T_o(s_1 - s_o) + \frac{1}{2}u_1^2 \right) \quad (36)$$

where  $h$  is the specific enthalpy in  $J$ ,  $T$  is the temperature in  $K$ ,  $s$  is the specific entropy in  $J/K$ ,  $u$ : is the flow speed in  $m^3/s$ ,  $\dot{m}$  is the mass flow of the gas in  $kg/s$ . Index (1) indicates the actual gas state, index (o) the reference state (Moran and Shapiro, 1998).

Nyerges and Zöldy, 2020 used estimation techniques to measure *EGR* mass flow rates by analysis of the sensors to measure the pressures, the temperatures, the mass fractions and other engine parameters. The results were compared and verified with other references.

Another advantage of the exergy study provides a way to better understand the role of turbocharger efficiency. Exergy analysis allows you to combine and compare the effects of components with completely distinct properties on total efficiency.

### 3.6. Active intake-and exhaust systems: Active noise control (ANC)

The active noise control system (ANC) is a method for noise control by using secondary source. There are three ways to control and reduce the noise from intake and exhaust system:

- i. Absorptive materials: A good sound absorbing material is one that is able to absorb and transmit more sound waves than it reflects. A material's capacity to absorb is influenced by characteristics such as thickness, density, and porosity. Although the allowable aperture ratios are considerable, sound absorption structures have the drawback of being costly. As a result, general sound-absorbing/insulating material efficiencies are difficult to predict (Amares et al. 2017).
- ii. Resonator for noise reduction: In the case of resonator for intake and exhaust systems, Helmholtz resonator is an acoustic device consisting of a large-volume cavity and a thin connecting pipe that has the property of reducing intake noise with a strong pure tone component extremely effectively .

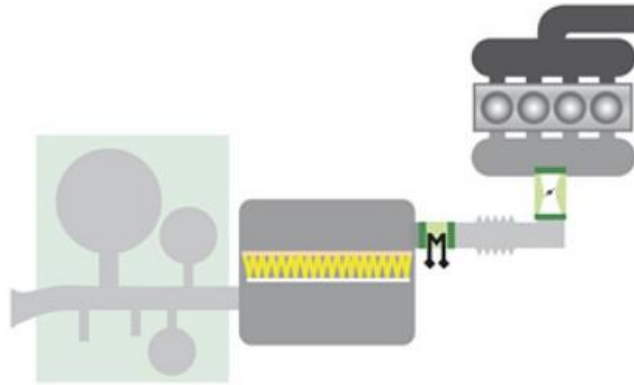


Figure 10 Intake system with fixed resonates (Mann-Hummel, 2010).

Resonance muffler usually is used in various applications, and it is mounted to the intake and exhaust system of the internal combustion engines to absorb a specific frequency band occurs due to flow noise. The equation to calculate target frequency in a Helmholtz resonator:

$$f = \frac{c}{2\pi} \sqrt{\frac{A_n}{L_n v_c}} \quad (37)$$

where  $A_n$  is the neck cross section area in  $m^2$ ,  $L_n$  is the neck length in  $m$ ,  $v_c$  is the cavity volume in  $m^3$ ,  $c$  is the speed of sound in  $m/s$ .

Based on this equation, ( $v_c$ ) shall be larger or the cross section of neck shall be wider if the low range frequency band is the target which is the intake noise range, as shown in figure 11.

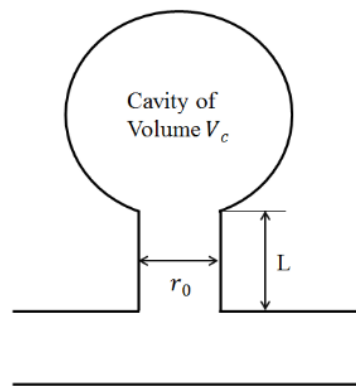


Figure 11 Helmholtz resonator.

- iii. Active noise control system: Consists of microphone and loudspeakers and its function to generate sound. The essential principle is that the controller sends a signal to the loudspeaker with the correct phase dependent on the speed and load. The sound component emitted by the loudspeaker then overlaps with the engine noise as shown in figure 12. The peaks and valleys of sound oscillations meet and cancel each other out in this process. (Pricken, 2000).

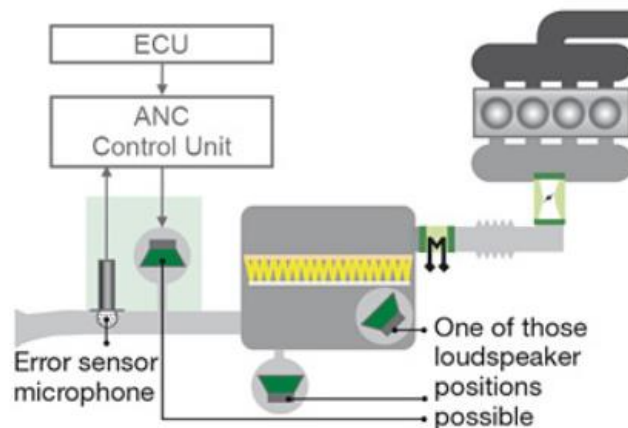


Figure 12 Intake system with active noise control (ANC) (Mann-Hummel, 2010).

### 3.7. Noise contribution of intake and exhaust noise to pass-by and to interior noise

The noise of intake and exhaust parts from vehicles with internal combustion engines is very important to focus for quality purpose. It must provide good engine sound quality without being distracting or in violation of noise regulations. In general, in order to improve the subjective sense of the sports cars, therefore, the exhaust system noise that is up to 20 dB greater than intake system noise under full load. However, these noise emissions must comply to current regulations. Primary and secondary noise sources can be found in the intake and exhaust systems. The opening and shutting events of the engine valves create pressure pulses, therefore, the engine's combustion rate is linked to valve motion which are the primary noise generators.

The pulses travel through the intake and exhaust systems to the orifices, where they are radiated into the environment as noise. The engine noise character and sound pressure level (*SPL*) are mostly determined by the intake and exhaust systems, which must be calibrated to meet the desired performance. The engine sound quality should notify the driver about engine speed (*rpm*) as well as offer a sound that is appropriate for the vehicle type, such as powerful and sporty during acceleration but quiet during constant speed driving. This is also true for exterior sound, where the sound character should be consistent with the vehicle's brand identity.

- i. Test rig and measurements on dynamometer: This setup essentially consist of four microphones, a power amplifier with speaker as excitation source, the object to be tested, and an anechoic termination at the downstream end. This testing is done at the component supplier or the original equipment manufacturer (*OEM*). The result is used for verification of requirements and benchmarking, computer-aided engineering (*CAE*) correlation and during development.

In a semi-anechoic test cell with a noise, vibration, and harshness (*NVH*) chassis dynamometer, the radiated noise from the intake, exhaust system parts, and tailpipe noise is measured on a full car. This is necessary for verification and benchmarking, as well as for determining the source contribution to car interior and pass-by noise. The microphones are kept near the muffler or other sections that need to be checked. (Gras, 2020).

Tailpipe noise microphones are frequently positioned at an angle to prevent direct exhaust flow. If the microphone has to be near a highly hot part or in the exhaust flow, probe microphones should be utilized. The relationship between sound pressure levels and engine orders versus engine speed is investigated.

Acoustic transfer function (*ATF*) measurements from the exhaust pipe to the vehicle interior are used to validate *CAE* models and verify the acoustic package, but they can also be used as one of several inputs for vehicle simulators to evaluate sound quality design targets subjectively before hardware is available.

- ii. Pass-by noise : The pass-by noise measurement is a crucial last test to ensure that the legislation's standards are met and, if not, to identify the cause of the problem. This is carried out on a designated test track in accordance with international standards. Additional exhaust system muffling can be employed to determine if tailpipe noise is the issue.
- iii. Acoustic test types within pass-by noise testing: pass-by noise testing is the most important part of troubleshooting in the mass production of cars. It includes two types of measurements: Indoor and outdoor. Indoor pass-by noise is used for development and requires a very large semi-anechoic chamber and a line of microphones on each side of the vehicle to simulate the actual pass-by. For source contribution analysis, the acoustic

transfer function (*ATF*) from the exhaust system to these microphones needs to be measured .

Testing in the outdoors Outdoor tests, which are utilized for both development and certification, are the most traditional and crucial aspect of pass-by-noise testing. Acceleration tests, constant speed tests, and static tests for a motionless vehicle on a specific test track are all part of pass-by noise testing. According to the requirements, two microphones are placed on either side of the test track to measure sound pressure levels, and further thorough analysis in the frequency and engine order domain is used for development . During the measurement, systems for logging vehicle speed and weather conditions are required. Around the world, there are some regional disparities in legislation , but the tests are based on the latest version of *ISO362*. The microphones and measurement equipment must be calibrated before and after testing (Braun, 2013).

iv. Vehicle interior *NVH* testing: Vehicle interior noise, vibration and harshness (*NVH*) involves a number of different tests – all related to noise inside the vehicle originating from road, body, chassis and components of the vehicle. The main focus areas are:

- a) **Total interior noise** : This is an excellent benchmarking measurement and one that automotive magazines frequently use to compare different car models. It is a method of testing the entire experience of a vehicle's acoustic comfort by measuring the overall noise level within the vehicle at full speed.
- b) **Road noise** : is one of the most terrible automobile interior noises. Road excitation contributes to both structure-borne and airborne interior noise. Subjective judgement, benchmarking, and experience are typically used to develop requirements. Noise level and frequency balance are two of the considerations. Tire cavity resonance noise at *200-250 Hz* and tread noise are given special attention..
- c) **The sound packages**: Is linked to the majority of *NVH* areas . The first step is to ensure that the body is as completely sealed as possible. This improves overall *NVH* performance by reducing high-frequency leakage. For maximum performance and lowest weight and cost, structural damping and heavy-layer isolation mats must be tuned. Finally, acoustic absorption material is applied at crucial areas to improve the acoustic comfort of the interior.
- d) **Component noise** : Is commonly divided into two major categories : customer-actuated sounds and system-actuated sounds. Customer-actuated sounds are associated with a specific activity, such as opening or shutting a door or activating power windows, and give user feedback. System-actuated sounds are not always simple to comprehend because they controlled independently of any activity by the driver or passengers. During cool down or heat up, the *HVAC* system is one of the most prominent noise generators in the vehicle, and it necessitates extensive design considerations (Gras, 2020).

- e) **Brake noise** : is a chassis-related noise that *OEMs* all over the world are concerned about. Friction-induced vibrations cause the braking system to emit noise, which causes the noise. When this happens, it will irritate and annoy the automobile owner as well as anybody else who is near the vehicle. The braking noise can lead to low customer satisfaction ratings and expensive warranty costs. As a result, the automobile industry places a great priority on the development of braking systems with minimal noise concerns. Brake noise is a difficult topic to solve, and study in this field is ongoing.
- f) **Computer model validations**: Before any prototype item or vehicle is built, several design choices and verifications are made. Body and chassis design have a significant influence on vehicle *NVH* performance, particularly in terms of powertrain and road noise, and should be validated early on. The simulations are correlated using measurements from current automobiles or systems. Mule vehicles (existing automobiles that have been modified to include new ideas) are also utilized.

General measurements include modal analysis and transfer function measurements, acoustic transfer function (*ATF*). Excitation is handled with an impact hammer, shakers, and volume velocity sources. The standardized vehicle verification tests are also used to verify computer-aided engineering (*CAE*) models.

Experimental approaches are used to identify the noise source contributions at discrete track positions, which are then combined with the transfer path characteristics from the source site to the pass-by noise microphone position to estimate pass-by noise. The calculations can be performed in either the time or frequency domain. In order to derive the noise source contributions, the operational source strengths are convolved with the associated impulse response functions in the time domain. The source contributions are determined in the frequency domain at a discrete track point by multiplying the operational source strengths by the associated transfer functions (Fleszar et al. 2001).

## 4. ANALYSIS OF RACE CAR ENGINE INTAKE SYSTEM

### 4.1. Air intake system: Location and function

There are three basic tasks of an engine's intake system. Its primary duty is to filter the air so that the engine receives clean, debris-free air. The flow and acoustic performance of the intake system are two more features that engineers consider when developing it. The intake system's flow efficiency has a huge influence on the engine's power output. As can be seen in ( Winterbone and Pearson, 2000) In a common internal combustion engine (*ICE*), during the air intake phase, when the intake valve is open, the cylinder volume is not totally filled, as one would expect theoretically. This is due to pressure losses and variations in air density along the feeding system. As a result of this procedure, real cylinder volumetric efficiency and engine performance as a whole will not reach design expectations if all effects are not properly handled. The intake manifold (*IM*) is one of the components that plays a crucial part in air supply process in engines, which has physical features such as pressure loss imposed on air and lack of homogeneity of the loss between the runners (air supply unbalanced) are some of the aspects that have been connected to engine emissions and fuel consumption efficiency. In current research work, Honda CBR 600RR (PC 37) engine was conducted to optimize intake manifold including plenum and channel ducts as shown in figure 13.



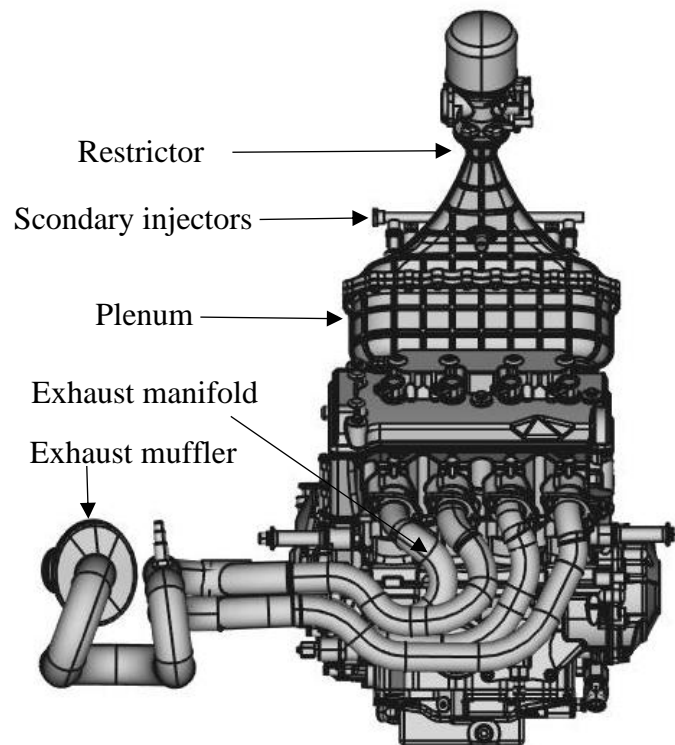


Figure 13 Honda CBR 600RR (PC 37) race car engine components.

The investigation consists of three parts:

- a) three-dimensional *CFD* analysis on the performance of the intake and exhaust system,
- b) one-dimensional analysis of a Honda *4-stroke* gasoline engine ,
- c) experimental study of a Honda engine operating with gasoline fuel.

The three-dimensional analyses based on Reynolds-averaged Navier–Stokes equations to describe the turbulent flow and fluctuating quantities have been conducted to study the effects on the intake, exhaust system and engine performance.

In order to improve understanding on the flow wave action on the intake and exhaust system of a Honda gasoline engine, one-dimensional engine simulations have been conducted using commercial AVL Boost software.

## 4.2. Model description

Several manufacturers have already incorporated a number of technologies who sell vehicles with technology that exploits the varying geometry of *IMs*, intending to appropriately tune it for each engine speed or range of rotation, in table 4 the entire engine descriptions were illustrated. A simple form is presented by (Juliano Vaz et al. 2017), where two different arrangements are switched in a specific rotation. See figure 14 for an illustration of the concept of varying geometry .

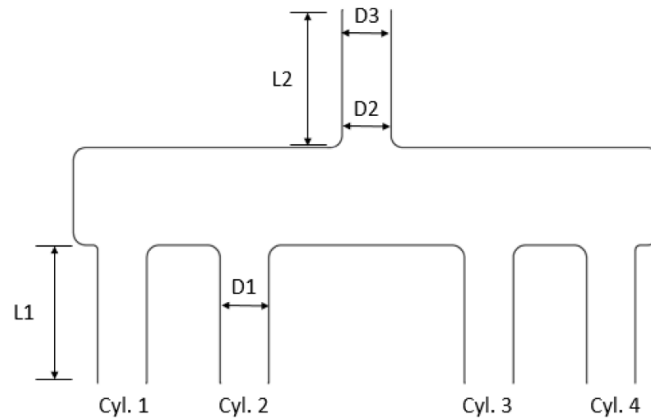


Figure 14 Intake manifold with variable geometry scheme taken from (Juliano Vaz et al. 2017).

In figure 14, a simplified representation of intake manifold switches the two sets composed by plenum and tubes with various shapes and sizes, appropriate for varied ranges of *ICE*'s rotation. *Cyl. 1, 2, 3, 4* represent number of cylinders, the length of primary duct ( $L1$ ), the length of secondary duct ( $L2$ ), the diameter of primary and secondary ducts ( $D1, D2$  and  $D3$ ) and air box (plenum) volume ( $PL$ ). In practice, the mechanism works as shown on a Honda's product in (Kenji, 2011), It highlights how to switch between channels and redirect flow in every circumstance in detail.

Other products are presented by (Joo, 2009), (Mashiko, 2006), (Stefan, 2006) and (Pascal, 2006), which illustrate various alternative approaches used by Hyundai, Mitsubishi, Volkswagen and Renault respectively to vary the length of the runners, change volume, combinations of these, and other characteristics of geometry, which must supply the combustion chamber in each circumstance, as well as the intake valve's opening time.

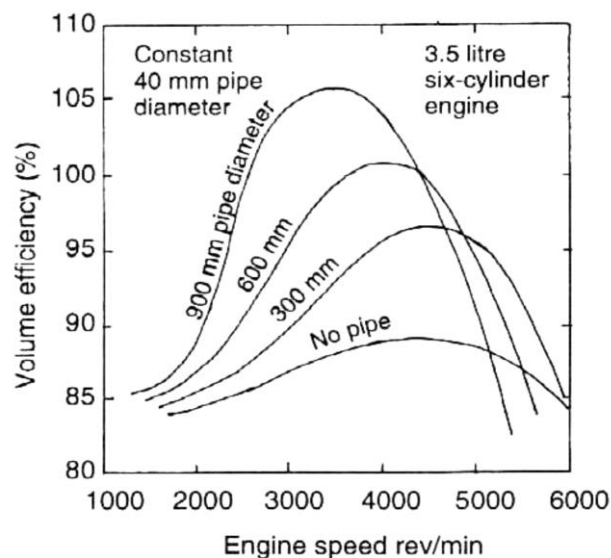


Figure 15 Relationship between inlet tract lengths and volumetric efficiency with constant diameter (Heisler, 1995).

The charge column peak ramming impact increases with the length of the tract for a fixed tract diameter; but the increased flow resistance causes the charge column pressure to peak at lower engine speeds (Heisler, 1995). This might be a disadvantage for our Formula Student because we need both the maximum performance and the volumetric efficiency at high engine speeds. For a given tract length, both small and large tract diameters offer about the same peak volumetric efficiency in the cylinder. The volumetric efficiency of the smaller diameter tract, on the other hand, peaks significantly earlier than the larger one. The engine design parameter were described in table 4.

Table 4 Formula race car engine parameter.

Powertrain	Units						
Manufacturer / Model		Honda CBR600 RR (PC37)					
Cylinders & Fuel		Cylinders:	4	Fuel Type:	RON98		
Displacement & Compression		Displacement (cc):	599	Compression (.:1):	12,2:1		
Bore & Stroke	mm	Bore:	67	Stroke:	42.50		
Connecting Rods Length	mm	91					
Engine Output		Peak Power (kW)	61	Peak Torque (Nm)	67		
Design Speeds	rpm	Lower Design Limit	7000	Upper Design Limit	11000	Peak Power and Torque Range	8500-10500
Valve Train		Chain driven, DOHC					
Valve Diameters	mm	Intake	27.5	Exhaust	23		
Valve Timing	deg	Intake	Opens	at 1 mm lift	22° BTDC		
			Closes	at 1 mm lift	43° ABDC		
		Exhaust	Opens	at 1 mm lift	40° BBDC		
			Closes	at 1 mm lift	5° ATDC		
Firing Order		1-2-4-3					
Fuel Pressure	bar	4.00					
Injector Type		Bosch EV14 ES (0 280 158 013), 4 pcs					
Injector Capacity	g/min	150					
Intake Plenum		Volume (cc):	N/A	Runner length (mm):	112		
Exhaust System Configuration		4-2-1					

Figure 13 shows a typical structural design, especially for four-cylinder engines. It has a little disadvantage in terms of *COG* (Center of Gravity) location, but on the other hand, the system is located in the opposite direction from the driving direction, allowing the engine to be blast overloaded. Because the air stream-lines do not have to make any severe bends, there are less

velocity fluctuations and hence a better flow coefficient. The airbox or plenum, and the runner in figure 16 is quite small and short for a 4-cylinder engine - Honda race car; it could bring worse charging, especially at higher engine speeds when the engine needs more air and has very short time for the induction. In figure 17 current racing engine manifold also have extend (runners) inside to plenum to secure better air flow. Sharp edges can create flow separation, resulting in a reduction in mass air flow via the runners and valve seat.

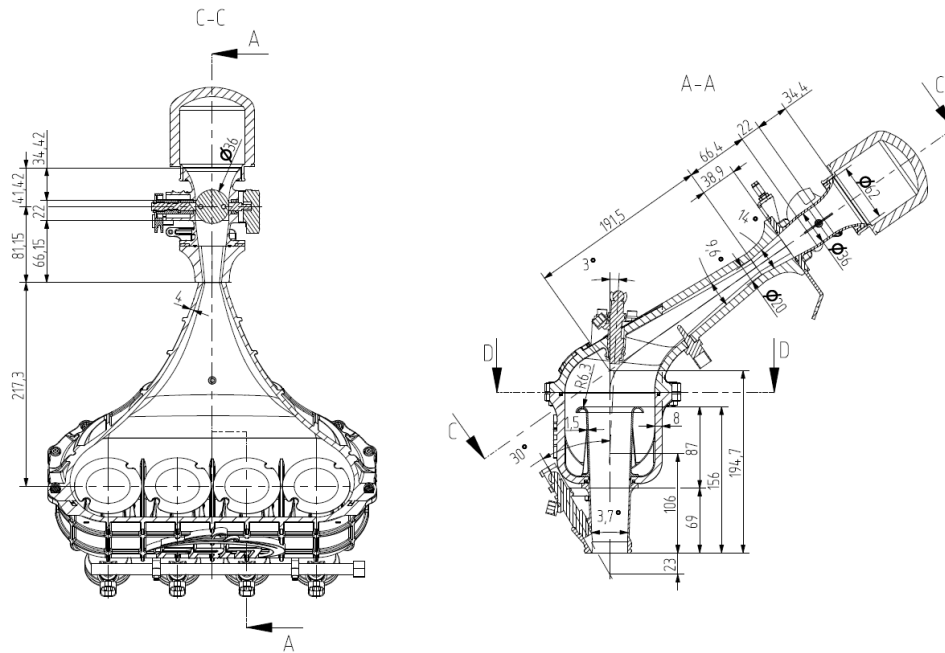


Figure 16 Honda CBR 600RR (PC 37) current intake manifold dimensions.

Pressure waves from the intake runner spread into the plenum, and the pressure wave extends to the plenum wall along the inserted half of the restrictor due to a large area difference between the restrictor outlet and the plenum wall. That implies the restrictor is only slightly influenced by pressure waves, leading to low turbulent flow and velocity variations, and thus better air flow through the restrictor.

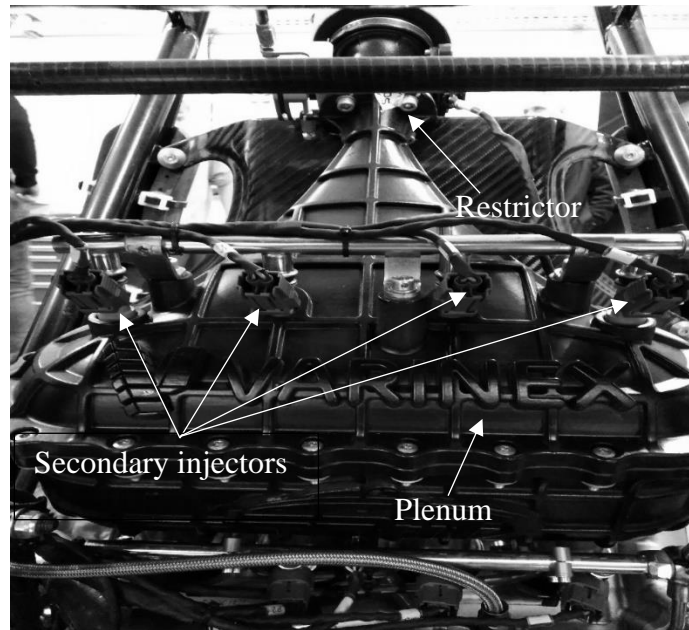


Figure 17 Honda CBR 600RR (PC 37) current engine intake system.

#### 4.2.1. Wave ram cylinder overcharging

When the engine is running, the reduction in the cylinder produces a negative pressure wave (primary wave) that travels at the speed of sound through the column of air from the back of the inlet valve to the open atmospheric end of the intake manifold (equation was used for the speed of sound calculation) (Mohamad & Amroune, 2019). Due to the inertia of the air, a reflected positive pressure-wave is formed when this pressure-wave pulse hits the atmosphere, causing the pressure pulse to return to the inlet valve port. This wave, if timed correctly, is responsible for ramming the air into the cylinder when the piston is behind the *BDC* (Bottom Dead Centre) and is rising. The pressure wave reverses direction and is reflected outwards when it hits the inlet valve again. Until the inlet valve is closed, these negative and positive pressure waves are continuously reflected backwards and forth. The movement of these waves in a column of air is comparable to that of a coil spring. As you can see in figure 18.

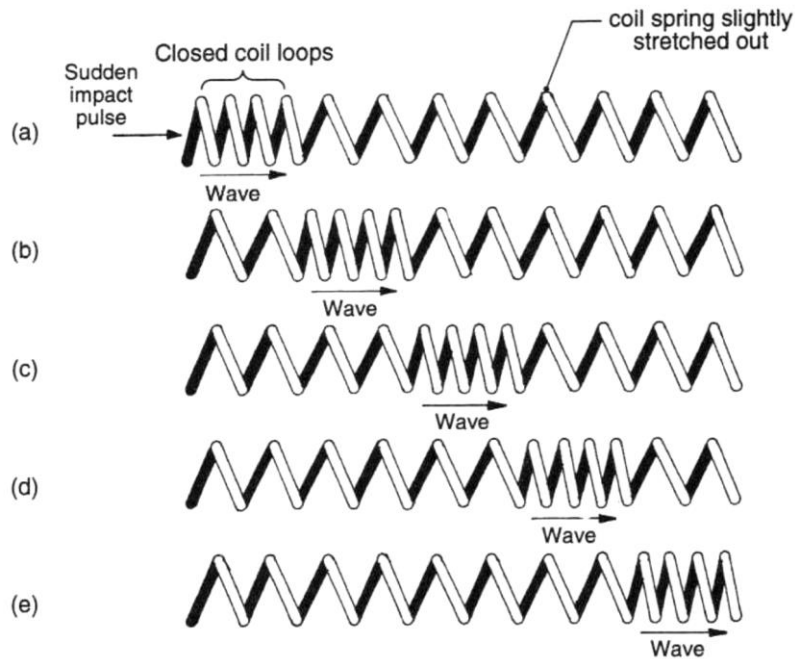


Figure 18 Illustration of wave moving (Heisler, 1995).

To use the pressure wave pulse, it must be timed so that the first positive pressure wave arrives at *BDC* at its peak amplitude at the middle of the induction stroke. The cylinder pressure has increased to around atmospheric pressure at *BDC* and then advances to a positive pressure before the effective inlet valve closing point (*EIC*) that is effective inlet valve closing is achieved if the induction length is selected so that  $\theta_t = 90^\circ$  in figure 19. The pressure wave has likewise peaked at *BDC*, providing appropriate time for the charge at the intake port to be transferred to the cylinder before cutting off the cylinder's supply.

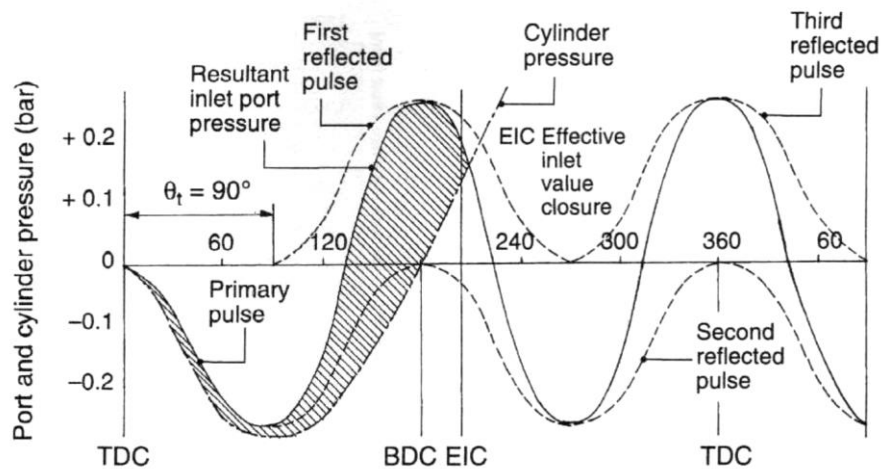


Figure 19 Pressure wave movement (Heisler, 1995).

The speed of sound theorem has two constants, and it is self-evident that temperature has a significant impact on the magnitude of sound speed, which also can be seen in figure 20.

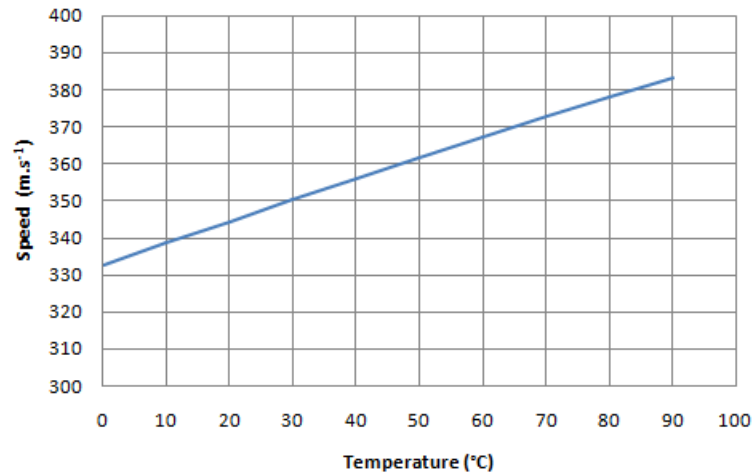


Figure 20 Speed of sound on temperature relationship (Adámek, 2011).

That is why there are replaceable intake runners in racing cars which use the induction ram wave overcharging and which can be replaced when the weather changes before the race. The primary principle is to select the appropriate manifold volume as well as the resonator resonating at an engine speed where torque boost is needed; it is also necessary to experiment with tuned pipe length to achieve the best results. However, interferences between the pressure wave pulses and the regular inertial ram effects can cause problems, and cylinder filling may be delayed as a result (Mohamad et al. 2019). As a result, extensive experimentation is required to achieve the greatest feasible compromise between the inertial and wave ram effects .

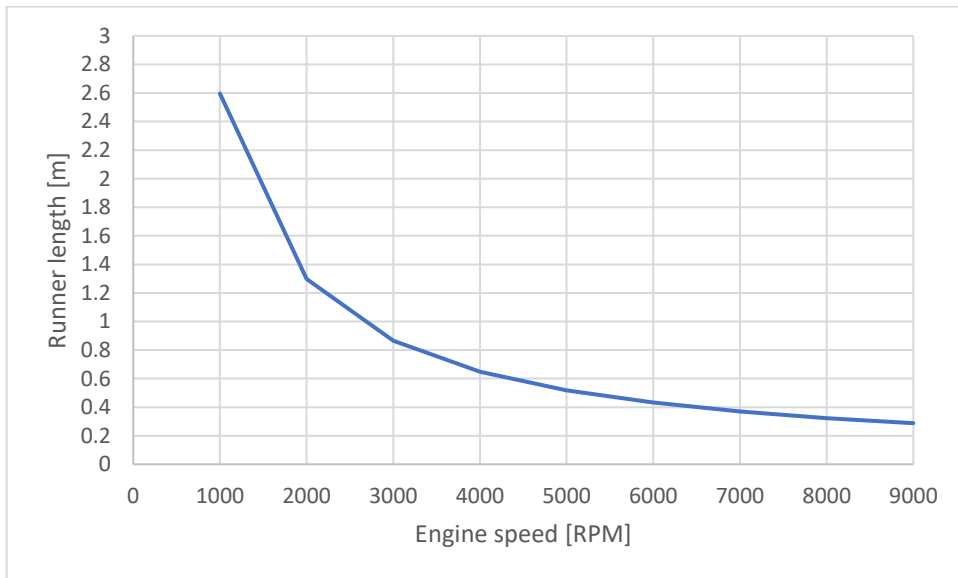


Figure 21 Intake runner length to engine speed relationship (Adámek, 2011).

#### 4.2.2. Variable intake system

The optimum intake system for today's naturally aspirated engines is a full variable intake system with an equivalent intake runner length for each engine speed. In figure 22, there is a

BMW full variable intake system (Autozine, 2011). The rotating labyrinth is located within the resonator and spins to achieve optimum volumetric efficiency at all engine speeds.

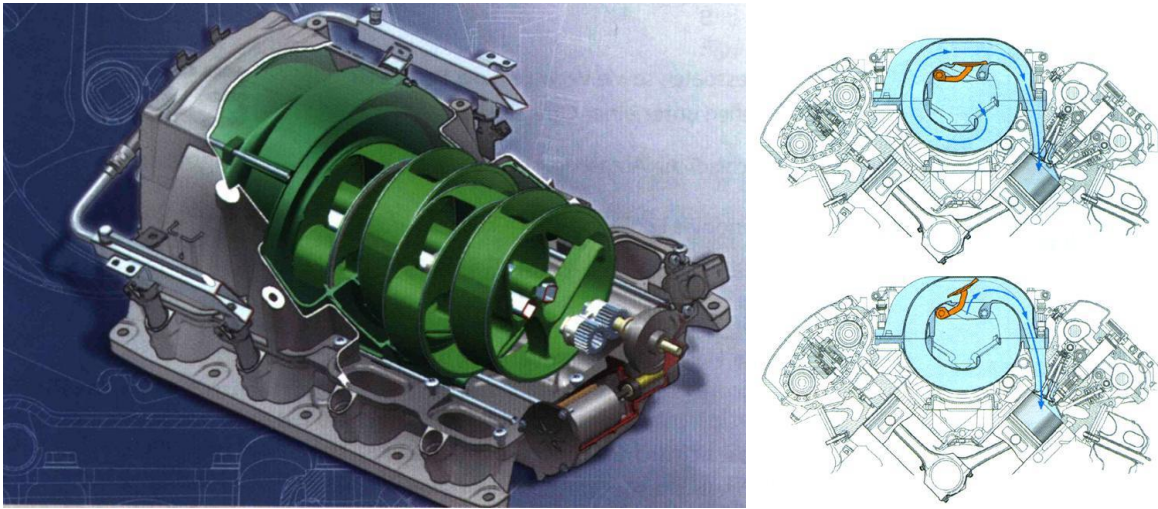


Figure 22 Full variable intake system (Autozine, 2011).

### 4.3. Numerical analysis

#### 4.3.1. Overview

The investigation of fluid dynamic and thermodynamic phenomena characterizing internal combustion engine operation retains practical relevance in the activity devoted to select the configurations able to ensure the optimized matching between noise radiation, pollutant emission and engine performance. In order to analyze and evaluate various configurations and operating points, experimental and computational approaches have been developed to provide a better understanding of the complex processes occurring inside intake systems. A variety of modelling procedures have been proposed in the literature and are currently applied to predict the propagation of pressure waves in the gas flowing along intake systems. These procedures may be collected in two main groups, linear acoustic and non-linear fluid dynamic models, according to the assumptions on which they are based (Mohamad, 2019). The intake system is made up of a few components placed in series and lie between the atmospheric air (intake orifice) and the intake valves of the engine. The primary function of the air intake system is to deliver air to the engine. It would be important to calculate the amount of air charge that can be sucked into the cylinder, as a ratio of the theoretical mass of air that can be contained in the cylinder. Essentially, for a naturally aspirated gasoline engine, it is the ratio of the trapped volume of gas to the volume of the cylinder (Claywell et al. 2006).

$$\lambda_a = \frac{m_g}{m_{th}} = \frac{m_g}{v_H \rho_{th}} = \frac{v_g}{v_H} \quad (38)$$



where  $\lambda_a$  is the volumetric efficiency,  $m_g = v_g \rho_g$  is the mass of air that is trapped in cylinder in  $kg$ ,  $m_{th}$  is the theoretical mass of air that can be trapped in cylinder in  $kg$ ,  $v_H = v_{th}$  is the volume of cylinder, which equals theoretical volume,  $\rho_{th}$  or  $\rho_g$  are the theoretical density of air in cylinder in  $kg/m^3$ ,  $v_g$ : Volume of gas trapped in cylinder in  $m^3$ .

The method of charging the engine is by the depression (partial vacuum) created by the expanding of the combustion chamber due to the downwards moving piston. Theoretically it is possible to achieve a maximum volumetric efficiency of 100%. This value could be reduced by intake components start from restricted flow through the throttle body and intake valves, the energy loss through friction with the inner walls of the air intake system, as well as the propagation of reduced air pressure when the cylinder's vacuum initiates (Mohamad, 2019). The mass flow rate under a choked flow condition can be defined by the equation (39):

$$\dot{m} = C_D A_c \sqrt{K \rho P \left( \frac{2}{k+1} \right)^{\frac{(K+1)}{(K-1)}}} \quad (39)$$

where  $\dot{m}$  is the mass flowrate  $kg/s$ ,  $C_D$  is the discharge coefficient,  $A_c$  is the discharge hole cross-sectional area,  $m^2$ ;  $k = c_p/c_v =$  of the gas,  $c_p$  is the specific heat of the gas at constant pressure in  $J/kg K$ ,  $c_v$  is the specific heat of the gas at constant volume in  $J/kg K$ .

### 4.3.2. Geometrical model

Definition of the geometry of the region of interest: the computational domain. Because of its convenience and minimal computing costs in the representation of complex geometries, one-dimensional linear acoustic models are extensively used to evaluate the noise performance of intake systems (Mohamad, 2020).

Honda CBR 600RR (PC 37) intake manifold 3D geometry was sketched based on real dimensions using advanced design software Creo 4 see the figure 23 (a, b, c).

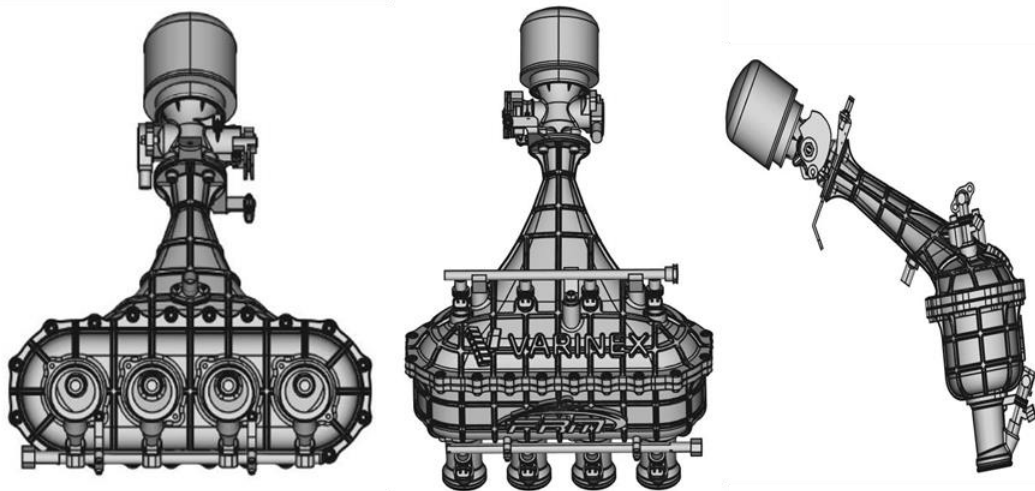


Figure 23 Honda engine Intake manifold 3D geometry along with restricted, primary injectors and secondary injectors.

4.3.3. Software

To implement the calculation, the AVL package software was used included Boost and 3D Fire solvers, based on finite volume method and those two solvers were coupled to indicate boundary conditions as in table 5 between virtual engine scheme and valid part of engine (Intake manifold). Every part of the manifold in the AVL simulation software can be described by the inlet diameter, the outlet diameter, the length, the wall thickness, the material and friction and heat transfer coefficients as in figure 24. Values of pressures and temperatures for the individual cylinders of the engine in relation to time were subsequently generated from the 1D model .

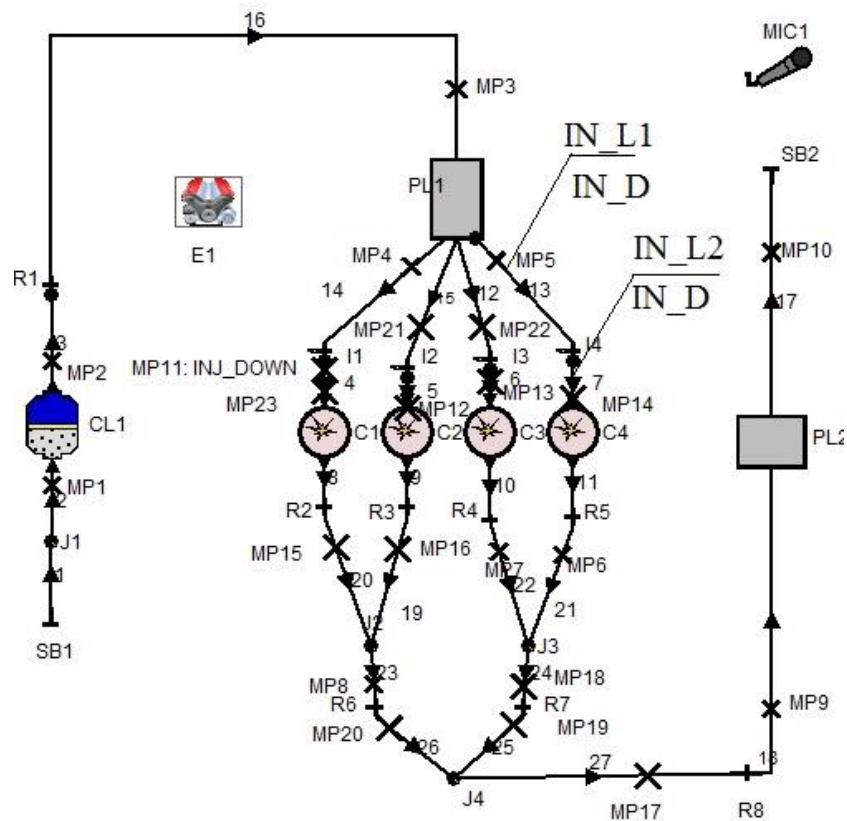


Figure 24 1D model of the Honda CBR 600RR (PC 37) engine.

The software also allows you to utilize a manifold model that is defined by an exact diameter for each length. The software generates its own set of elements, which may be quite accurate, slowing down the calculation. As a result, customizing your own parts will be a superior option.

Table 5 Material properties and analytic boundary conditions.

Density	1.2041 kg.m <sup>-3</sup>
Air temperature	293.15 K
Viscosity	1.817. 10 <sup>-5</sup> Pa.s
Flow compressibility	Incompressible
Atmospherical pressure	101,325 Pa
Inlet pressure (Relative)	0
Outlet pressure (Relative)	8,000 pa

The basic method is used to refine the background mesh in the region of the surfaces defined in the *STL* file, then remove cells that are external to the flow path, and finally snap the vertices of the cells to the *STL* surfaces. The quality of the applied mesh as indicated in table 6 also the control of the mesh resolution is available at various points in the meshing see figure 25.

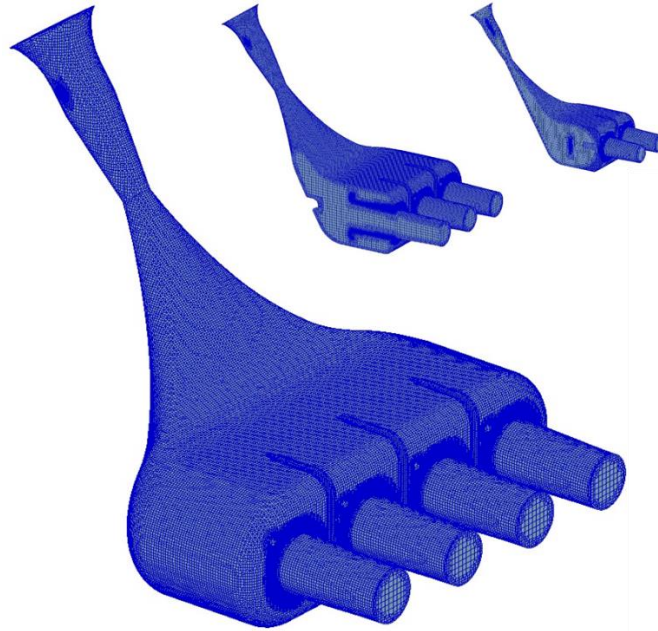


Figure 25 Intake manifold model with mesh.

From the *3D* scan of the engine, all geometric characteristics of the intake manifold and other parts of the engine were transformed into the *ID* model (such as variable diameters of the intake and exhaust pipes dependent on their length, angles in the pipe joints of the intake and exhaust manifold, materials with thermal properties, etc.).

Table 6 Model properties .

Type of model	3D
Type of mesh	Mapped
Total number of elements	3115552
Volume of model	0.004449 $m^3$
Surface area	0.346168 $m^2$

For the heat transfer calculation through the runners the ordinary equation for simple convective heat transfer in the radial direction from the gas to the manifold:

$$q = \frac{4h_{conv}}{\rho D} (T_w - T_g) \quad (40)$$

where  $q$  is the heat transfer in  $W$ ,  $h_{conv}$  is the convective heat transfer coefficient in  $W.K/m^2$ ,  $T_w$  is the temperature of the pipe inner wall in  $K$ ,  $T_g$  is the temperature of gas in  $K$ ,  $D$  is the manifold diameter in  $m$ ,  $\rho$ : is the gas density.

The calculation of the length of ram wave intake runner at mean temperature in the intake system  $T_s$  around 296 K that means around 23°C, the adiabatic index of air  $k = 1.4$  and Specific Gas constant  $R = 287 \text{ J/kg/K}$  (Mohamad et al. 2019).

Mean speed of sound calculation:

$$c = \sqrt{k R T_s} \quad (41)$$

$$c = \sqrt{1.4 \cdot 287 \cdot 296}$$

$$c = 344.86 \text{ m.s}^{-1}$$

Then, the length of the ram wave intake runner can be calculated from the equation below:

$$L_{rez} = \frac{c}{8n} \quad (42)$$

where  $n$  is the engine speed  $s^{-1}$ .

The intake manifold material set as in table 7 below. To utilize for the pipes, as well as the thickness of the walls. This gives us a more realistic model of the engine, and the final calculation can be more precise. Some basic pre-set materials are included in the *ID Engine Simulation* .

Table 7 Intake manifold material properties.

Material	Density [ $\text{kg/m}^3$ ]	Thermal conductivity [ $\text{W.m}^{-1}.\text{K}^{-1}$ ]	Specific heat capacity [ $\text{kJ.kg}^{-1}$ ]
Steel	7900	48	490
Aluminium	2700	204	940
Plastic ( <i>Polyamide 6,6</i> )	1400	0.25	1.256
Magnesium alloy ( <i>AS21</i> )	1760	86	1.005

I have chosen types of materials based on the real situation on the engine for both simulations covered in the next chapter so that the model is as accurate as feasible. Because these two ports are inside the cylinder head, which is made of steel alloy, and because the exhaust system is also built of steel alloy. The plastic was chosen for the intake runner and steel for the inlet and exhaust ports.

#### 4.3.4. Computational methods

*CFD* tools are useful in a wide variety of applications and here we note a few of them to give an idea of its use in industry. To start modelling the engine part we must disassemble the intake manifold from restricted, primary and secondary injectors. As you see in figure 26. *CFD* can be used to simulate the flow of air inside the Intake system include restricted, ducts and plenum. For instance, it can be used to study the interaction of flow gas with a manifold wall and optimization. The model was completely sealed to extract inner volume for it. The following figure shows the Internal volume for the *3D* solid geometry extracted by *Creo advanced design* software.

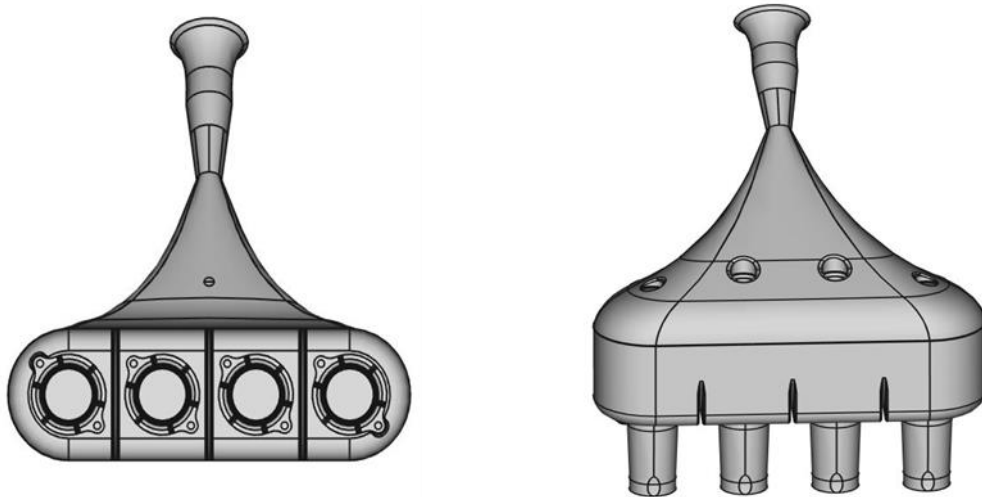


Figure 26 Internal volume of intake manifold.

*CFD* is structured around the numerical algorithms that can tackle fluid flow problems. In order to provide easy access to their solving power these include sophisticated user interfaces to input problem parameters and to examine the results. Hence all contain three main elements: Pre-processor, Solver and Post-processor.

The pre-processing consists of the input of a flow problem to a *CFD* problem by means of an operator-friendly interface and the subsequent transformation of this input into a form suitable for use by the solver (Mohamad et al. 2020). The user activities at the pre-processing stage involve:

- Meshing process:
  - Grid generation-the sub-division of the domain into a number of smaller sub-domains: a grid (or mesh) of cells (or control volumes or elements).
  - Selection of the physical and chemical phenomena that need to be modelled.
  - Definition of fluid properties .
- Finite volume method (*FVM*) model: The *FVM* model was solved using AVL *3D Fire* software adopting engine intake manifold geometry considering symmetry and three-dimensional fluid dynamics and heat transfer. The fundamental hypotheses adopted are (a) Turbulent flow, (b) Steady state condition, (c) The mass flow rate and flow temperature, are known, (d) Ambient temperature  $27^{\circ}\text{C}$ , (e) The intake manifold standard wall function was selected for this type of modelling (AVL GmbH, v2014).
- Boundary conditions: AVL *3D Fire*, like other commercial *CFD* codes, offers a variety of boundary condition options such as velocity inlet, pressure inlet, pressure outlet, etc. It is very important to specify the proper boundary conditions in order to have a well-defined problem. Table 8 shows physical properties of air ( $p = 101.13 \text{ kPa}$ ). It gives values

of some physical properties - density and viscosity in relation to the temperature of gases (Perry, 1984).

Table 8 physical properties of air (DieselNet, 2006).

T	$\rho$	h	s	$C_p$	$\mu$	$k_{cond}$
260	1.340	260.0	6.727	1.006	0.165	0.0231
280	1.245	280.2	6.802	1.006	0.175	0.0247
300	1.161	300.3	6.871	1.007	0.185	0.0263
350	0.995	350.7	7.026	1.009	0.208	0.0301
400	0.871	401.2	7.161	1.014	0.230	0.0336
450	0.774	452.1	7.282	1.021	0.251	0.0371
500	0.696	503.4	7.389	1.030	0.270	0.0404
600	0.580	607.5	7.579	1.051	0.306	0.0466
800	0.435	822.5	7.888	1.099	0.370	0.0577
1000	0.348	1046.8	8.138	1.141	0.424	0.0681
1200	0.290	1278	8.349	1.175	0.473	0.0783
1400	0.249	1515	8.531	1.207	0.527	0.0927

$T$  temperature,  $K$ ;  $\rho$  density,  $kg/m^3$ ;  $h$  specific enthalpy,  $kJ/kg$ ;  $s$  specific entropy,  $kJ/(kg \cdot K)$ ;  $C_p$  specific heat at constant pressure,  $kJ/(kg \cdot K)$ ;  $\mu$  viscosity,  $10^{-4} Pa \cdot s$ ;  $k_{cond}$  thermal conductivity,  $W/(m \cdot K)$ .

- Loss junctions: In addition to inlet ports, exhaust ports, and exhaust branch pipes, intake and exhaust manifolds have junctions. It's crucial to include the loss junctions in order to create a simulation model of the engine that is as realistic as feasible, see figure 27.

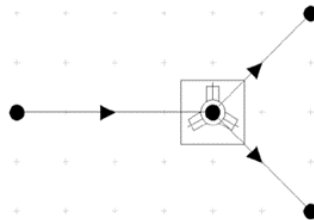


Figure 27 Loss junction at some locations in intake manifold model.

These loss junctions should resemble hydrodynamic losses caused by friction between the pipe wall and the gas or air fuel mixtures when they flow through a physical junction, such as the above-mentioned intake or exhaust ports. Flow velocity has a significant impact on hydrodynamic losses, as we all know. Greater flow velocity causes more losses, and higher engine speeds naturally increase flow velocity.

- Flow dynamics: Randomly moving particles move in the flow direction at the same time to generate the flow. The flow's essential condition is its hydraulic gradient.

In terms of thermodynamics, the intake air that passes through the engine may be characterized as an inert gas combination that can be considered ideal gas if the atmospheric boundary conditions are favorable. A set of randomly moving, non-interacting point particles with a zero volume make up an ideal gas. It has consistent physical characteristics as well.

Intake air can be parametrically described by the state quantities like the temperature, density, velocity and the pressure that are described at equation (43):

$$\begin{aligned}
 T &= f(x, y, z; t), \\
 \rho &= f(x, y, z; t), \\
 v &= f(x, y, z; t), \\
 P &= f(x, y, z; t),
 \end{aligned}
 \tag{43}$$

The flow can be categorized into two types: steady-state and unsteady (Mohamad, 2019). The term "steady-state flow" describes a situation in which the fluid characteristics at a given location in the system do not vary over time. The flow is described as unstable if it is not otherwise. Because it is difficult to compute an unsteady flow, it is usually solved as a steady-state flow.

A quasi-stationary solution is the name for this method. Each flow particle follows its own streamlined path. Streamlines are a group of curves that are always tangent to the flow's velocity vector. These show the direction in which the fluid element will travel at any point in time figure 28.

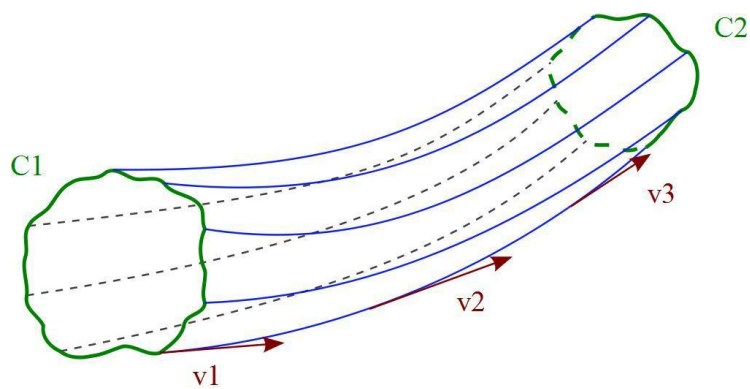


Figure 28 Flow streamlines (Adámek, 2011).

- Governing equations: The Conservation of Mass Equation: It is based on the principle of conservation of mass. Net mass flow out of control volume equal to time rate of decrease of mass inside control volume:

$$\frac{\partial \rho}{\partial t} + \nabla \cdot (\rho \vec{V}) = 0
 \tag{44}$$

The conservation of momentum equation: It is based on the law of conservation of momentum, which states that the net force acting in a fluid mass is equal to change in momentum of flow per unit time in that direction:

$$\rho \frac{\partial \vec{V}}{\partial t} + \rho(\vec{V} \cdot \nabla)\vec{V} = -\nabla P + \rho \vec{g} + \nabla \cdot T_{ij} \quad (45)$$

These equations along with the conservation of energy equation form a set of coupled, nonlinear partial differential equations.

The energy equation: It is based on the principle that total energy is conserved. Total energy entering control volume equal to total energy leaving control volume. The energy equation for a fluid region can be written in terms of sensible enthalpy :

$$\frac{\partial}{\partial t}(\rho h) + \nabla \cdot (\vec{V} \rho h) = \nabla \cdot (k_{cond} \nabla T) + S_h \quad (46)$$

$$h = \int_{T_{Ref}}^T C_p dT \quad (47)$$

where,  $\partial$  is partial derivative,  $\rho$  is density,  $\vec{V}$  is mean velocity,  $t$  is time in second,  $h$  is enthalpy,  $g$  is gravitational acceleration in  $m/s^2$ ,  $T$  is temperature,  $k_{cond}$  is thermal conductivity in  $W/m.K$ ,  $S_h$  is volumetric heat sources,  $C_p$  is specific heat (Mohamad, 2019).

Euler's equation for hydrodynamics: The second Newton's law in hydrodynamics is described by the equation for hydrodynamics. When the external forces have dissipated, the equation (48) expresses this theory for a compressible flow..

$$\frac{\partial \vec{c}}{\partial t} (C \vec{V}) \vec{c} + \frac{1}{\rho} \vec{V} \rho = 0 \quad (48)$$

The first equation term represents a local acceleration. The second equation term represents a convective acceleration, which is formed when the fluid flows through the manifold with a variable section .

- Turbulent model: Turbulent flows are characterized by large value of Reynolds number,  $k$ - $\zeta$ - $f$  model is used to treat the turbulence regime in the present study in the simulation, and nearly random fluctuations in velocity and pressure in both space and time. Instabilities increase until nonlinear interactions lead them to break down into finer and finer whirls, which are finally dissipated (as heat) via viscosity. Turbulent flows occur at the other end of the Reynolds number spectrum from high Reynolds numbers.

## 4.4. Calculation Results

### 4.4.1. Design of Simulations

It is necessary to perform sensitivity analysis to improve predictions based on simulation models. The first step in the pre-processing phase is to obtain a digital image of every inner



part of the intake system and to proceed to creating a representative mesh of these surfaces. The volume mesh where the air circulates is built from this surface mesh. These meshes were produced with the software AVL Fire. Special attention was given to the intake manifold, the plenum, and the regions where air enters and leaves the system such as runners, treated by the solver as regions of inlet and outlet. All other regions, comprising boundaries of the control volume, are defined as wall. Table 9 a brief of input and output data were demonstrated, indicating how the system was improved.

Table 9 The data of input and output for intake system at certain operating conditions.

Simulations	Inputs					Outputs			
	Speed in rpm	Runner diameter in mm	Runner inlet length in mm	Runner outlet length in mm	Plenum vol. in liter	Power in hp	Torque in Nm	BSFC in g/kWh	SPL in dB
run 1	2000	33.5	100	100	4	11.81	42.06	396.4	90
run 2	4000	33.5	100	100	4	28	47.5	370	97
run 3	6000	33.5	100	100	4	41.81	49.63	366.6	99.8
run 4	8000	33.5	100	100	4	64.53	57.44	350.2	101.7
run 5	10000	33.5	100	100	4	86.36	61.5	350.5	103.4
run 6	2000	42	100	100	2	11.54	41.09	383.4	91
run 7	4000	42	100	100	2	28	46.5	368.2	95.8

Simulations	Inputs					Outputs			
	Speed in rpm	Runner diameter in mm	Runner inlet length in mm	Runner outlet length in mm	Plenum vol. in liter	Power in hp	Torque in Nm	BSFC in g/kWh	SPL in dB
run 8	6000	42	100	100	2	44.72	53.07	340.4	99.6
run 9	8000	42	100	100	2	58.97	52.49	356.4	101.2
run 10	10000	42	100	100	2	84.66	60.29	335.7	103
run 11	2000	32	250	100	3	11.78	41.95	397.7	91.8
run 12	4000	32	250	100	3	28	48.11	374.8	96.2
run 13	6000	32	250	100	3	47.79	56.72	365.1	100.3
run 14	8000	32	250	100	3	71.72	63.84	349.7	102.4
run 15	10000	32	250	100	3	70.58	50.26	361.4	102.2

#### 4.4.2. Velocity distribution

The velocity of quantity of air in intake system (channel) can be calculated of the flow from the conservation of energy equation. The potential energy component will be removed or neglected, due to a *zero* difference in the altitude. The other quantities will be specified. The inlet velocity is  $u_1$  equal to *zero*, the outlet velocity is  $v_2$ , the inlet pressure  $p_1$ , and the outlet pressure is  $p_2$ .

The pressure difference from the Energy equation gave us the dynamic pressure between the inlet and the outlet and on its basis. The flow velocity can be expressed as below:

$$v = v_2 = \sqrt{\frac{2(p_1 - p_2)}{\rho}} = \sqrt{\frac{2p_d}{\rho}} \quad (49)$$

After the substitution  $v = 91.13 \text{ m/s}$ .

To calculate the mean velocity which is one of the Reynolds number equation terms. The expression for the mean velocity from the mathematical equation of the turbulent velocity profile below:

$$u_s = u_{Max} \left[ \frac{y}{r} \right]^n \quad (50)$$

where  $y$  is representing the distance from the pipe wall in  $m$ ,  $n$  is representing the function of Reynolds number ( $Re$ ),  $r$  is the pipe radius in  $m$ .

Mean speed of turbulent flow is approximately 85% of maximum flow velocity:

$$u_s = (0.82-0.87) u_{Max} \quad (51)$$

After the substitution  $u_s = 77.46 \text{ m/s}$ ; Substituting in Reynolds number equation 52:

$$Re = (u_s L) / \nu \quad (52)$$

$Re = 4.26 \times 10^6$  so the flow is turbulent.

The mass flow  $Q_m$  and volumetric flow  $\omega$  through the intake channel can be calculated:

$$\omega = \pi r^2 u_s \quad (53)$$

$$\omega = 0.095 \text{ m}^3/\text{s}$$

The mass flowrate  $Q_m$  can be expressed:

$$Q_m = \omega \cdot \rho \quad (54)$$

$$Q_m = 0.12 \text{ kg/s.}$$

The mass flow pass into the cylinder, therefore the analysis of in-cylinder flow structures over a range of realistic engine speeds were done using *1D* simulation with AVL software as well for predicting engine performance as shown in figure 29. The greatest cyclic mass flow occurs in the *8000 rpm* case due to the amount of air required for combustion process, therefore to boost the volumetric efficiency. At *5000 rpm*, the mass flow rate is reduced with the piston movement, and engine speed, while at *2000 rpm* mass flow of air decreases due to less need for air for combustion process. The simulated peak in-cylinder mass flow rate varies with varies engine speed, but the rate remains stable within cylinders at designed crank angle degrees, which correlate well with the measured peak in-cylinder mass flow rate from the engine.

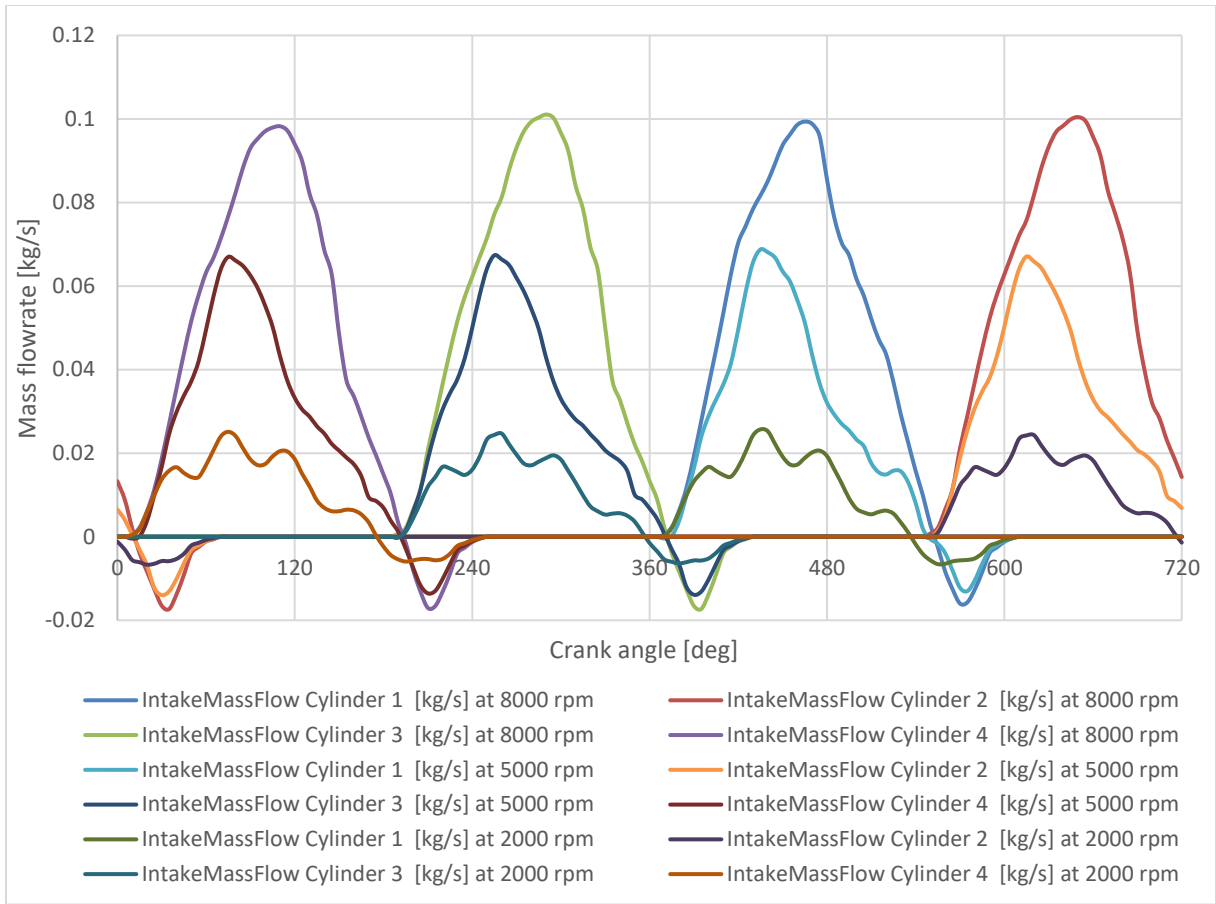


Figure 29 Mass flowrate at intake manifold restrictor for complete cycle and various engine speed (2000, 5000, 8000) rpm.

3D CFD analysis was performed at various stages in the design. Simulation was used to evaluate two important flow properties which were velocity and pressure. The velocity logically high in plenum zone and runner part which may lead to fluctuation in amount of air into the combustion chamber at high engine speed (figure 30, 31).

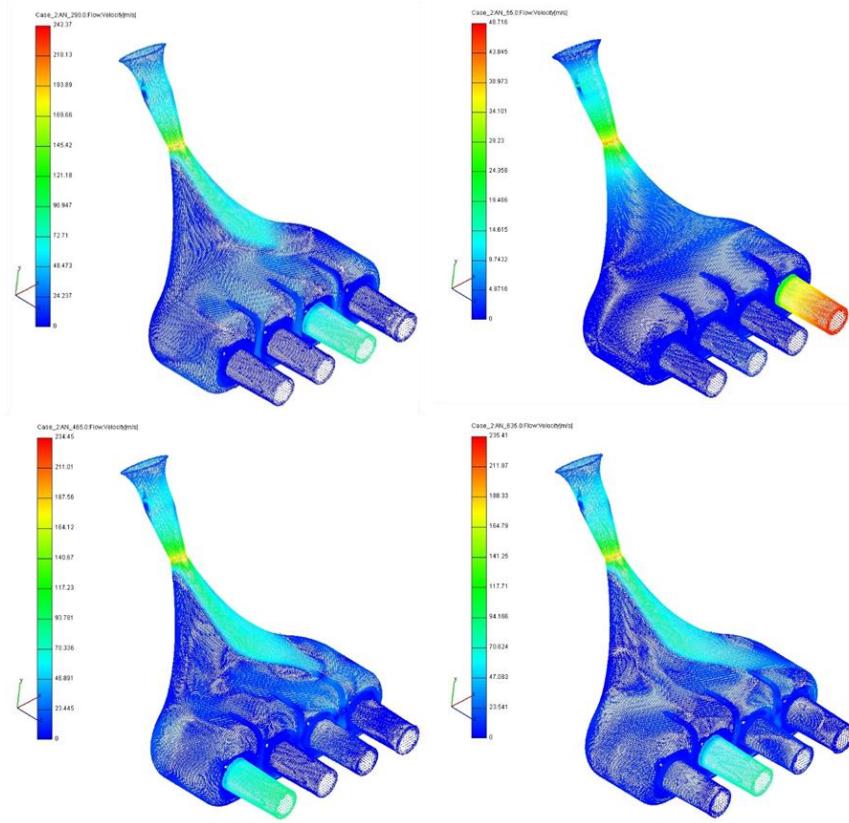


Figure 30 Velocity contour  $Min = 0$ ,  $Max = 262.4$  m/s at 8000 rpm.

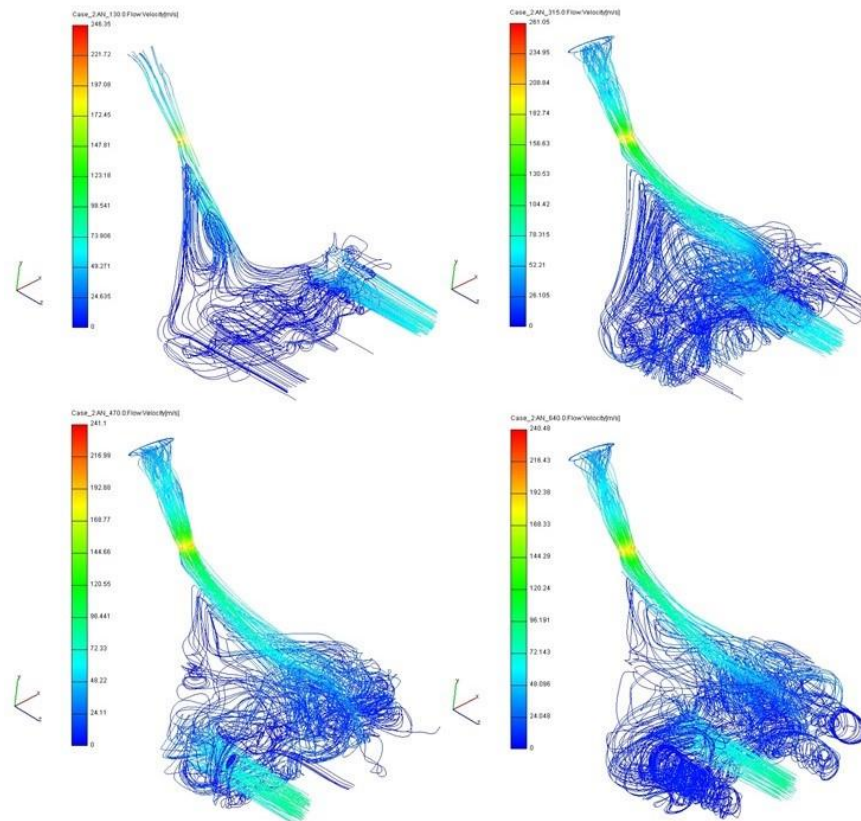


Figure 31 Velocity streamline  $Min = 0$ ,  $Max = 262.4$  m/s at 8000 rpm.

#### 4.4.3. Pressure loss

This type of analysis is very problematic because there is high speed, compressible flow of air in the intake system, pressure drops and changes of temperatures. The final distribution of the pressures of the air in the airbox are given in figures 32 the generated pressure reach  $100500 \text{ Pa}$  at  $5000 \text{ rpm}$  with less oscillate at  $8000 \text{ rpm}$  and almost steady at  $2000 \text{ rpm}$ . Figure 33 demonstrates the pressure and it was elevated in restriction area by  $1.00036e+05 \text{ Pa}$  at  $8000 \text{ rpm}$ . The pressure pulsation can be seen at  $2000 \text{ rpm}$ , and have higher amplitude for  $5000 \text{ rpm}$  than  $8000 \text{ rpm}$ ; this was mainly due to the induced frequency change of the pressure waves (reflected pressure wave) in the intake manifolds, and this is agreed with (De Risi et al. 2000) and (How Heoy Geok et al. 2009).

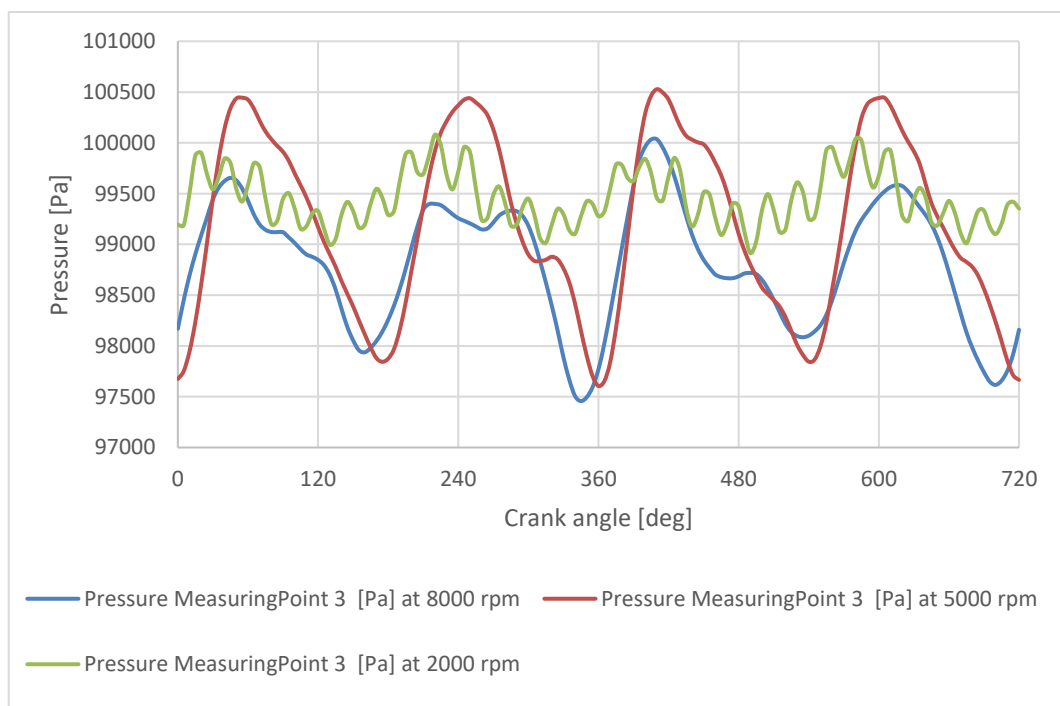


Figure 32 Pressure at intake manifold restrictor for complete cycle and various type of engine speed (2000, 5000, 8000).

The values are evaluated at the outlets of the pipes of the plenum for one operational cycle of the engine (rotation of the crankshaft  $720^\circ$ ) at  $8000 \text{ rpm}$ . The initial conditions were the pressure and temperature inside the calculated volume at the initial moment of calculation (the data were taken from the calculation results in *ID Boost*). The temperature were monitored for three type of engine speed rpm, and more details will illustrated in next sections.

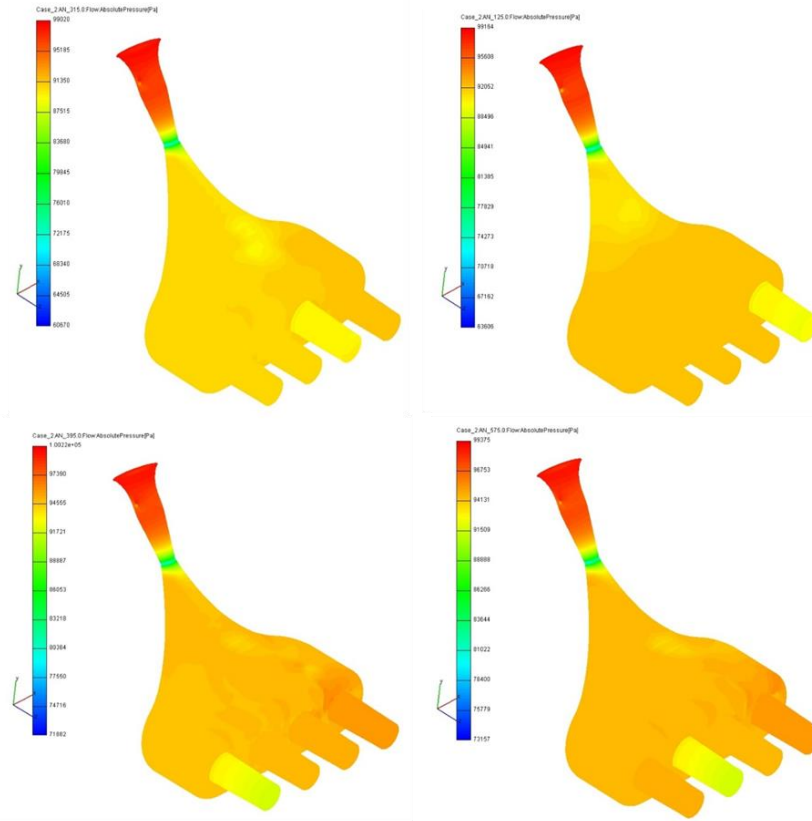


Figure 33 Pressure contour  $Min = 72217$ ,  $Max = 1.00036e+05$  Pa at 8000 rpm.

#### 4.4.4. Sound pressure level for the intake system

The analytical solution of sound pressure level (*SPL*) of a simple plenum was performed and optimized based on intake system geometry modification. Details are given in figure 34. From the result, it shows that there is no significant effects of changing design parameter on the sound pressure emitted from intake system were found.

The iteration was then carried out to reach optimum improvement with flow being implemented in the three conditions; In comparison with the base case, in the suggestions *Mod 1* and *Mod 2* the next design parameters are modified:

- *Mod 1* –The diameter of the inlet channel *IN\_D* was increased from 33.5 to 42 mm (see engine scheme in figure 24), as well as the volume of the intake manifold *PLI* was decreased from 4 to 2 litres.
- *Mod 2* –The length of inlet port *IN\_LI* was increased from 100 to 250 mm, *IN\_D* diameter was reduced from 33.5 to 32 mm, *PLI* volume was reduced from 4 to 3 litres.

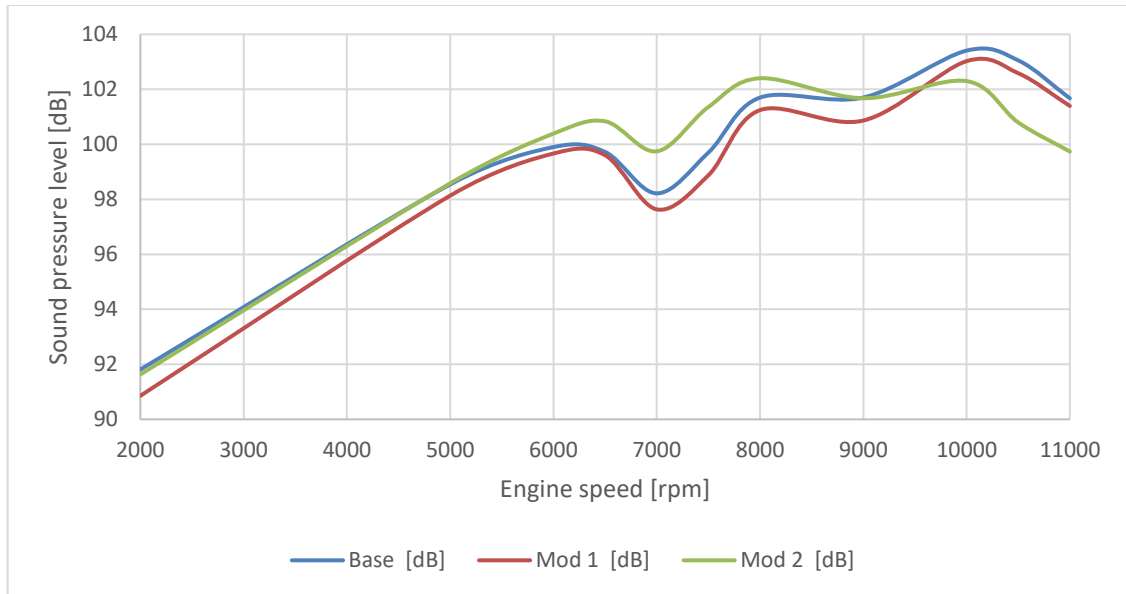


Figure 34 The comparison of sound pressure level for the base case, and the suggested improvement data (modifications 1 and 2) by software.

#### 4.4.5. Temperature at restrictor

Managing the temperature of the cylinder contents at the time of fuel injection in petrol engines is critical to ensure proper engine operation, and to achieve proper charge temperature, the air temperature at the restrictor has been monitored. The inlet air temperature is higher difference on the variable engine speed since the diameter of restrictor is fixed due to Formula standards.

As the fixed load applied, the increasing engine speed has higher number of power strokes per period of time which has more combustion process than lower engine speed and flow velocity increases the restrictor inlet temperature as explained in the ideal-gas equation of state,  $pV = mRT$ . The results are shown in figure 35.

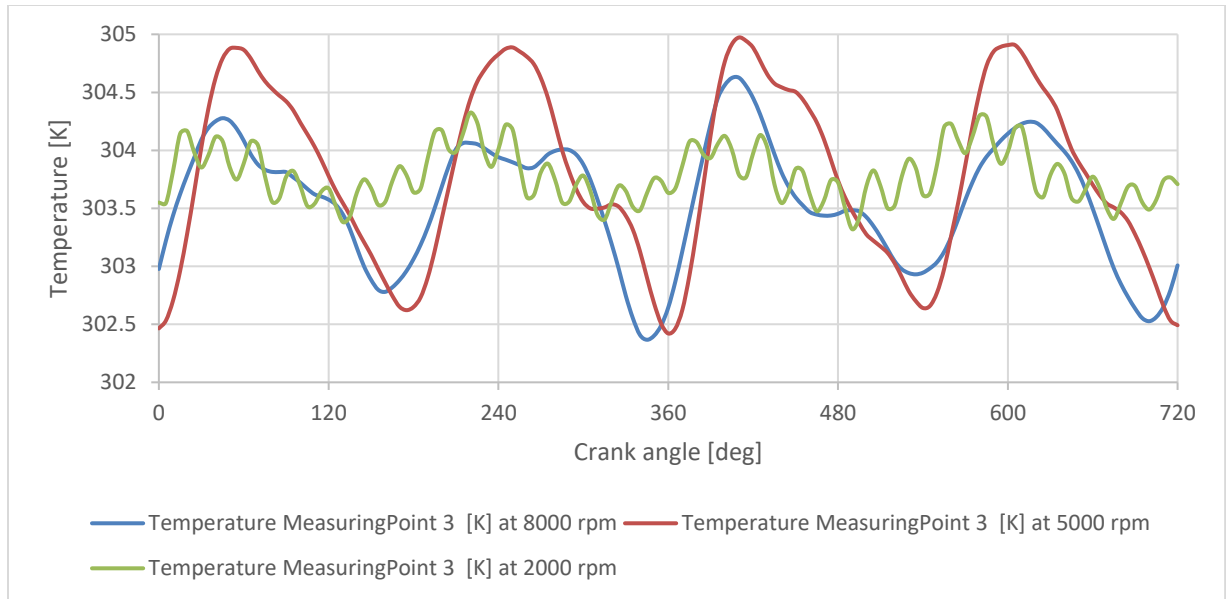


Figure 35 Temperature at intake manifold restrictor for complete cycle at various engine speeds (2000, 5000, 8000 1/min).

#### 4.5. Experimental results of the engine power output

To be able to compare the simulation model results with the dynamometer testing results and manufacturing company data. Every parameter of the simulation model was set as closest to reality as feasible.

At the purchase of the engine the salesman gave us approximate values of the torque and engine performance (engine dynos), see the appendix *A1 Dyno test 1*. Nevertheless, we performed the performance test at the University of Miskolc chassis dynamometer (chassis dynos) see the appendix *A2 Dyno test 2*. The results are shown in figure 36 along test results of two variants resulted of my research work.

The peak of power at engine speed *10500 rpm* was *78.3 hp*. This monitored the following engine calibration will be based on the data. The test shows a severe drop in power output from *6000-7500*, *7500 – 10500* and *10500 - 11500 rpm* (figure 36 orange curve).



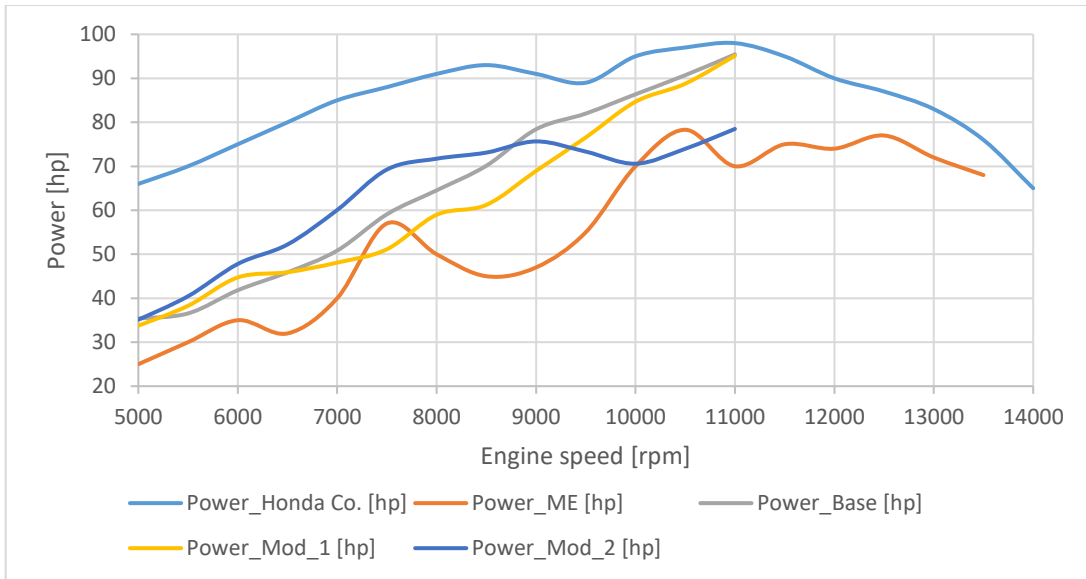


Figure 36 Honda CBR 600RR (PC 37) engine performance and torque recorded in manufacturing company.

The maximum torque was around  $48 \text{ Nm}$  and  $95 \text{ hp}$ . The results were compared with the dynamometer (Base data) which is shown in the appendix *A2 Dyno test 2* and improvement suggested by simulation results (*Mod\_1 and Mod\_2*). There is a performance and torque characteristic of a simulation model of the Honda CBR 600RR (PC 37) engine. As it is shown in figure 37, the peak of torque is showing up at engine speed around  $11000 \text{ rpm}$  and its value is  $48 \text{ Nm}$  on the basis of factory data. In addition, an apparent torque loss between  $12,000\text{-}14,000 \text{ rpm}$  as shown in the appendix *A1 Dyno test 1*. This is due to a resonance intake system that has been modified for a wider range of engine speeds.

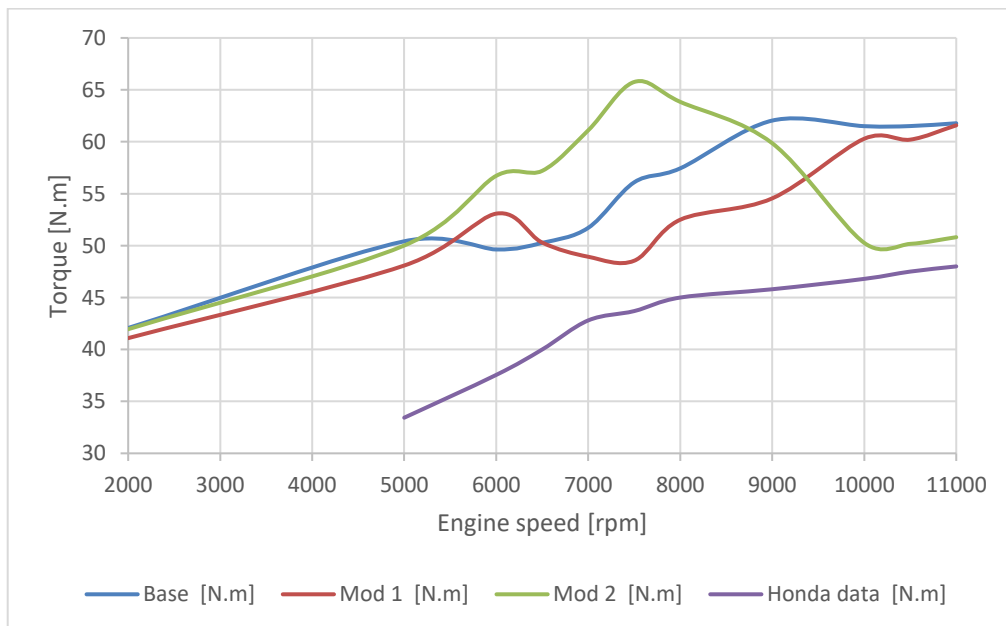


Figure 37 Honda CBR 600RR (PC 37) engine performance (Power output) recorded in University of Miskolc/Formula workshop.

## 5. ANALYSIS OF RACE CAR ENGINE EXHAUST SYSTEM

### 5.1. Structural design of formula race car exhaust system

The factory exhaust system (manifold, muffler and ducts) as shown in figure 38 is made of high quality of titanium alloy, therefore the exhaust system is light-weight, and it meets all noise requirements .

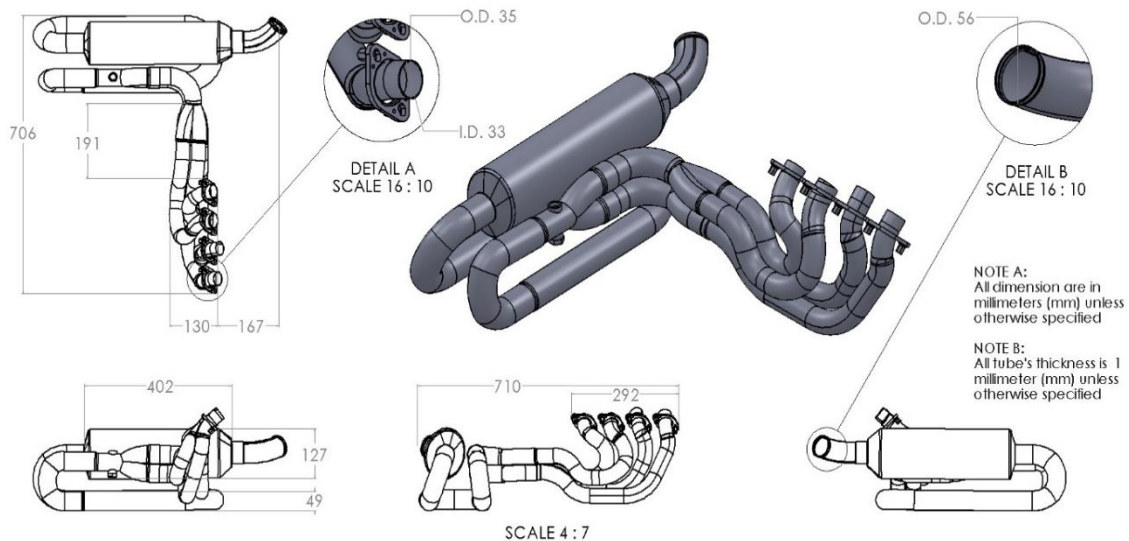


Figure 38 Honda CBR 600RR (PC 37) current engine exhaust system dimensions without perforated pipe inside (*PPiP*) the muffler.

The term *ID* model (figure 25) implies a one-dimensional approach to the description of processes in the exhaust systems of the piston engine. The one-dimensional statement of the problem allows estimating the influence of pipelines and channels dimensions (diameters, lengths, fillet radii) on the gas flow.

At the same time, despite the name "one-dimensional model", the processes inside the cylinder are considered in the zero-dimensional formulation. With this approach, the entire cylinder (section) is considered as a single volume in which the processes of intake, compression, combustion, expansion and outlet occur. This volume, unlike the three-dimensional approach, is not divided into subdomains (control or finite volumes). The system of equations (energy, continuity, gas state) is written only for one volume that changes with time (in the three-dimensional approach – the system of equations is solved for each control volume) (Mohamad et al. 2020).

### 5.2. Model description

A part of pre-processing was done using advanced design software Creo V2014, because the models are a difficult task as far as the shape is concerned and therefore, as seen in figure 39 exhaust system has to be designed in surfaces. To construct the surface model, the functions should be the multi-section surface, which draws the surface from part to part along the designed spine or guides. The dimensions were illustrated in table 10. The functions trim, revolute and extrude tools were used for the model build. The fluid volume or internal volume should be extracted due to the *CFD* simulations.

Table 10 Engine exhaust system dimensions.

Exhaust Dimensions	mm				
		1. Pipe Inside Diameter ( $D_1$ ):	36	1. Pipe ( $D_1$ ) Length:	420
		2. Pipe Inside Diameter ( $D_2$ ):	43	2. Pipe ( $D_2$ ) Length:	240
		3. Pipe Inside Diameter ( $D_3$ ):	46	3. Pipe ( $D_3$ ) Length:	425
		4. Pipe Inside Diameter ( $D_4$ ):	48	4. Pipe ( $D_4$ ) Length:	1075
		5. Pipe Inside Diameter ( $D_5$ ):	52	5. Pipe ( $D_5$ ) Length:	140

The majority of the locations in the frame consisted of sections where mating and had a small gap which means that in order to bridge that gap and make them air tight, the bridging process has to be done on each part and filled then capping the ducts. The inner volume was extracted from the solid model.

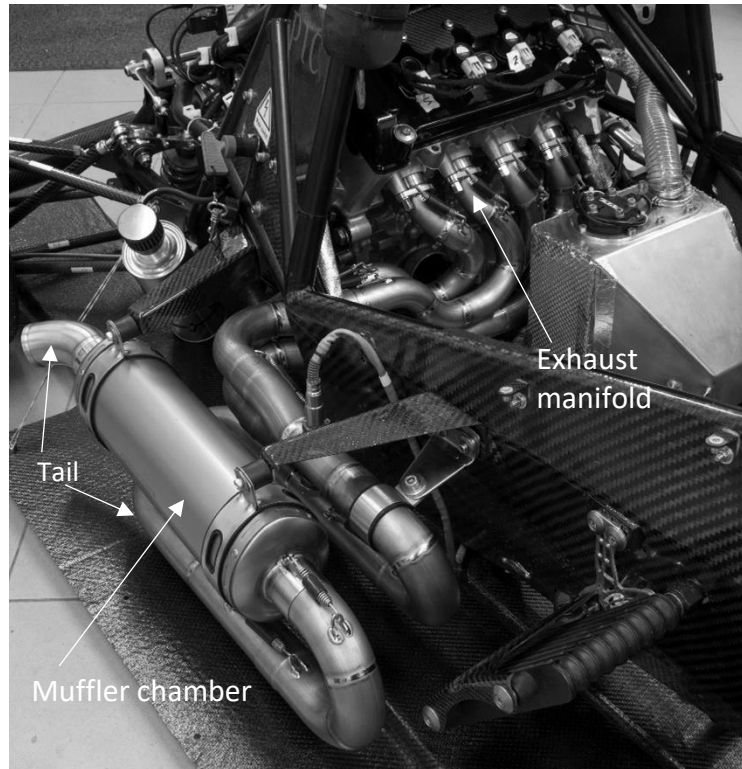


Figure 39 Honda CBR 600RR (PC 37) current engine exhaust system.

### 5.2.1. Exhaust manifold

Exhaust manifolds are a part of *IC* engines, they are used to collect and carry the exhaust gases away from the cylinder head and send them to the exhaust tail, with a minimum back pressure. More so, the intake and compression strokes are one of the most significant processes which influences the behaviour of air flow structure inside cylinder (Mohamad et al. 2020). The BOOST software package includes an interactive pre-processor that aids in the preparation of input data for the main computation (AVL BOOST, 2014). The engine was designed and successfully tested, as in figure 40.



Figure 40 Honda CBR 600RR (PC 37) current engine exhaust manifold.

For compressible flows, it is based on the solution of multiple local Favré–Reynolds stress closures, each one centered on a face constituting the boundary patch which interfaces the  $1D$  domain with the  $3D$  one. This approach allows to locate the  $1D$ - $3D$  interface even in regions close to highly  $3D$  shapes, therefore allowing the treatment of non-uniform fields on the  $3D$  side without compromising the stability of the solution (Mohamad et al. 2020).

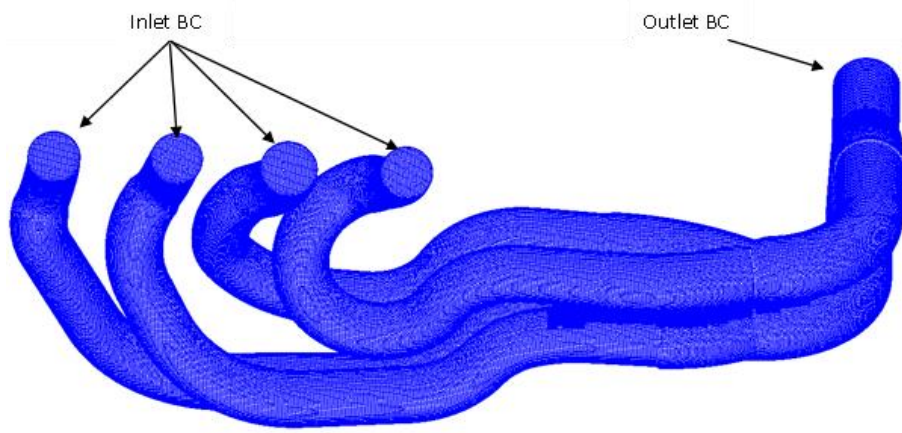


Figure 41. Control volume mesh as well as the options of the boundary conditions ( $BC$ ).

In addition, the wall temperature of an external pipe was set  $T_w = 573 K$ , heat transfer coefficient ( $h_{conv}$ ) =  $50 W/m^2/K$  and ambient temperature  $300 K$ . The mesh properties detailed in table 11.

Table 11. Mesh parameter.

Mesh information	Value
Number of nodes	2066942
Number of surface faces	394779
Number of edge elements	0
Number of tria elements	0
Number of quad elements	0
Number of tet elements	462

Number of hex elements	1737050
Number of pyramid elements	89711
Number of octa elements	0
Number of prism elements	174660
Number of other elements	0
Total number of elements	2001883
Surface area	0.31953816606
Volume	0.00297471268

The flow characteristics of the exhaust manifolds of the Honda CBR 600RR (PC 37) engine were calculated using 3D computational fluid dynamics (AVL Fire). The emitted noise has a significant impact. The pulsing flow in the duct system creates flow noise through vortex shedding and turbulence at geometrical discontinuities, which I emphasized on in this research section. Figure 42 shows an example of pressure contour at the exhaust ducts (manifold) for each stroke, maximum pessusure was  $1.8166e+05$  at 8000 rpm.

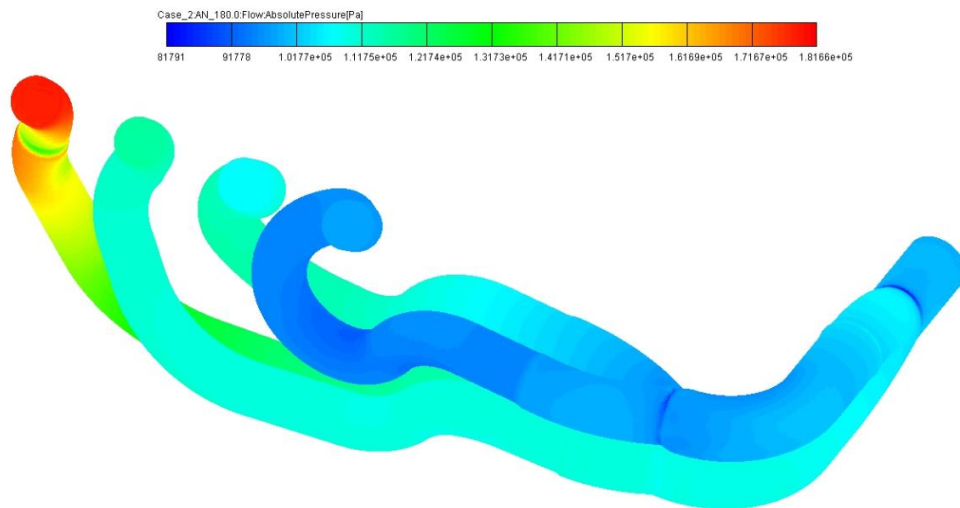


Figure 42 Exhaust manifold pressure contour at 8000 rpm.

The dimensions and acoustic absorption qualities of the component in the exhaust line impact the propagation properties of these pulses (muffler). Noise created by high flow velocity is, in general, a disadvantage, as shown in figure 43 flow distribution may be improved with the right modification. The current findings reveal three basic distinctive factors ( $E$ ,  $M$  and  $\zeta$ ) to control flow distribution and pressure drop in manifolds. However, adjustments of these parameters are not straightforward due to complexity of flow in manifolds. There is a significant difference of the friction factor and the pressure recovery factors on flow distribution. At the former half manifold, the influence of the friction factor can be neglected.



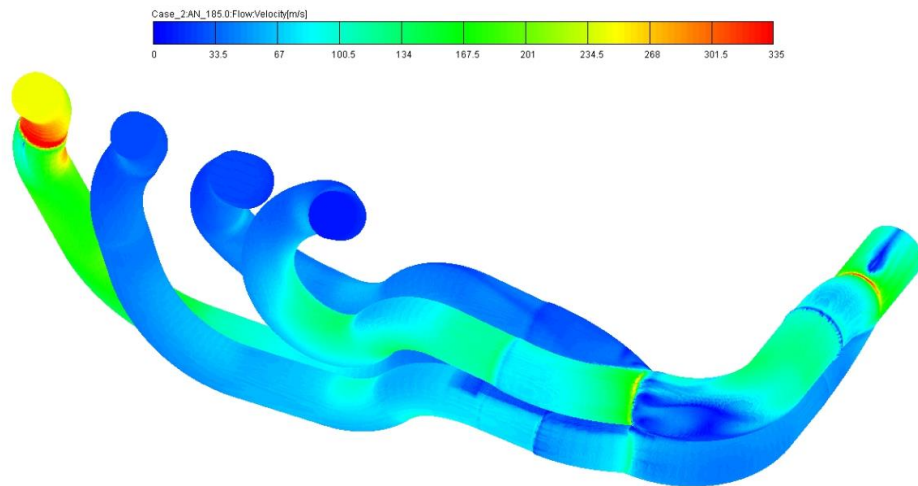


Figure 43 Exhaust manifold velocity contour at 8000 rpm.

To generate the homogeneity structure of gas flow entering into the muffler, both bulk gas motion and turbulence characteristics of the flow are necessary. The other system variables which influence on the flow distribution are the friction slope  $S_f$  and the orifice discharge coefficient  $C_D$ . In general, the objective of uniform discharge is satisfied by ensuring that the ratio of total head variation in the manifold system to the head loss across individual outlets is kept low (figure 44). This is influenced by the ratio of manifold cross-sectional area to the sum of the outlet cross-sectional areas and the spacing of the outlets. Swirl generation was identified by tracking the direction of flow vectors.

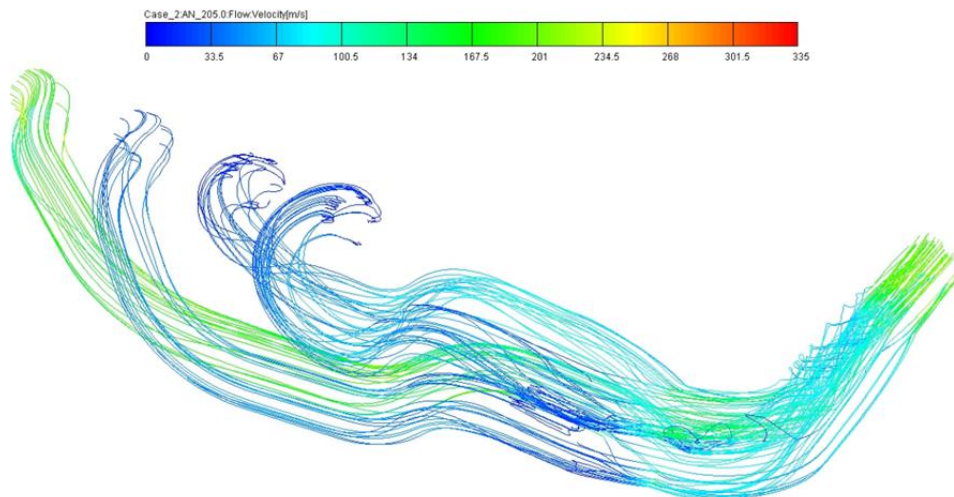


Figure 44 Exhaust manifold velocity streamline at 8000 rpm.

### 5.2.2. Exhaust muffler

The principal goal of the exhaust muffler is to minimize the automobile's engine radiated noise. They either dissipate or absorb the exhaust noise energy of systems. The constant pressure made by international organizations to decrease noise levels.

Recently updating the Environmental Noise Directive (2002/49/EC), encouraged the development of new muffler schemes and other techniques for noise attenuation. In the design of muffler, the problem is appropriately treated as consisting of three parts:

- Sound source (e.g., fan and internal combustion engine);
- Duct system (e.g., ventilation channel, exhaust gas system and air pressure ducts);
- Termination (e.g., exhaust gas outlet nozzle).

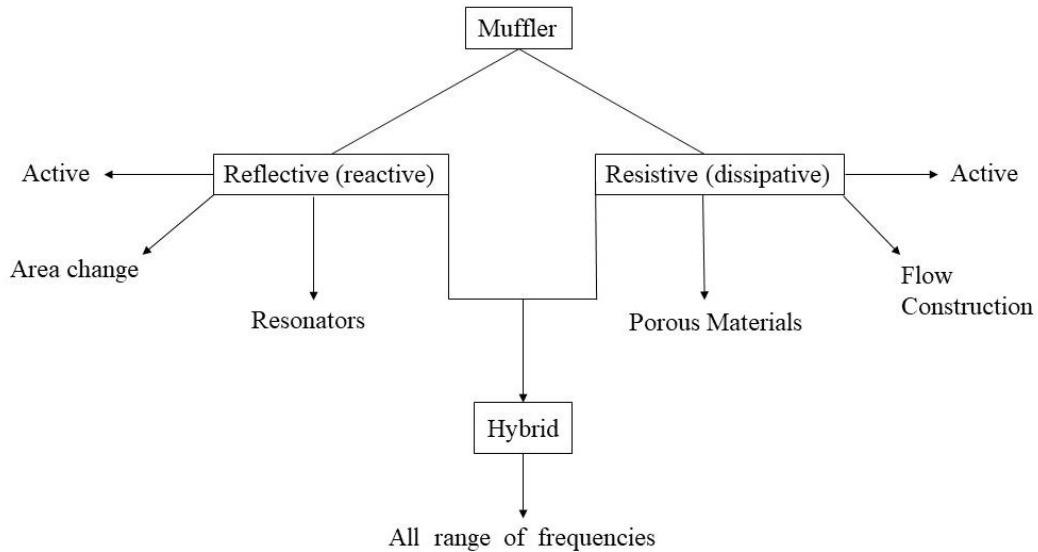


Figure 45 Type of exhaust muffler.

The mufflers can be said to be based on three different principles: reflective (reactive) of sound waves, resistive (dissipation) of acoustic energy and the combination of reflective and resistive called hybrid. Mufflers based on the first principle are said to be reactive and are used to mitigate sound consisting of discrete tones, especially in the low frequency region. Mufflers based on the latter principle are called dissipative, and are most suited to deal with high frequency, broad-band noise. Hybrid mufflers are more used in modern cars, and it is based on combination suited all range of frequencies.





Figure 46 Honda CBR 600RR (PC 37) current engine exhaust muffler.

The original (base) muffler of Honda CBR 600RR (PC 37) is hybrid type muffler which consists of perforated pipe inside the muffler chamber (*PPiP*) and absorptive material (*AM*). When the gas flows between the chambers, through the perforated pipe, part of the acoustic energy is transformed into turbulent vortices that form at the perforations part.

The geometry was created using SolidWorks 2017 advanced design software, including inlet, outlet, perforated pipe inside pipe (*PPiP*), and chamber, based on the existing Formula Student (*FS*) hybrid muffler prototype. The perforated pipe was situated in the centre of the muffler's cylindrical chamber. The dimensions and cross section of a muffler were explained. in Figure 47.

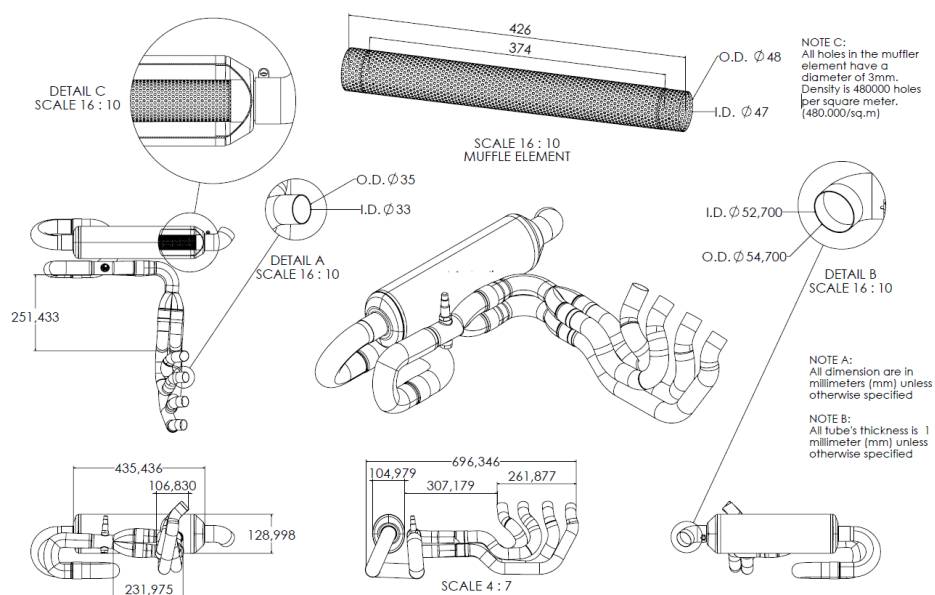


Figure 47 The porosity parameter of the perforated pipe of Honda CBR 600RR (PC 37) exhaust system.

The initial typical concept is quite clear to allow *3D CFD* simulation to collaborate with *1D CFD* or systems simulation (figure 48). Although the phrase zero-one-dimensional is more accurate, the term 1D approach is more commonly used, and it was used to describe the model developed in AVL Boost.

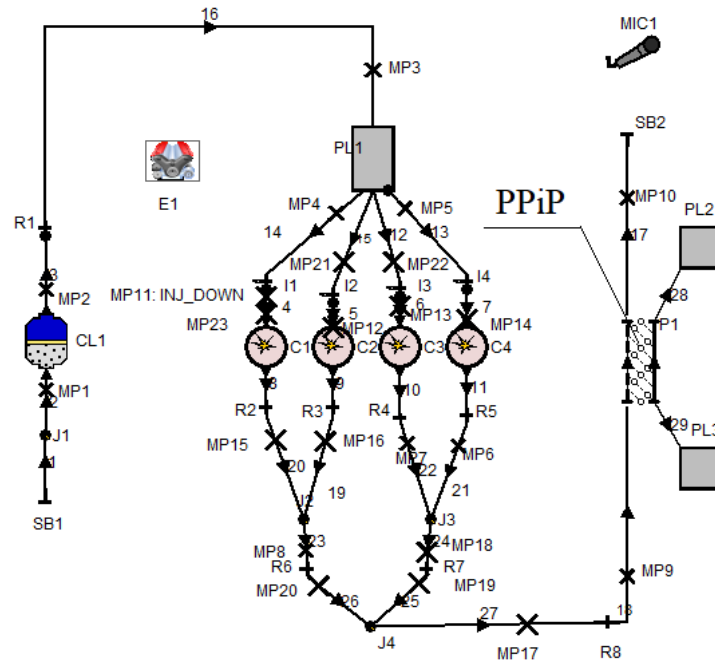


Figure 48 Scheme of Honda CBR 600RR (PC 37) engine with perforated pipe in pipe (*PPiP*) as part of muffler.

We had to consider two kinds of analysis: the *1D* user who is looking for a local detail coupled the *3D* user who would like the more real as possible boundary conditions. Inlet boundary conditions (*BC*) were mass flow and temperature values from virtual measuring points *MP 19, 9, 21, 10* (Figure 48), outlet *BC* – pressure in *MP 10*. In addition, the wall temperature of an external chamber of the muffler was set:  $T_w = 573\text{ K}$ , and heat transfer coefficient  $h_{conv} = 50\text{ W/m}^2/\text{K}$ .

The initial conditions were the temperature and pressure inside the calculated volume at the initial moment of calculation (the data were taken from the calculation results in Boost). The pressure drop was defined as the difference between the pressure in the exhaust manifold at the cylinder outlet and the cross section at the outlet of the muffler (computational volume).

Figure 49 shows different techniques for modeling using computational fluid dynamics tools and creating the best design for the case studies with AVL BOOST optimization. The flow acoustic analysis' boundary conditions are typical of the exhaust system at various engine speeds. The program's results were verified and issued at the end of the process.

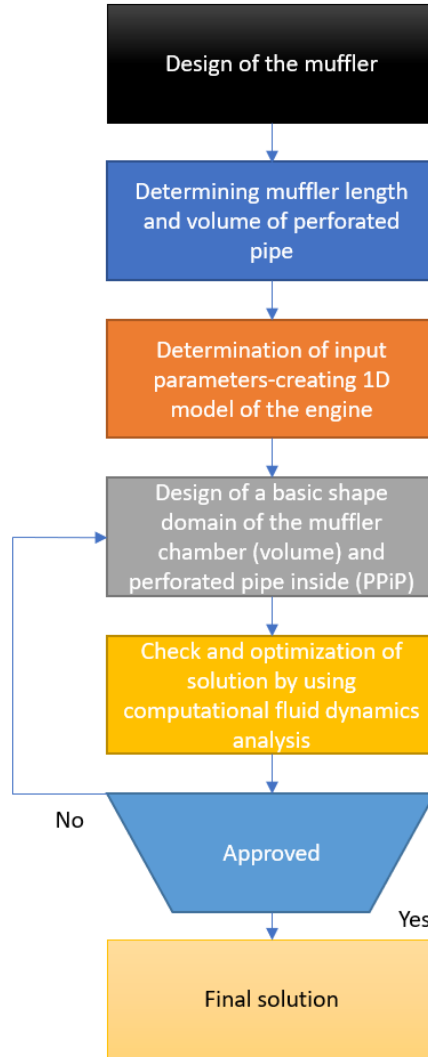


Figure 49 Flowchart of the design and an optimization process.

The mathematical model is based on the fundamental equations of three-dimensional unsteady transport equations: the equations of momentum (Navier-Stokes), energy (Fourier-Kirchhoff) and the conservation of mass (continuity), which take the form of Reynolds after the averaging procedure by the Favre method :

$$\begin{aligned}
 \bar{\rho} \frac{D\bar{W}_i}{d\tau} &= \bar{G}_i - \frac{\partial \bar{p}}{\partial x_i} + \frac{\partial}{\partial x_j} \left[ \mu \left( \frac{\partial \bar{W}_i}{\partial x_j} + \frac{\partial \bar{W}_j}{\partial x_i} - \frac{2}{3} \delta_{ij} \frac{\partial \bar{W}_k}{\partial x_k} \right) - \bar{\rho} \overline{W'_i W'_j} \right], \\
 \bar{\rho} \frac{D\bar{H}}{d\tau} &= \bar{G}_j \bar{W}_j + \frac{\partial \bar{p}}{\partial \tau} + \frac{\partial}{\partial x_i} (\bar{\tau}_{ij} \bar{W}_j) + \frac{\partial}{\partial x_j} \left( \lambda \frac{\partial \bar{T}}{\partial x_j} - c_p \bar{\rho} \overline{T' W'_j} \right), \\
 \frac{\partial \bar{\rho}}{\partial \tau} + \frac{\partial}{\partial x_j} (\bar{\rho} \bar{W}_j) &= 0,
 \end{aligned} \tag{55}$$

where  $W_i$ ,  $W_j$ ,  $W_k$  are the projections of velocity vector,  $m/s$ ;  $p$  is the pressure,  $N/m^2$ ;  $G_i$  is the projection of the density vector of the volume forces ( $N/m^3$ ) onto the  $O_{xi}$  axis of a rectangular Cartesian coordinate system;  $H$  is the total specific energy,  $J/kg$ ;  $T$  is the temperature,  $K$ ;  $\mu$  is the dynamic viscosity,  $kg/(m \cdot s)$ ,  $\tau_{ij}$  is the averaged Reynolds stress for components,  $c_p$  is the

heat capacity at constant pressure in  $J/(kg \cdot K)$ ,  $\lambda$  is the thermal conductivity  $W/(m \cdot K)$ ,  $\delta_{ij}$  is the Kronecker symbol,  $t$  is the time value in  $s$ ; and  $d/dt$  is the substantial derivative. The equations use the representation of any parameter  $\varphi$  (it can be velocity  $W$ , pressure  $p$ , enthalpy  $H$ , etc.) as the sum of its averaged  $\bar{\varphi}$  and pulsation  $\hat{\varphi}$  values. In equation (55), the Einstein summation convention is used for the twice repeated  $i, j$ , and  $k$  indices.

The system of transport equations in the Reynolds form equation (55) is closed by the  $k$ - $\zeta$ - $f$  model of turbulence specially developed and verified for the processes of flow, combustion, and heat transfer in piston engines (Tatschl et al. 2005), and (Tatschl et al. 2006). Hanjalić et al. 2004 proposed three equations: for the  $k$  kinetic energy of turbulence, for the  $\varepsilon$  dissipation rate of this energy known from the  $k$ - $\varepsilon$  model of turbulence, and the equations for the normalized velocity scale  $\xi = \bar{W}^2/k$ . The  $k$ - $\zeta$ - $f$  turbulence model by contains the Durbin elliptical function of  $f$ , which takes into account the near-wall anisotropy of turbulence.

The equations of the system (55) are used to describe, respectively, the flow velocities  $W$  (Navier-Stokes equation), the enthalpy  $H$  (energy equation) and the mass  $m$  or density  $\rho$  (continuity equation) for each control volume of the considered computational domain. Wall heat transfer is determined through the thickness of the boundary layer using hybrid wall function (Popovać and Hanjalić, 2005).

Merker et al. 2019; Basshuysen and Schäfer, 2007 and Kavtaradze et al. 2009 they emphasized that this mathematical model is typical for *CFD* calculations of processes in piston engines.

For the exhaust muffler of engines, different muffler structures and parameters obviously have different influences on reducing the noise. Due to the complex work process of the muffler, how to theoretically compute and design the inner structure of the muffler has been a topic which was constantly discussed.

Material distribution is tailored to the interior design of hybrid mufflers. Such devices are typically acoustically small, except in the length direction, and their interior consists of a combination of pipes, expansions, and contractions. In order to design the interior layout using material distribution technique, it is necessary to be able to resolve thin porosity of materials. To show the effect of absorptive material (*AM*) and perforated pipe on sound pressure level can be described as equation below:

$$\text{Material Porosity} = 1 - (\text{Packing Density})/(\text{Material Density})$$

$$\varphi = \frac{V_V}{V_T} = \frac{V_T - V_M}{V_T} = 1 - \frac{\rho_T}{\rho_M} \quad (56)$$

where  $\varphi$  is the porosity (unitless),  $V_v$  is the void (air) volume in  $m^3$ ,  $V_T$  is the total (bulk) volume in  $m^3$ ,  $V_M$  is the material volume in  $m^3$ ,  $\rho_T$  is the apparent density of the material in  $kg/m^3$  and  $\rho_M$  is the density of the material in  $kg/m^3$ .

Unstructured mesh is chosen to discretize the computational field of the muffler and its components due to its high flexibility, the details in figure 50. According to the geometric model of the muffler, its surface mesh was refined to establish the finite element analysis of *PPiP* muffler. All internal walls are set as real walls with a surface roughness of *0.5 micrometres*.

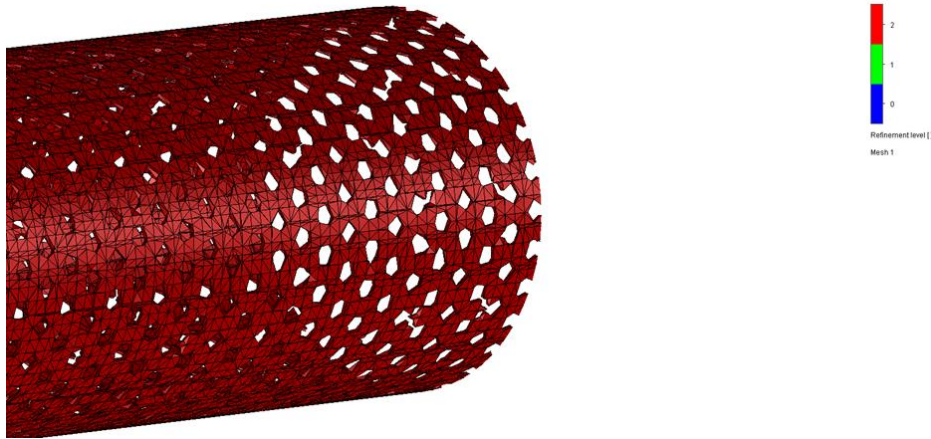


Figure 50 Refinement mesh of perforated tube

### 5.3. Calculation results

#### 5.3.1. Velocity and pressure distribution in muffler

The results below adopted finite element analysis to compute the flow trajectories of the muffler. The flow rates, pressures and fluid temperatures will be communicated through the linked boundary conditions nodes throughout the solution process. The input parameter and solution status were given in details in table 12.

Table 12 Volume muffler case study.

Iteration	173
Total cells	432742
Fluid cells	201809
Solid cells	230933
Trimmed cells	0
Muffler capacity	3.767028 Litre
High Mach number flow	No
Time-dependent	No
Heat Conduction in Solids	Yes
Radiation	No
Porous Media	No
Internal	Yes
Gravity	Yes
Basic Mesh Dimensions	$N_x = 150, N_y = 30, N_z = 36$
Reference Pressure	101325.00 Pa
Software Calculation Warnings	No Warnings

Further to this analysis, a pressure-based solver was used for visualize the flow characteristics in the muffler. The pressure field in this case is obtained through software inbuilt pressure solver, which is solving interlinked continuity and momentum equation. As show in figure 51. The maximum pressure was  $102384.37 Pa$  and the minimum was  $100181.23 Pa$  observed in the muffler without perforated tube. The non-colorful arrows represent gas flow while the colorful arrows represent reflected gas flow inside the muffler chamber. The internal pressure of the expansion chamber is relatively stable, and the distribution is relatively uniform. It can be concluded that one cause of a significant elevated pressure in the muffler part (chamber) is reflected part of gas flow at the chamber outlet. The reference values were computed from the left side (inlet).

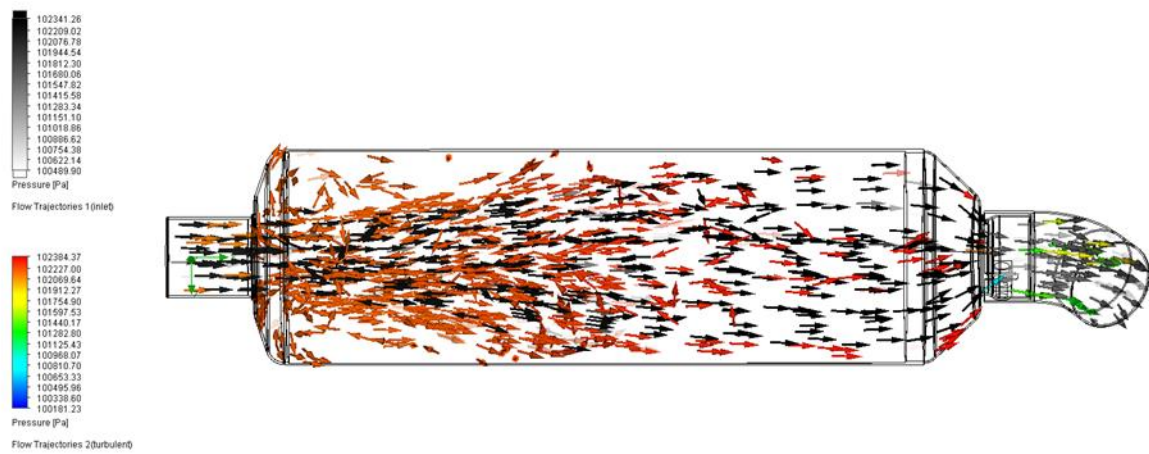


Figure 51 The volume muffler's pressure contour (flow trajectories).

Mutations in the gas flow cross-section can have a greater pressure loss. If the flow direction and the gas flow conditions change with a greater degree, it not only will generate the eddy current phenomenon, but also consume more energy. The flow velocity inside circular tube shows that there are infinite number of pulses produced. The more continuous the exhaust flow is that a fast-moving pulse creates a low-pressure area behind it. Figure 52 shows the velocity variation through different zones in geometry. It is found higher in the constrained ipipe.

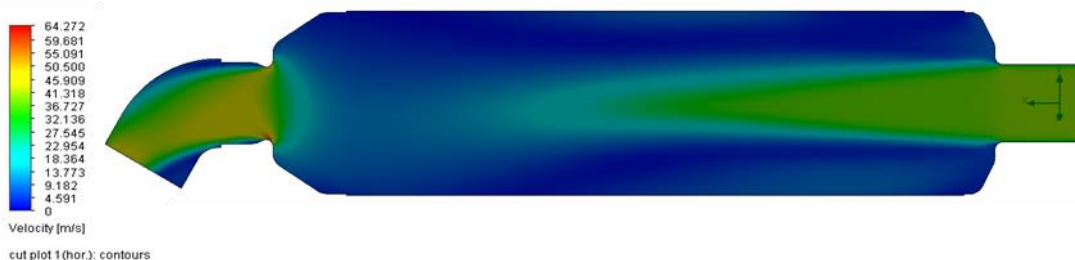


Figure 52 Velocity distribution in volume muffler.



For analyzing perforated pipe inside the muffler whose geometry is relatively complex, the computational model is split into several parts to generate mesh individually in order to decrease computational time. An element size and input information were given in table 13.

Table 13 PPiP Muffler case study.

Iteration	443
Total cells	824962
Fluid cells	565554
Solid cells	259408
Trimmed cells	0
Muffler capacity	3.767028 <i>Litre</i>
High Mach number flow	No
Time-dependent	No
Heat Conduction in Solids	Yes
Radiation	No
Porous Media	No
Internal	Yes
Gravity	Yes
Basic Mesh Dimensions	$N_x = 82, N_y = 16, N_z = 20$
Reference Pressure	101325.00 <i>Pa</i>
Software Calculation Warnings	No Warnings

In the figure 53 the contour of flow field distribution of the muffler system is shown at the entrance and the exit as well. As can be seen, the largest flow velocity (52.799 m/s) was in the connection pipe of PPiP at the outlet of the muffler and the largest pressure of the body muffler (102325.35 Pa) was at the inlet, and minmum observed (100778.85 Pa) as seen in figure 54.

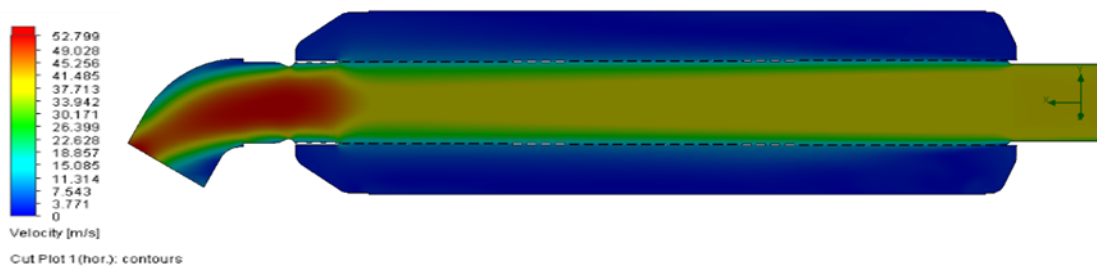


Figure 53 Velocity distribution in PPiP muffler.

As seen in figure 54 the majority of fluid in the interior of the PPiP muffler entered the muffler volume directly through the perforated pipe. Furthermore, the perforated tube inside the muffler featured holes with a very small diameter (3 mm). When fluid flowed from perforations, it was substantially reduced due to high resistance. The non-colorful arrows represent flow vector inside the perforated pipe in the muffler and the colorful arrows represent reflected flow vector or flow outside the perforated pipe.

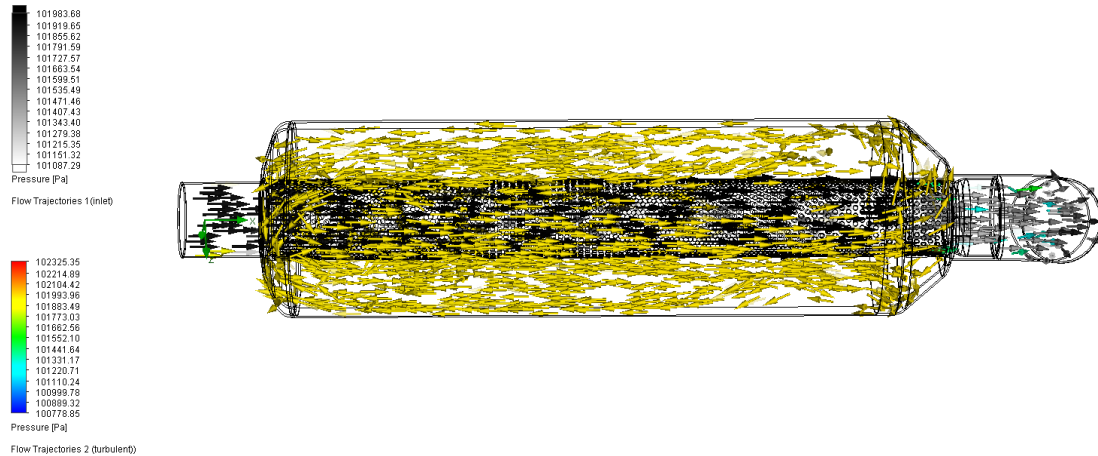


Figure 54 Pressure contour (Flow trajectories) in perforated tube and the volume part of muffler.

The pressure drop in the modeled muffler was calculated using three-dimensional calculations and the existence of an interior perforated pipe was taken into consideration. Additionally, three-dimensional models enabled the significance of Material Porosity to be clarified. These data were also utilized in AVL Boost to calibrate the *ID* exhaust system model. During intake operation, most of the flows in cylinder are generally turbulent due to the high velocity inside the Internal Combustion Engine (*ICE*), as seen in figure 55.

### 5.3.2. Exhaust gas flow distribution

The intake and compression strokes, in particular, are two of the most important activities that affect the dynamics of the air flow structure within the cylinder, as shown in figure 55. Due to the high velocity of exhaust gas out of the combustion chamber during exhaust operation of Internal Combustion Engine (*ICE*), all the flow in cylinders are typically turbulent due to swirl motion.

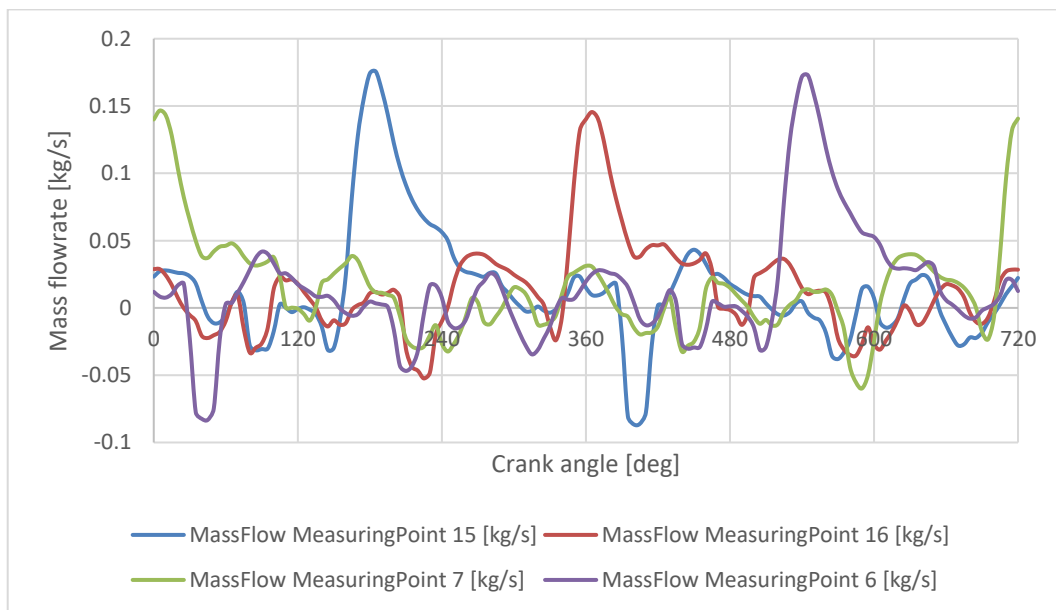


Figure 55 Mass flow rate for complete cycle at 8000 rpm through exhaust manifold.



### 5.3.3. Pulsating and flow acoustic

In the BOOST model, the measurement points for the sound pressure levels (*SPL*) are marked *MP9* and *MP10* in the figure 48 basing on the transfer matrix method for calculating *SPL*. As it can be seen from figure 56, for current *FS* muffler (installed *PPiP*) makes it possible to decrease the noise level but for  $n > 3000$  rpm noise level is still higher than in case of muffler construction with only volume. This part of research work focuses on the improvement of the average *SPL* of the muffler instead of taking *SPL* at all frequencies. So in the next part of results will discuss the suggestions for making improvement of the *FS* muffler.

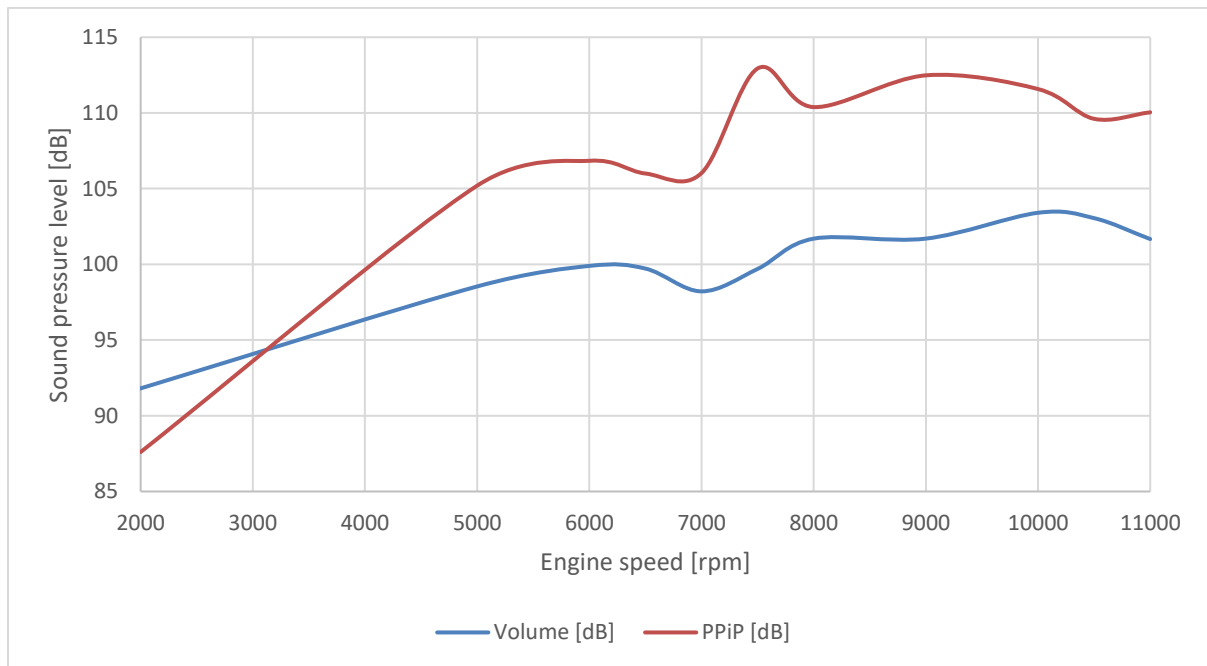


Figure 56 The effect of muffler structure on the sound pressure level (*SPL*) at different engine speed (*rpm*).

### 5.3.4. Thermodynamic analysis

During the compression stroke, the optimum exhaust manifold and duct design creates the ideal conditions for fuel injection. Because there was no catalyst or intercooler in the racing car system to absorb additional pollution or heat, the exhaust gas had a high temperature at the exhaust pipe, especially under low engine rotation circumstances. Figure 57 demonstrates how much the exhaust gases' bulk temperature drops through each particular channel. Since the channels are different lengths, and the input gas temperature for a given diameter is more or less the same at both channels. Also the temperature profiles were obtained to identify irregularity of temperature. However, it can be seen that the outlet temperature is significantly higher in the outer channel.

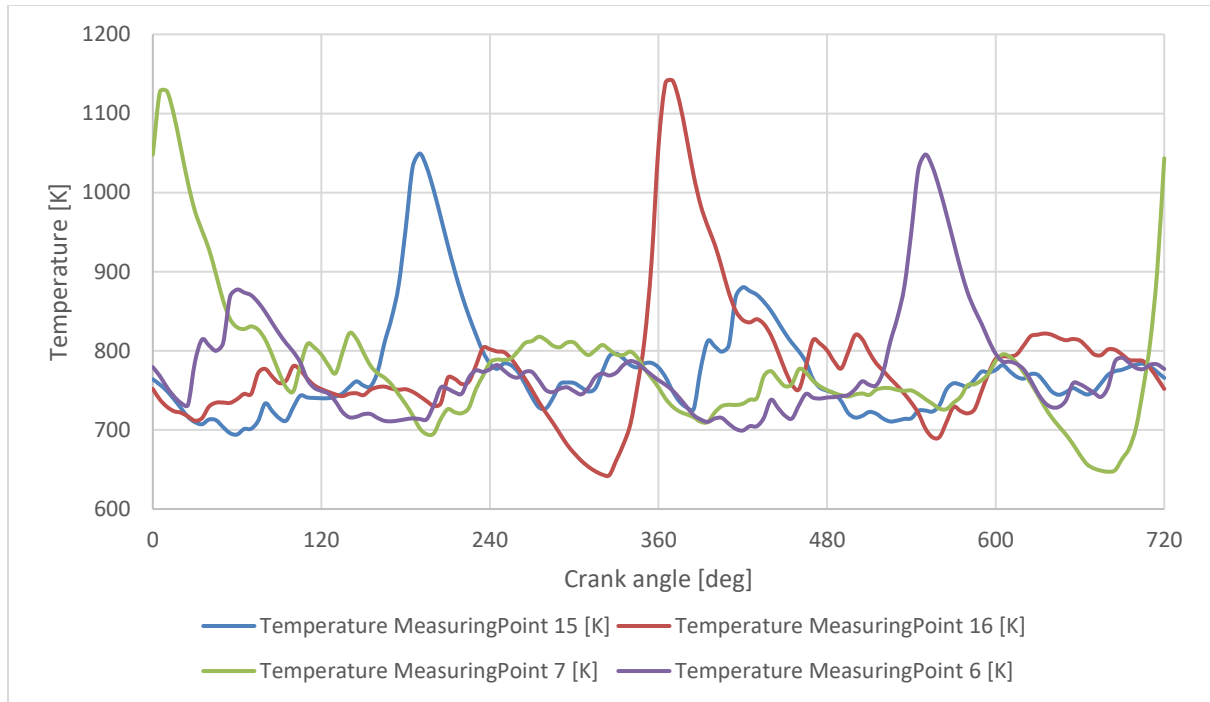


Figure 57 Temperature of *FS* engine exhaust gas at the exhaust manifold for complete cycle and  $n = 8000$  rpm.

### 5.3.5. Engine combustion

We really have to know how much heat was released during combustion and what the combustion route was in order to accurately replicate the flow through the exhaust manifolds. The engine thermodynamic computations are built on the premise of mathematical combustion models. Fundamental theoretical models exist, however they are inapplicable since they are based on ideal thermodynamic processes. The *ID* Boost solver employs combustion models to describe changes in state values in the cylinder. The following sections in this chapter will present combustion characteristic including heat release in details.

### 5.3.6. Fuel type and their effects on exhaust gas properties

The basic and suitable fuel for the Formula *SAE* race car engine is unleaded gasoline with an octane rating of  $93 (R+M)/2$  (about 98 *RON*) and *E85*. Nothing can be added to the fuels that have been delivered. The use of nitrous oxide or any other oxidizing agent is prohibited. Prakash Chandra Mishra et al. 2018 studied the effect of perforated and non-perforated muffler on outlet temperature. A computational fluid dynamic method was used to develop muffler performance. Based on the solver, the effect of back pressure, temperature, density and velocity streamline of exhaust gas on the muffler performance was studied for different blends (5%, 10%, 15%) of gasoline and methanol by volume percentage. The result shows clear variations of these parameters are observed between non-perforated and perforated type turbo pipe mufflers. For different design parameter and fuels, the results of *CFD* analysis show great difference of gas properties during damping process. Mohamad et al. 2017 used *ID* AVL-Boost software to describe

the effect of using different kind blend fuels on engine performance and exhaust properties. The result shows variation of outlet temperature, and emission gas characteristics for  $CO$ ,  $NO_x$ , and  $CO_2$  by using different volume percentage of alcohol-gasoline blends. Mohamad et al. 2018 studied the effect of Ethanol-Gasoline blend fuel on engine power output and emissions, the literatures results show great improvement in combustion process and exhaust gas characteristics. Mohamad et al. 2017 presented a study of mufflers applied in industry in their technical paper, and this evaluation illustrates flow and temperature distribution along the muffler ducts. Experimental and practical approaches for diverse methodologies utilized in the design, calculation, and construction of mufflers, as well as transmission loss features, were presented. *ID* calculations are much faster, and still give a good overview of the system under investigation.

The energy transformation in the cylinder is based on the heat generated during the combustion of the air-fuel mixture. However, the quantity of heat emitted is not the only factor that impacts values such as engine heat efficiency, indicated engine performance, and so on. Another aspect is the combustion course, which has a significant impact on the results. The quantity of heat emitted is determined by the calorific value of the fuel, and the amount of fuel burnt is determined by the amount of fuel consumed. As seen the equation 57:

$$dQ_B = H_u dm_b \quad (57)$$

Where  $dQ_B$  is the heat released from fuel,  $H_u$  is the calorific value of fuel,  $dm_b$  is the amount of burned fuel in  $kg$ .

The process of combustion influences several factors (such as cylinder pressures and temperatures) that have a significant impact on ultimate engine performance. The aforementioned parameters  $m$  and  $a$  are used in the Vibe combustion model. These characteristics cannot be set at random since they are dependent on a number of other factors such as the combustion chamber geometry, fuel charge, injection time, engine speed, and so on. In AVL *ID* Boost the data were selected according to the Honda CBR 600RR (PC 37) design and operation guidebook.

Heat transfer in exhaust system: During the combustion process the heat transfer occurs between gas and the cylinder wall then damped out to the exhaust system also the losses caused by the heat passage occur through the duct wall and expansion stage of exhaust system. We can divide the whole system heat transfer into three stages:

- Convection heat transfer between gas inside the exhaust manifold, ducts and exhaust muffler.
- Heat conduction through the duct wall.
- Heat transfer between the outside duct and the ambient (in our case, air).

The pipe wall temperature can be calculated through equation (58).

$$q_w = \frac{T_w - T_c}{\frac{1}{h_{conv}} + \frac{k_{cond}}{\lambda_w}} \quad (58)$$

where  $T_w$  is the wall temperature in  $K$ ,  $T_c$  is the coolant temperature in  $K$ ,  $h_{conv}$  is the heat-transfer coefficient of coolant in  $W/m^2.K$ ,  $k_{cond}$  is the heat conductivity of cylinder wall in  $W/m.K$ ,  $\lambda_w$  is the cylinder wall thickness in  $m$ .

This equation is similar to Ohm's law, as shown in figure 58. Like resistors, heat transfers are serially aligned. However, it does not represent a heat transfer between hot gas in the exhaust system and the duct wall on the inside. Another equation is used to calculate the convective heat transfer.

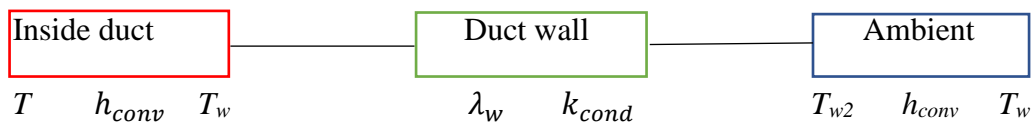


Figure 58 Heat transfer scheme.

Equation 58 is composed of two parts. The first part equation 59 is a part which specify heat convection through the duct wall.

$$q_{w2} = \lambda_w \frac{T_w - T_{w2}}{k_{cond}} \quad (59)$$

Second part equation 60 describes convection heat transfer between the outside duct wall and the ambient.

$$q_c = h_{conv}(T_{w2} - T_c) \quad (60)$$

Therefore, we can deduce temperature of the duct wall  $T_w$  from equation 58. The temperature is represented by equation 61.

$$T_w = q_w \left[ \frac{1}{h_{conv}} + \frac{k_{cond}}{\lambda_w} \right] + T_c \quad (61)$$

Values from the equation 61 can be selected by a user or can be pre-set like default values in the AVL engine simulation software. Ambient temperature and heat transfer coefficient for the air are one of these pre-set values. We may also specify the material of the exhaust system parts with pre-set values of the heat conductivity in table 14 or in case we have enough measured data we can define our own material with measured or computed values of the heat conductivity. In this research work, the steel alloy was selected for whole exhaust parts.

Table 14 Heat conductivity of default materials.

Material	Heat conductivity $w.m^{-1}.k^{-1}$
Aluminium	45
Cast Iron	150
Steel	48
Zirconium	4.1

Calculation of the convection heat transfer between exhaust gas inside the duct and the inside duct wall is the last step of the total heat transfer calculation. Heat transfer inside the duct can be described with the basic analytic equation 60:

$$\dot{Q} = h_{conv}A(T_w - T) \quad (62)$$

where  $h_{conv}$  the heat-transfer coefficient in  $W/m^2.K$ ,  $A_i$  is the instantaneous value of combustion chamber area depends on actual piston, location in  $m^2$ ,  $T$  is the gas temperature in  $K$ ,  $T_w$  is the cylinder wall temperature in  $K$ .

Annand, Woschni, and Eichelberg heat transfer models are also supported by the AVL Engine Simulation program. All of these models are used to calculate the heat-transfer coefficient of the exhaust system.

The main objective of this research work was to provide a numerical procedure in order to implement a reliable evaluation of the intake and exhaust system include heat release in *FS* engine. The technique was applied the first law of thermodynamics called single – zone model (*SZ*) *OD* model. The rate of heat release can be calculated for a wide range of engine operative conditions. However, considering the general good accordance along the entire crank angle interval, as shown in figures 59, 60 and 61. Although this combustion process can be distorted to a higher degree than in gasoline combustion engines, researchers can investigate the trade-off between a rapid and early heat release, which results in low exhaust losses but high heat losses per sub-volume of the cylinder wall and head, and having an extended heat release, which leads to lower heat losses to the walls but even more heat being dissipated through the head. This re-allocation is due to the fact that in the latter circumstance, the heat has less accessible duration to input force into the piston, resulting in greater residual energy at the final stage of the power stroke, which is later released as exhaust. Generally speaking, highly diluted mixtures will yield lower overall heat losses.

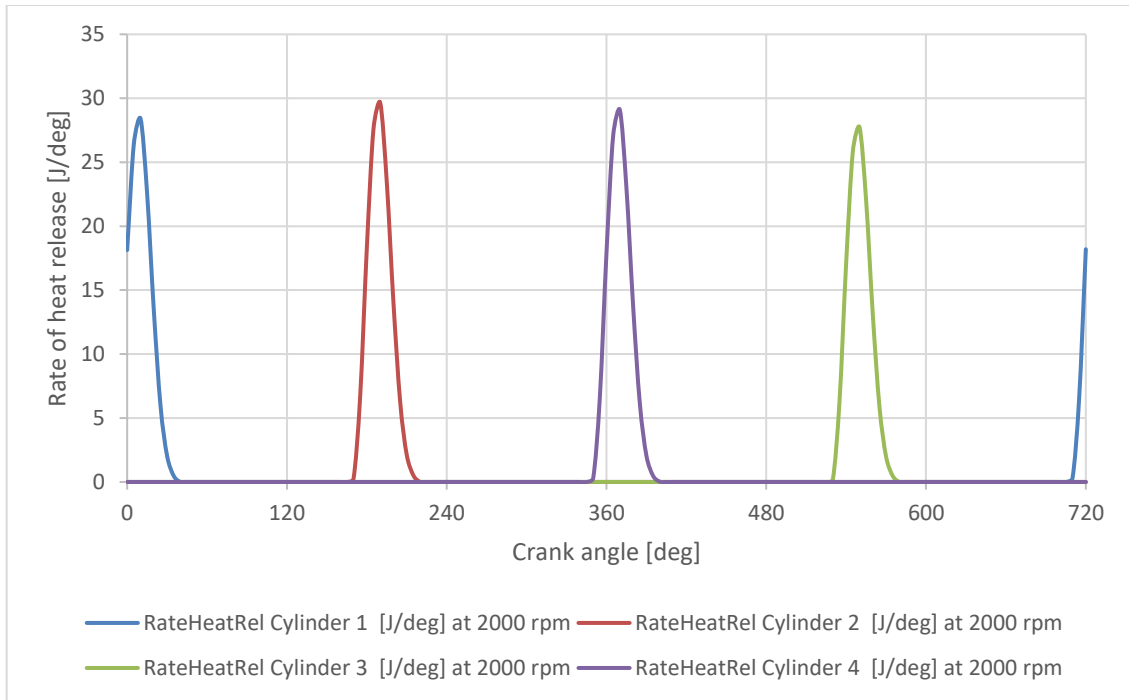


Figure 59 Rate of heat release for complete cycle at exhaust manifold for engine speed 2000 rpm.

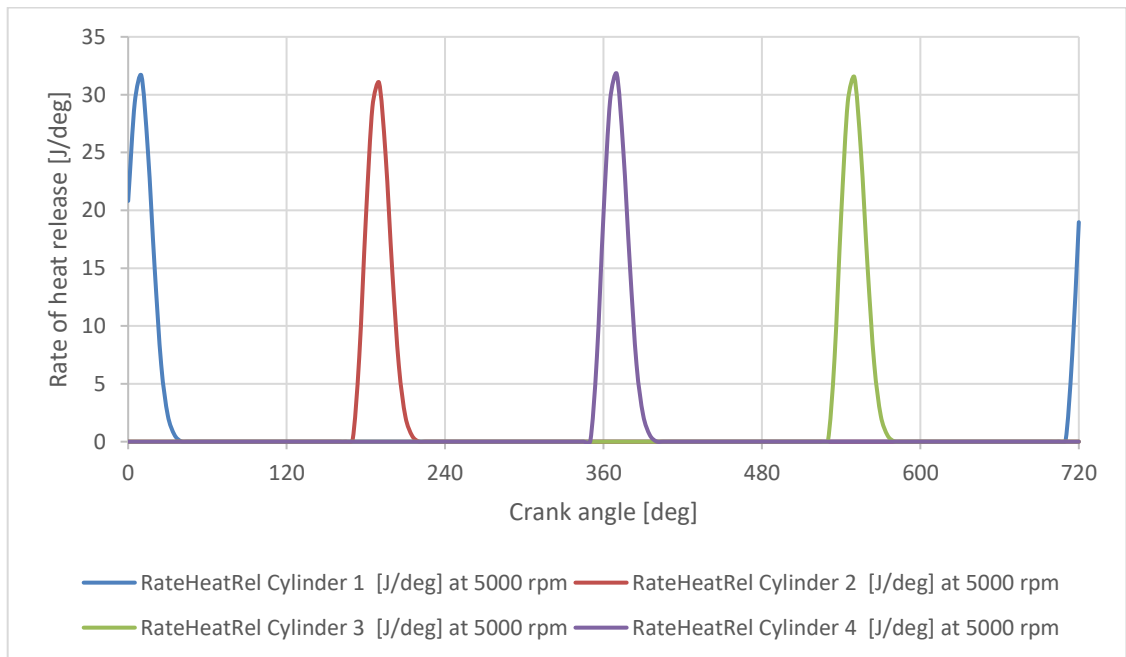


Figure 60 Rate of heat release for complete cycle at exhaust manifold for engine speed 5000 rpm.

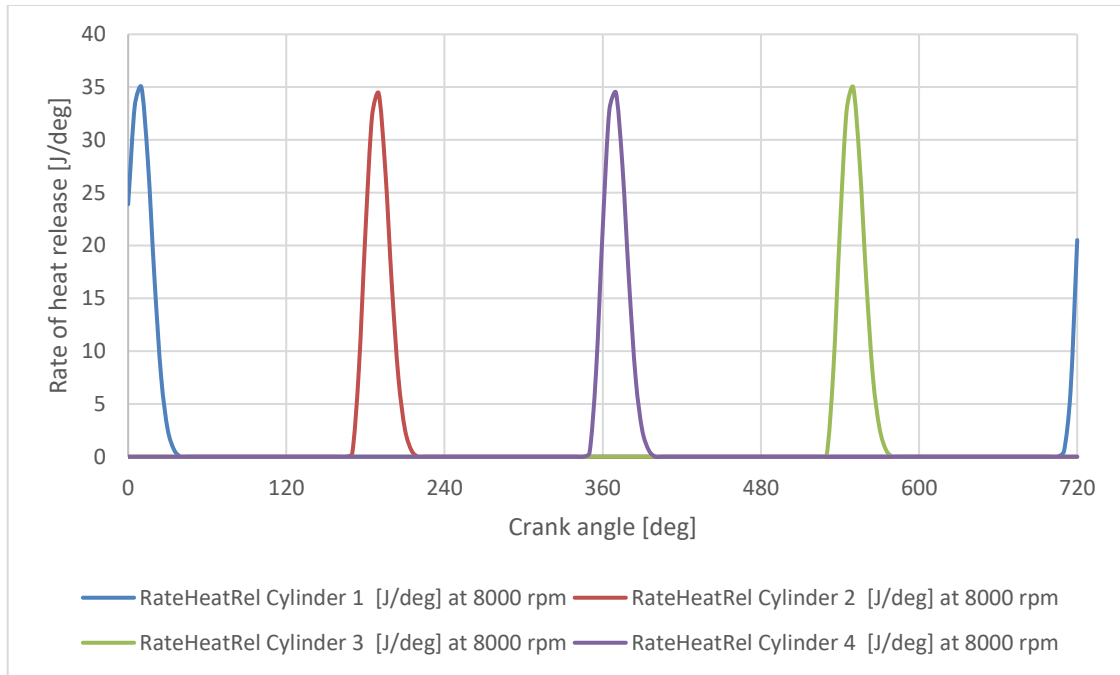


Figure 61 Rate of heat release for complete cycle at exhaust manifold for engine speed 8000 rpm.

### 5.3.7. The surface roughness and chemical composition of stainless steel alloy

The material used in this silencer is an austenitic stainless-steel type (*AISI 316*), is considered non-magnetic, highly resistant to corrosion, whose starting powder, gas atomised, and has a maximum particle size of  $22 \mu\text{m}$ . This steel has a homogenous microstructure with a homogeneous core in the surface, which enables high quality surface finishes and machining to be obtained. This steel is suitable for galvanic treatments as well as chemical and physical deposits with a chemical composition given in Table 15.

Table 15. chemical composition of *AISI316*.

%C <sup>(1)</sup>	%Mn <sup>(2)</sup>	%P <sup>(2)</sup>	%S <sup>(1)</sup>	%Si <sup>(2)</sup>	%Cr <sup>(2)</sup>	%Ni <sup>(2)</sup>	%Mo <sup>(2)</sup>	%N <sup>(2)</sup>	%O <sup>(2)</sup>	%Fe
<0.03	<2	<0.01	<0.005	<1	16-19	9-13	1.5-3	<0.003	<0.002	Compl.

### 5.3.8. Johnson–Champoux–Allard model (JCA)

This is a model utilized for the measuring the coefficient of acoustic absorption and the propagation of sound in porous materials. The advantage of the *JCA* model is based on the forecast data, that it not only predicted acoustic features very well but also showed general consistency with the results of the experimental tests (Taban et al. 2019). Allard and Champoux, 1992 defined the density module and the equivalent bulk as below:

$$\rho(\omega) = \alpha_{\infty} \rho_o \left[ 1 + \frac{\sigma \varphi}{j \omega \rho_o \alpha_{\infty}} \left( 1 + \frac{4i \alpha_{\infty}^2 \mu \omega \rho_o}{(\sigma \wedge \varphi)^2} \right)^{0.5} \right] \quad (63)$$

$$K(\omega) = kp_o \left( k - (k - 1) \left[ 1 + \frac{8\mu\alpha_\infty\varphi}{\lambda^2 \varphi i \omega \rho_o \alpha_\infty N_{Pr}} \left( 1 + \frac{4i\alpha_\infty^2 \mu N_{Pr} \omega \rho_o}{(\sigma \lambda \varphi)^2} \right)^{0.5} \right]^{-1} \right)^{-1} \quad (64)$$

The physical parameters of the sample include porosity  $\varphi$  [-], air flow resistivity  $\sigma$  [ $Ns/m^4$ ], viscous characteristic length  $\Lambda$  [ $\mu m$ ], tortuosity  $\alpha_\infty$  [-] and thermal characteristic length  $\Lambda$  [ $\mu m$ ]. Meanwhile,  $N_{Pr}$  is Prandtl number [ $\approx 0.71$ ], the  $\rho_o$  indicates air density [ $kg/m^3$ ],  $\mu$  is the dynamic viscosity of the air [ $\approx 1.85 \times 10^{-5} Pa.s$ ],  $\omega$  is the angular velocity [ $1/s$ ] and  $k$  is the ratio of the specific heat capacity [ $\approx 1.4$ ].

To express the characteristic wave number  $K(\omega)$  and the characteristic impedance  $Z_c(\omega)$ , the impedance of surface acoustic  $Z$  can be reformulated from the following equations [Allard and Daigle, 1994]:

$$Z_c(\omega) = \frac{1}{\varphi} \sqrt{\rho_\omega K_\omega} \quad (65)$$

$$K_c(\omega) = \omega \sqrt{\frac{\rho(\omega)}{K(\omega)}} \quad (66)$$

$$Z = Z_c(\omega) \cdot \cot(K_c(\omega) \times d) \quad (67)$$

$$\dot{R} = \frac{Z_c - \rho_o c_o}{Z_c + \rho_o c_o} \quad (68)$$

where  $\dot{R}$  is the reflection coefficient of sound pressure in ( $dB$ );  $d$  is the thickness of the prototype in ( $m$ );  $Z_c$  is the surface impedance. The absorption coefficient is calculated by equation 69:

$$\alpha = 1 - |\dot{R}|^2 \quad (69)$$

Finally, the prediction error rates ( $PERs$ ) of data collected from the  $JCA$  model at the frequency range between  $0-3000$   $Hz$  can be calculated for every condition by equation (70):

$$PER = \frac{|\alpha_m - \alpha_p|}{\alpha_m} \times 100 \quad (70)$$

where  $\alpha_m$  and  $\alpha_p$  are the measured and predicted absorption coefficients, respectively. The structural feature of perforated tube is summarized in table 16.



Table 16 The parameters of perforated pipe.

Porosity	0.047
Porosity Discharge Coefficient In	0.6
Porosity Discharge Coefficient Out	0.6
Perforated pipe capacity	0.738712 $dm^3$
Perforation-Hole Diameter	3 mm
Perforation-Wall Thickness	0.5 mm
Perforated pipe weight	191 g

The Transmission loss ( $TL$ ) in  $dB$  has been calculated for three porosity values (0.29, 0.6 and 0.9) on a similar model as shown in figure 62. For acoustic  $FEM$  analysis, Johnson–Champoux–Allard model ( $JCA$ ) has been used for porous medium.

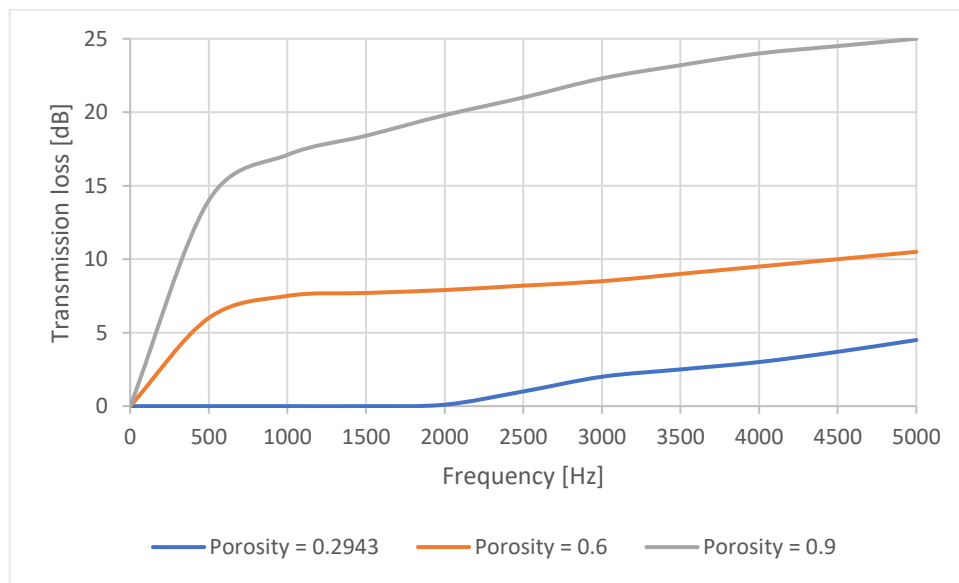


Figure 62. Transmission loss at different frequencies at different porosities.

For the same porosity back pressure has been calculated using  $CFD$  analysis, details in table 17. Steady and compressible flow has been carried out with heat transfer.  $K$ -epsilon model has been used for turbulent analysis.

Table 17 Back pressure at different porosities.

Porosity	0.29	0.6	0.9
Back Pressure	889 mbar	821 mbar	795 mbar

### 5.3.9. Design of Simulations

It is necessary to perform sensitivity analysis to improve predictions based on simulation models, The initial stage in the pre-processing phase is to capture a digital image of every internal component of the exhaust system before constructing a suitable mesh of these surfaces. This surface mesh is used to create the volume mesh in which the gas flows. These meshes were produced by the AVL Fire GmbH. Special attention was given to the exhaust manifold, the perforated element, and the regions where exhaust gas enters and leaves the system, treated by the

ANALYSIS OF RACE CAR ENGINE EXHAUST SYSTEM

solver as regions of inlet and outlet. All other regions, comprising boundaries of the control volume, are defined as wall. The flow considered as turbulent within the system. Table 18 a brief of input and output data were demonstrated, indicating how the system was improved.

Table 18 The data of input and output for exhaust system at certain operating conditions.

Simulations	Inputs			Outputs			
	Speed in rpm	Pipe diameter in mm	Hole diameter in mm	Power in hp	Torque in Nm	BSFC in g/kWh	SPL in dB
run 1	2000	47	1.5	11.82	42	393	88
run 2		47	2	11.78	41.95	399	85.5
run 3		47	2.5	11.78	41.96	398	87.7
run 4		47	3.5	11.79	42	395	86
run 5		47	4	11.81	42.06	398	87.5
run 6		45	3	11.79	42	394	85.5
run 7		46	3	11.76	41.91	404	85.5
run 8		47	3	11.77	41.94	394	84
run 9		48	3	11.78	41.95	403	85
run 10		49	3	11.79	41.98	400	86
run 11		50	3	11.78	41.95	394	85

Simulations	Speed in rpm	Muffler diameter in mm	Muffler length in mm	Power in hp	Torque in Nm	BSFC in g/kWh	SPL in dB
run 12	2000	106	406	11.79	42	383	87.5
run 13		111	406	11.79	42	390	88
run 14		116	406	11.77	41.94	395	85
run 15		121	406	11.79	41.95	395	84.5
run 16		126	406	11.78	41.95	395	85
run 17		131	406	11.77	41.9	400	84.5
run 18		106	416	11.79	42	385	87.5
run 19		111	416	11.8	42	395	86
run 20		116	416	11.78	41.95	395	84.5
run 21		121	416	11.77	41.91	400	84.5
run 22		126	416	11.77	41.92	405	84.5
run 23		131	416	11.79	41.95	400	85.5

Simulations	Speed in rpm	Muffler diameter in mm	Muffler length in mm	Power in hp	Torque in Nm	BSFC in g/kWh	SPL in dB
run 24	2000	106	426	11.79	42	395	86.5
run 25		111	426	11.78	41.95	398	86
run 26		116	426	11.77	41.94	402	85.5
run 27		121	426	11.81	42	385	87.5

run 28	126	426	11.79	42	395	86
run 29	131	426	11.79	42	395	85.5
run 30	106	436	11.78	41.95	390	85.5
run 31	111	436	11.78	41.95	395	87
run 32	116	436	11.77	41.94	402	85.5
run 33	121	436	11.79	41.95	395	86.5
run 34	126	436	11.78	41.95	395	84
run 35	131	436	11.81	42	400	85.5
run 36	106	446	11.79	42	395	87
run 37	111	446	11.76	41.87	398	85.5
run 38	116	446	11.79	42	402	87
run 39	121	446	11.78	41.95	390	85
run 40	126	446	11.79	42	395	85
run 41	131	446	11.82	42.05	395	87
run 42	106	456	11.79	41.95	400	88
run 43	111	456	11.8	42	390	88
run 44	116	456	11.81	42.05	387	88
run 45	121	456	11.78	41.95	395	84.5
run 46	126	456	11.8	42	398	87
run 47	131	456	11.79	42	399	86.5

### 5.3.10. Effect of muffler design on the engine characteristic

Engine performance is mainly characterized by the engine operating behavior in the speed-load domain, for example, the behavior of emissions, fuel consumption, noise, mechanical and thermal loading. Engine performance maps refer to the constant value contour plots of a given performance parameter in the speed-torque domain. For a system design engineers it's clear that the engine performance is essential and major task.

In figure 63 shows less effect on power output, after using different type of exhaust muffler for current FS engine, since there is no catalyst convertor or intercooler to create high back pressure.

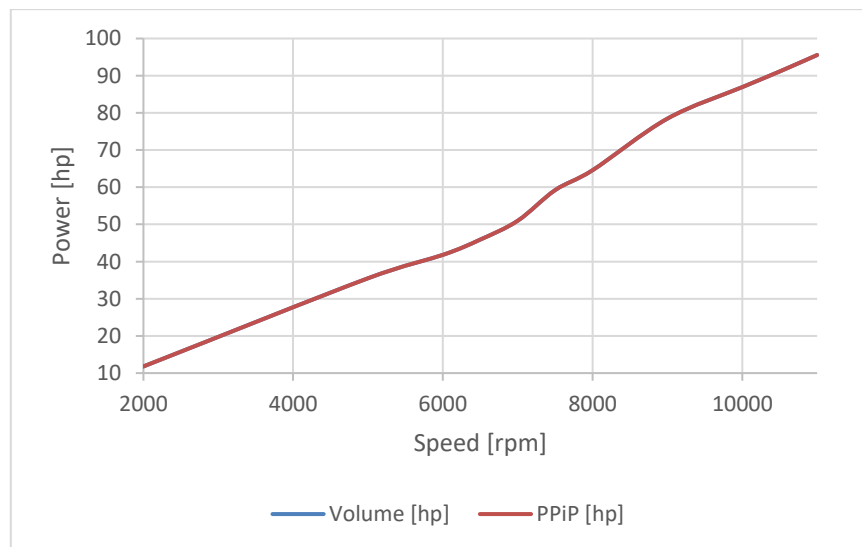


Figure 63 The effect of the difference structure of the exhaust muffler on the power output.

Influence of diameter  $PPiP$  of muffler ( $Dm_{in}$ ), diameter of hole of perforated inner pipe ( $Dm_{hole}$ ), diameter out of muffler shell ( $Dm_{out}$ ) and the length of the muffler variation on Honda engine performance was monitored and optimized based on AVL BOOST solver. As shown in figure 64 the differences were slightly detected of the torque characteristics as the effect of the diameter change of the perforated pipe inside the muffler. The formula team and the author select  $47\text{ mm}$  for the diameter of the installed perforated tube.

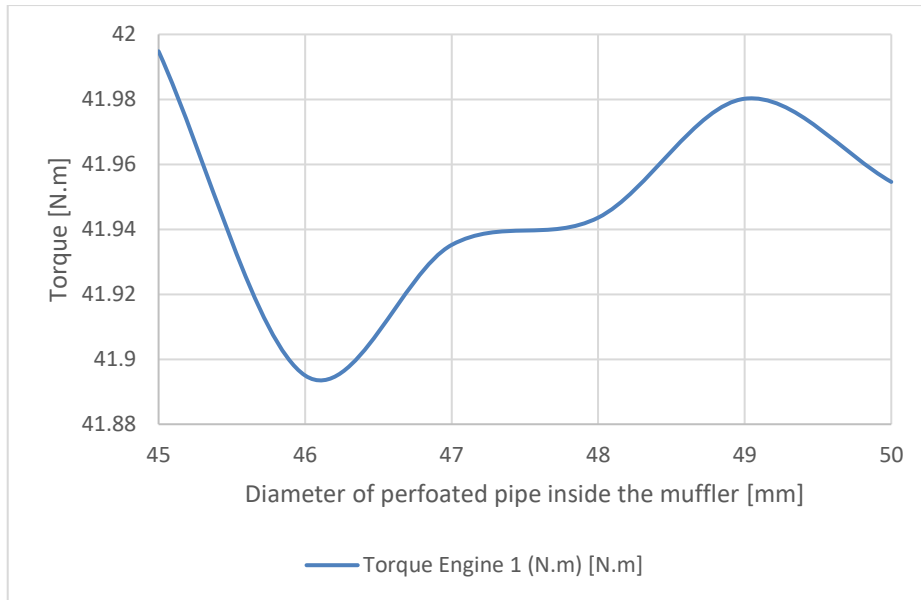


Figure 64 The result of variation of  $PPiP$  diameter on the  $FS$  engine torque (at  $n = 2000\text{ rpm}$ ).

The influence of different diameter of installed  $PPiP$  inside the muffler ( $Dm_{in}$ ) on the Brake Specific Fuel Consumption ( $BSFC$ ) in ( $g/kw.h$ ) was showed in figure 65, and significant change was done to reduce fuel consumption when the chosen diameter of  $PPiP$  is  $47\text{ mm}$ .

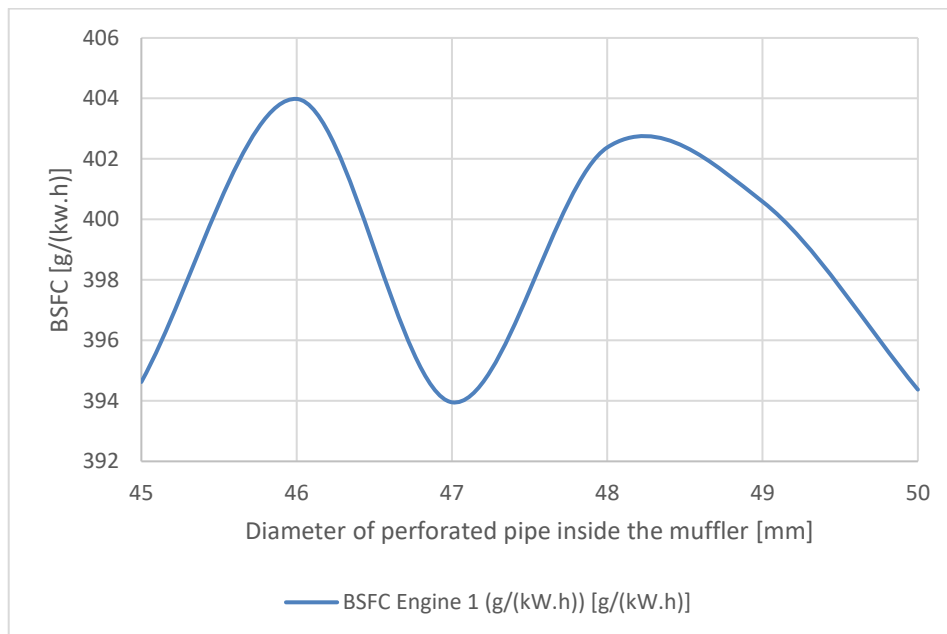


Figure 65 The effect of variation of  $PPiP$  diameter on the  $FS$  engine  $BSFC$  (at  $n = 2000\text{ rpm}$ ).

During its operation, the engine, as the power producing source, continually creates pressure waves. The pulsing action of the exhaust gases causes these pressure waves. Due to a differential pressure, these exhaust gas pulses propagate from the engine to the ambient environment. When these pulses interact with the environment, which is at a lower pressure than the combustion gases, they cause them to pulse. The exhaust orifice noise contributes to interior and exterior race car noise, as show in figure 66.

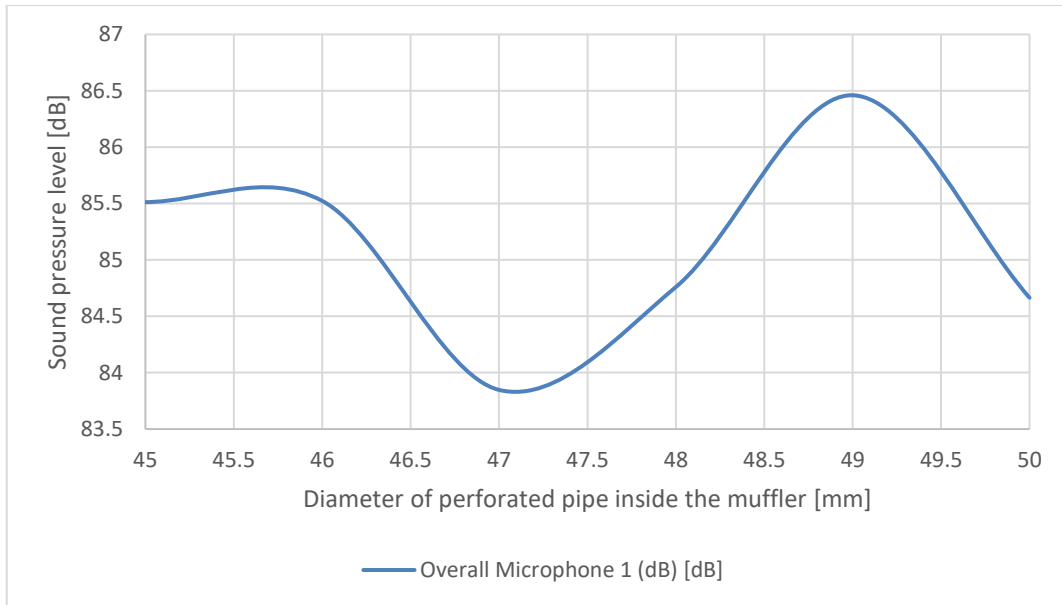


Figure 66 The result of variation of *PPiP* diameter on sound pressure level (*SPL*) at the muffler (at  $n = 2000 \text{ rpm}$ ).

As it can be noticed form figure 67, the effect of diameter of perforated tube inside the muffler on the power output and for engine speed ( $n$ ) = 2000 rpm, the power output remains almost the same and no significant effect was achieved for variation of the diameter of perforated inner pipe inside the muffler on the engine power output.

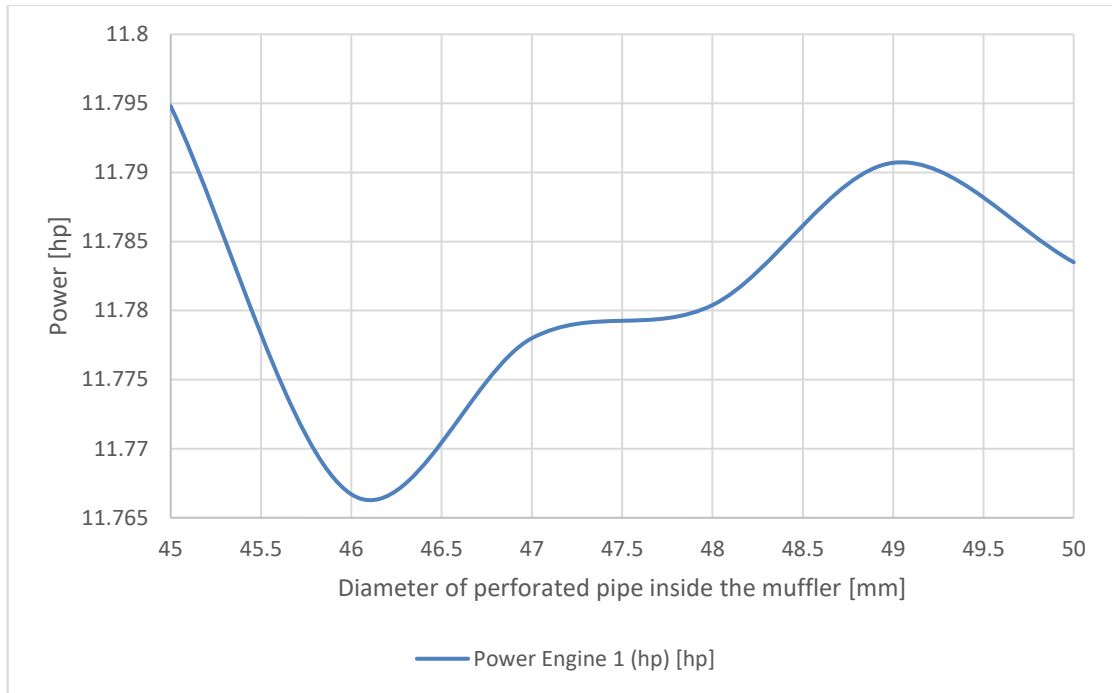


Figure 67 The effect of variation of *PPiP* diameter on the *FS* engine power output (at  $n = 2000$  rpm).

The results of this software calculation also showed the differences in indicated torque for the different diameters of holes on the installed perforated pipe (*PPiP*) inside the muffler. Based on the calculation results the 3 mm was the selected diameter of holes of installed *PPiP*. As shown in figure 68 the diameter of holes of *PPiP* has less effect on the indicated torque when is compared to the other given parameters.

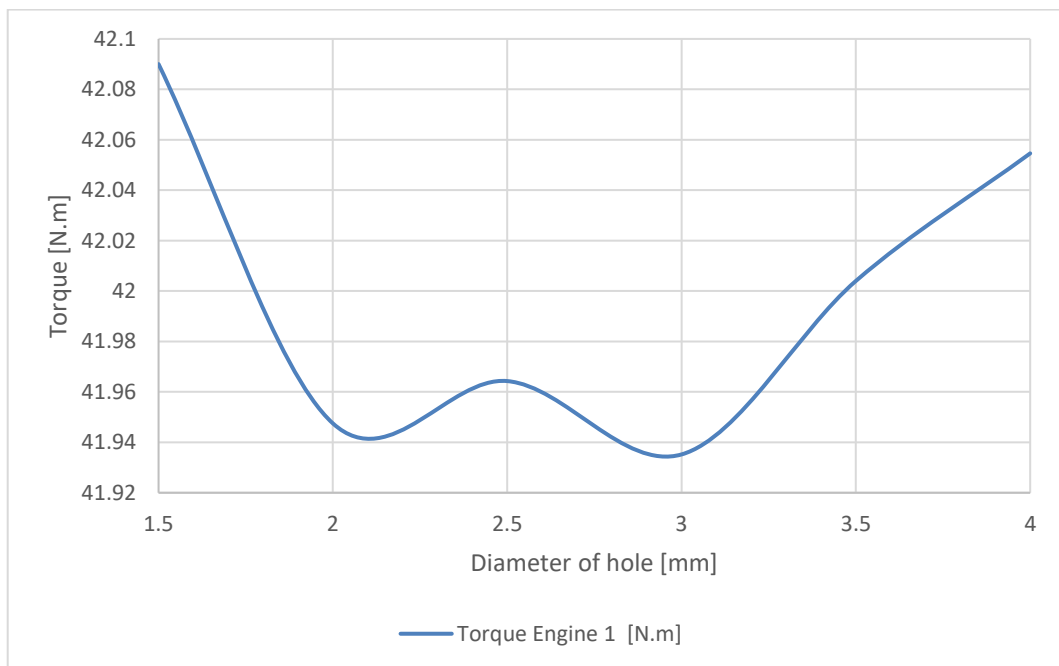


Figure 68 The effect of variation of *PPiP*-holes diameter on the *FS* engine torque (at  $n = 2000$  rpm).

The effect of different diameter of the holes of installed *PPiP* ( $D_{m\_hole}$ ) as shown in figure 69, on *FS* car engine performance include *BSFC* was observed and improved by suggest alternative values of diameter based on AVL BOOST simulation software. The selected diameter of holes on perforated pipe inside the muffler was  $3\text{ mm}$  in which achieved minimum rate of fuel consumption.

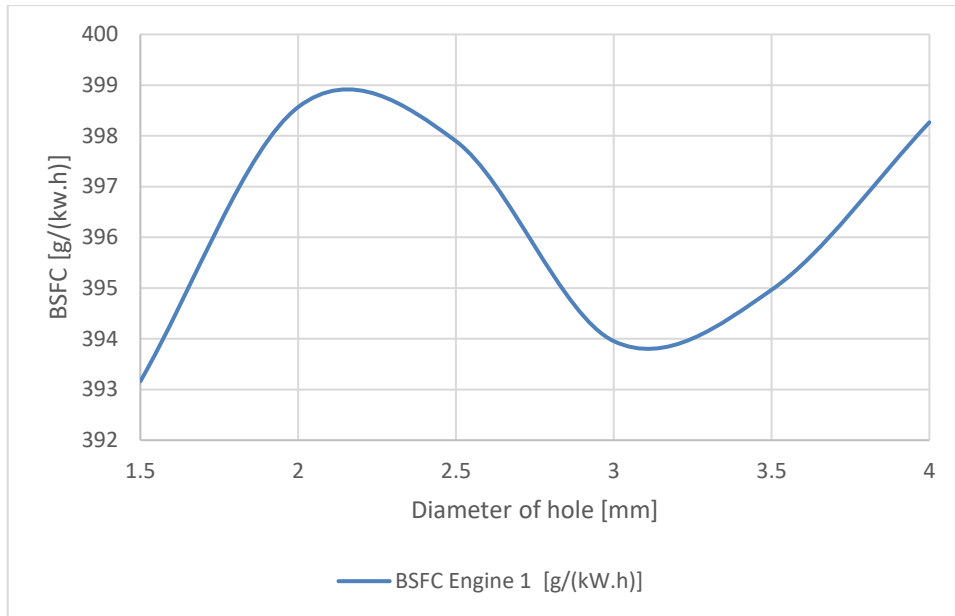


Figure 69 The effect of variation of *PPiP*-holes diameter on the *FS* engine *BSFC* (at  $n = 2000\text{ rpm}$ ).

The pressure pulses created by the periodic charging and discharging process induce the predicted noise emitted from the orifice of exhaust systems, which propagates to the open ends of the duct systems. As shown in figure 70 illustrates this point. The impact of the diameter of the hole in the perforated pipe within the muffler has been monitored.

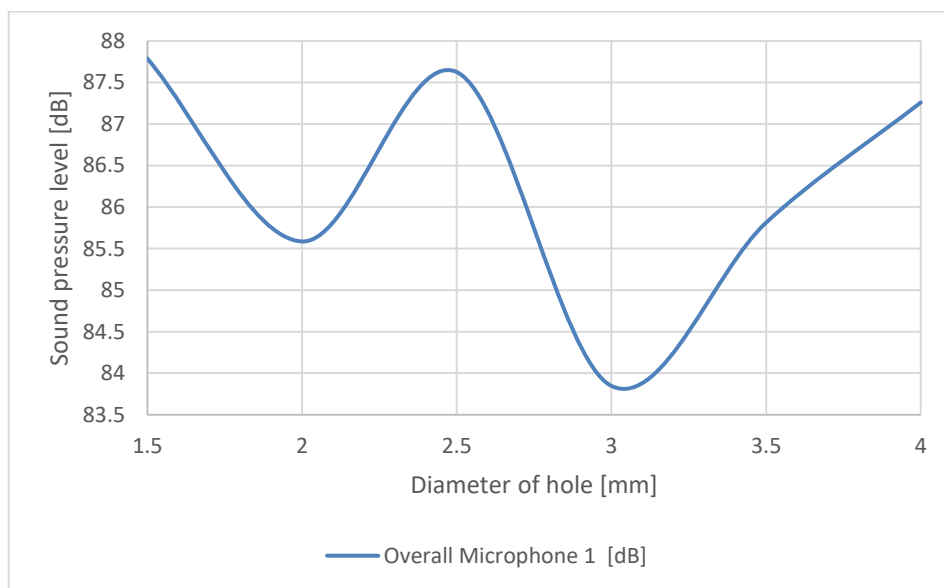


Figure 70 The effect of variation of *PPiP*-holes diameter in muffler on the sound pressure level (*SPL*) at  $n = 2000\text{ rpm}$ .

No significant effect was achieved for variation of the diameter of holes of perforated inner pipe inside the muffler on the engine power output as shown the details in figure 71.

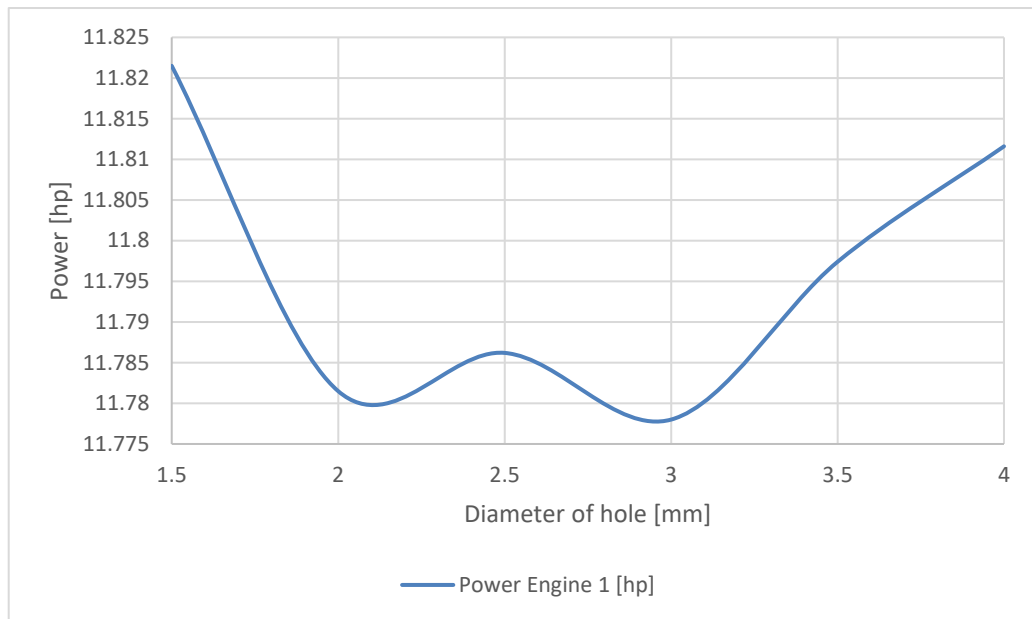


Figure 71 The effect of variation of *PPiP*-holes diameter on *FS* engine power output at  $n = 2000 \text{ rpm}$ .

In figure 72 it is possible to find the optimum torque profile for Formula-Student race car and the effects of pipe length ( $L_m$ ) and diameter ( $D_{m\_out}$ ) of outer pipe were clarified.

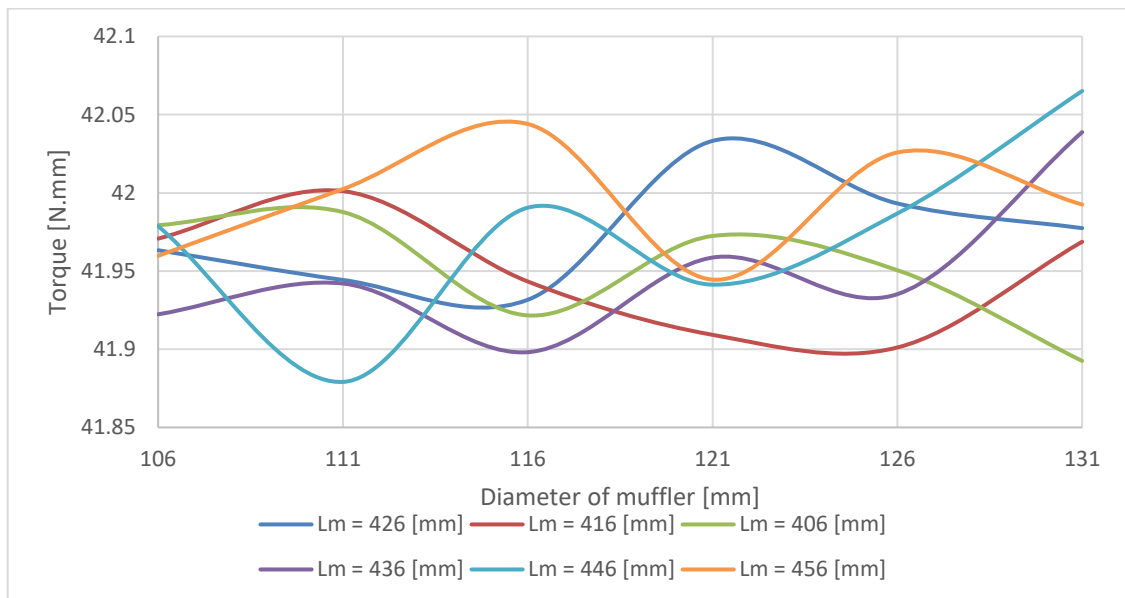


Figure 72 Results of variation of pipe length ( $L_m$ ) and the diameter of muffler volume ( $D_{m\_out}$ ) on the *FS* engine torque at diameter of perforated inner pipe  $D_{m\_in} = 47 \text{ mm}$ ,  $n = 2000 \text{ rpm}$ .

The muffler is a crucial component of an engine's performance. In general, a well-designed exhaust system reduces fuel consumption and exhaust pollutants. In today's environment, engine



designers' main goals are to accomplish the twin goals of highest performance and lowest cost. Figure 73 shows the effects of muffler dimensions on the brake specific fuel consumption (*BSFC*).

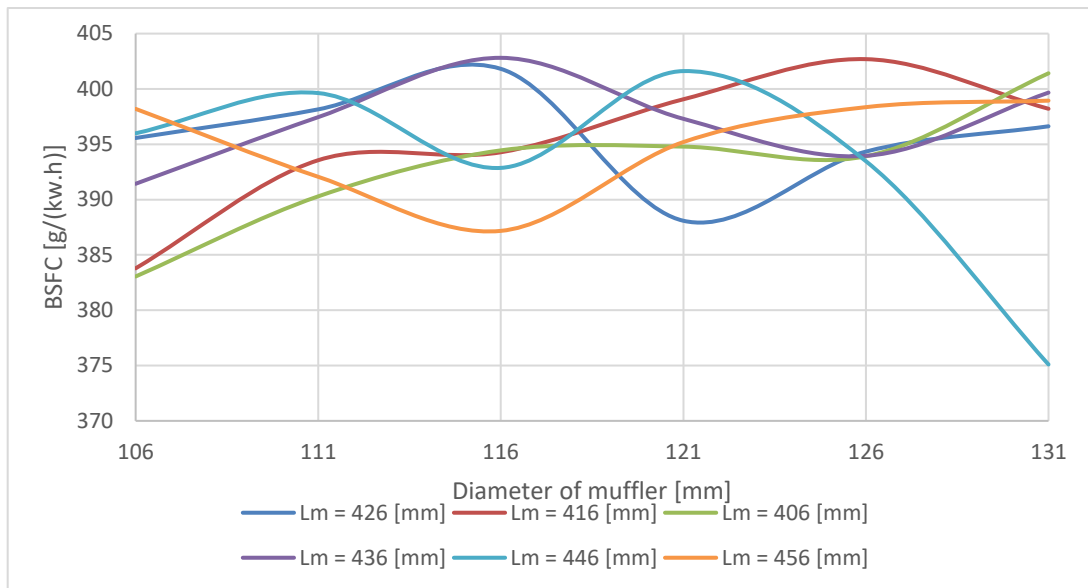


Figure 73 Results of variation of pipe length ( $L_m$ ) and the diameter of muffler volume ( $D_{m\_out}$ ) on the *BSFC* of the *FS* engine at the diameter of perforated inner pipe  $D_{m\_in} = 47$  mm,  $n = 2000$  rpm.

The propagation of backward waves from the open end of the pipe determines a severe influence of engine performance characteristics, including noise level, on the output pipe length. As a result, the lowest noise level while maintaining the power performance of the engine was achieved when  $D_{m\_out} = 126$  mm and  $L_m = 436$  mm, details in Figure 74.

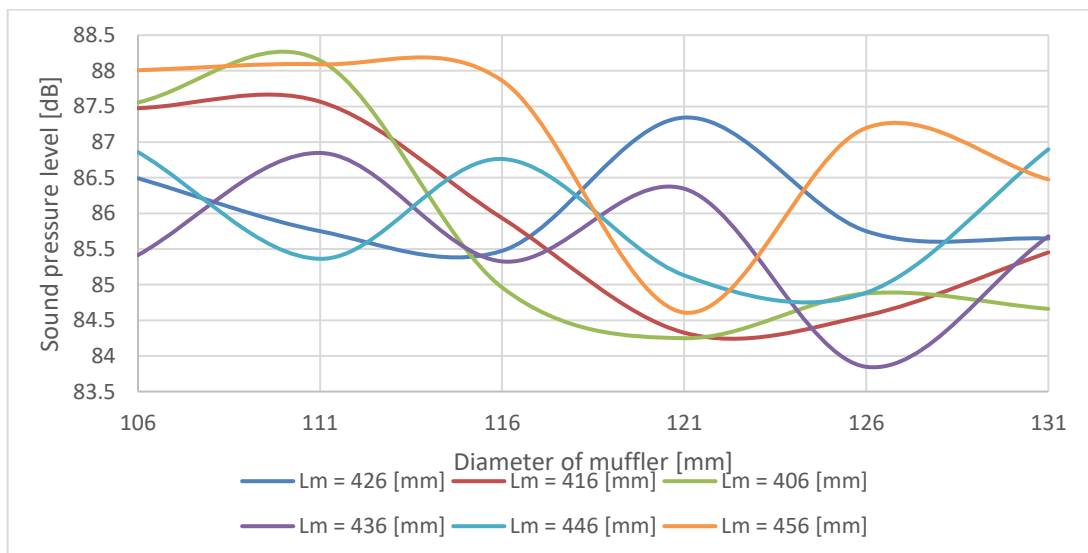


Figure 74 Results of variation of pipe length ( $L_m$ ) and the diameter of muffler volume ( $D_{m\_out}$ ) on the *SPL* at the diameter of perforated inner pipe  $D_{m\_in} = 47$  mm,  $n = 2000$  rpm.

Exhaust gas should also be led from the cylinder to the exhaust system smoothly, therefore, to maximize the engine power especially at high engine speeds, several suggestion were made for muffler dimensions to reach optimum value. Results are shown in figure 75.

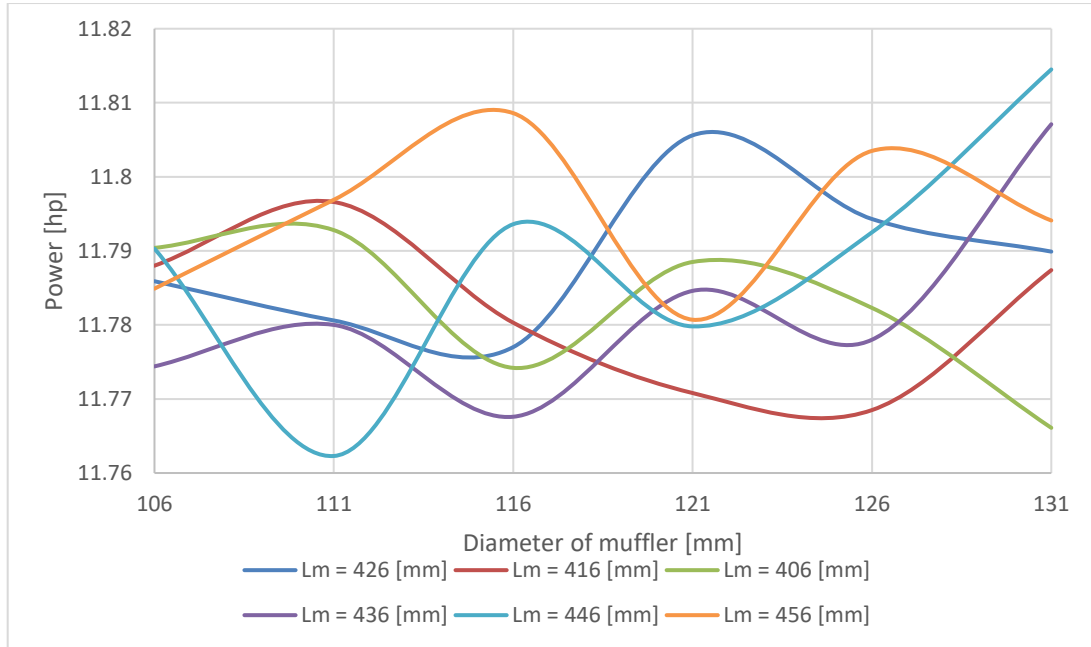


Figure 75 Results of variation of pipe length ( $L_m$ ) and the diameter of muffler volume ( $D_{m\_out}$ ) on  $FS$  engine power output at the diameter of perforated inner pipe  $D_{m\_in} = 47 \text{ mm}$ ,  $n = 2000 \text{ rpm}$ .

No significant effect was achieved for variation of the diameter of holes or diameter of perforated inner pipe inside or the length of the muffler on the engine torque as shown in figure 76.

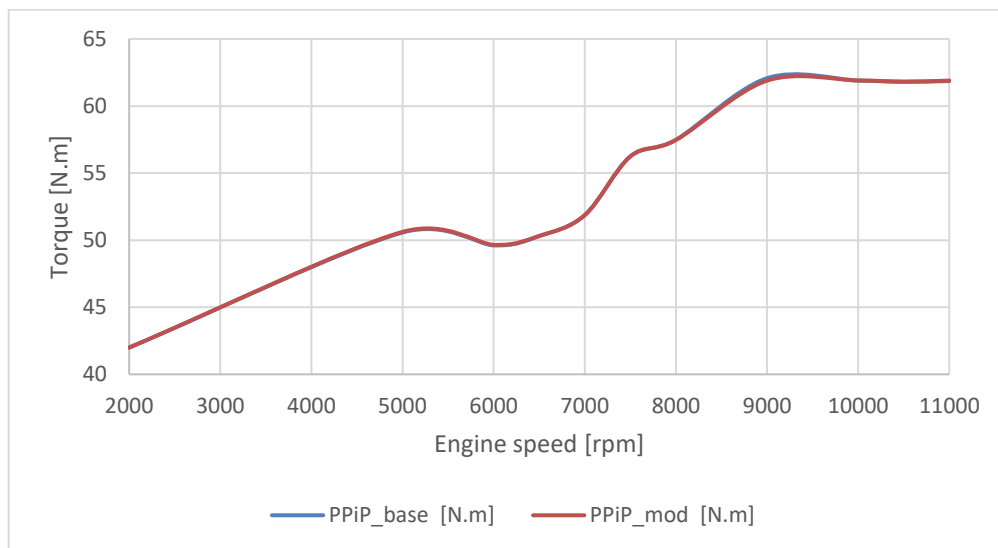


Figure 76 Comparison between base  $PPiP$  and modified (alternative)  $PPiP$  for torque measurement at different engine speed.

Other suggestions were made to improve sound pressure level. In figure 77 presents a comparison of engine sound pressure levels at a distance of  $1\text{ m}$  from the muffler cut-off when a base and a modified (alternative) muffler construction are used. Since this exciting source applied by the *FS* car engine to the muffler was sound pressure rather than vibration velocity when the muffler was connected with *FS* car. The simulation of flow noise propagation for base muffler, the discussion of their influencing factors, and the effectiveness of this combination theory in the field of flow noise in exhaust gas could reflect the practical condition.

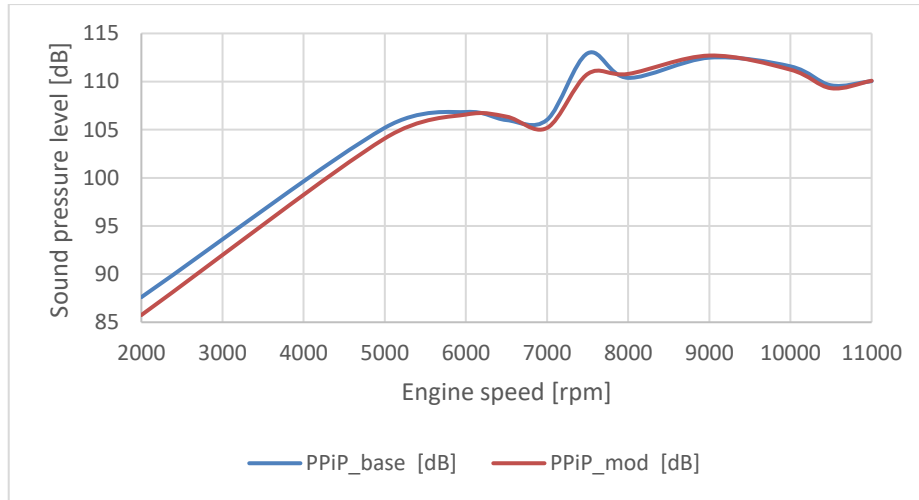


Figure 77 Comparison between sound pressure level in muffler with base *PPIp* and modified (alternative) *PPIp* at different engine speed.

Applied different exhaust muffler structure on the present *FS* engine has no influence on power output, since there is no catalytic convertor or intercooler to produce significant back pressure (as shown in figure 78).

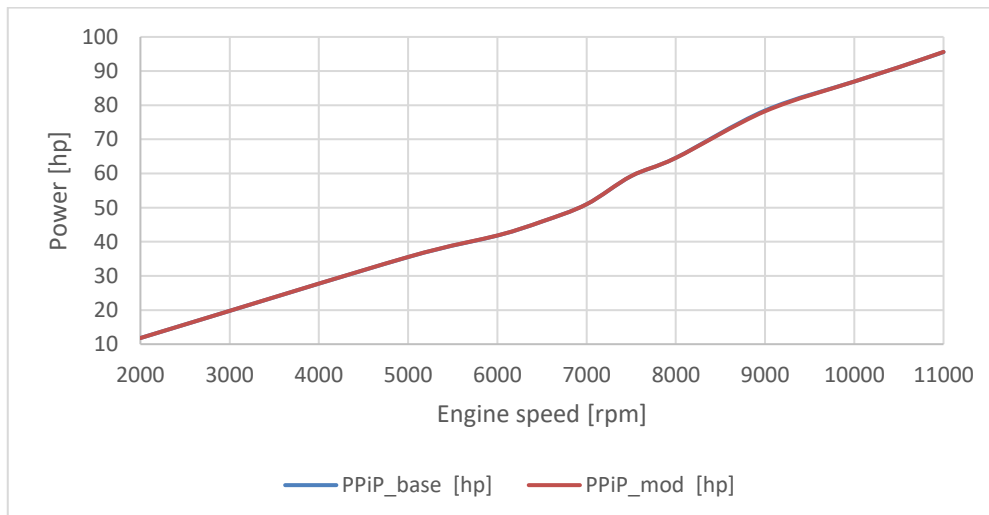


Figure 78 Comparison between power output from *FS* engine with base *PPIp* and modified *PPIp* at different engine speed.

The addition of sound-absorbing material allowed for a 15-20% reduction in *SPL* over the full engine speed range, as shown in figure 79. Meanwhile, the output flow resistance increases, lowering the engine's effective performance. Furthermore, during engine operation, the sound-absorbing material may get clogged with soot particles contained in the exhaust gases, resulting in an increase in resistance at the outlet and a worsening of the engine's operating conditions.

In the engine cylinders, the combustion process was modeled. It is also feasible to represent the production of soot in the applicable model, although for *SI* engines with external mixing, soot emissions may be ignored. Afterburning processes are not replicated in the exhaust system, and the temperature of exhaust gases changes due to heat exchange with the environment. A primary muffler also had a lower mass while maintaining adequate the lowest *SPL* at the output end, which was a multi-objective optimization challenge. The commercial software was used for all optimization stages.

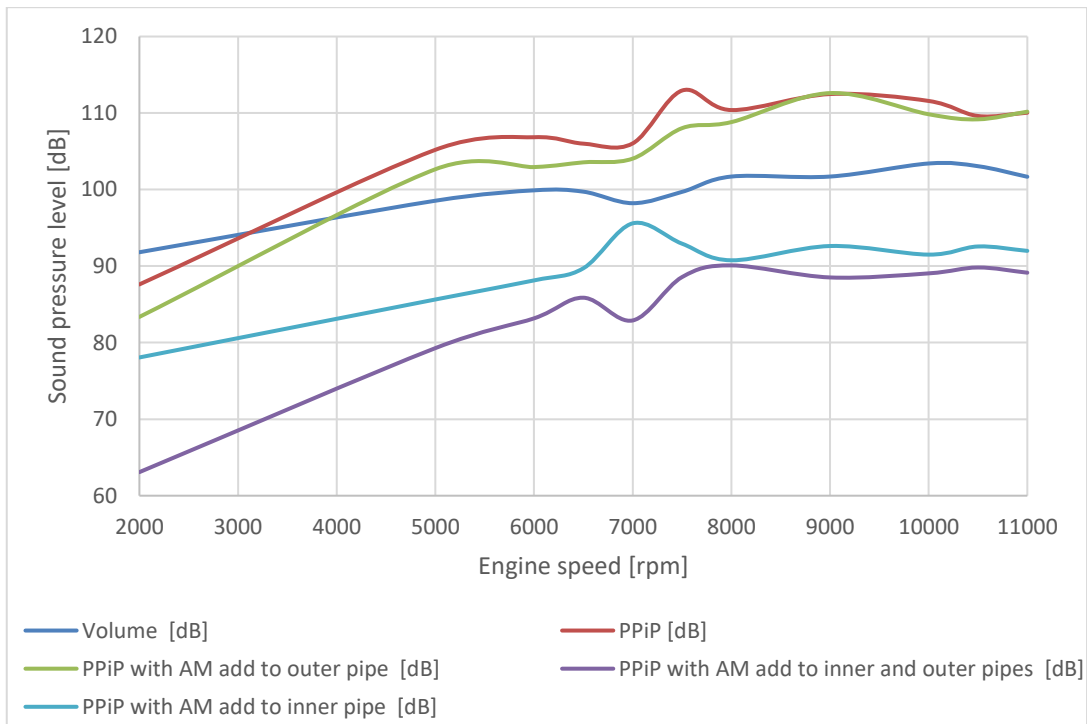


Figure 79 FS engine sound pressure level with different types of muffler materials; (AM) refer to absorbing material.

The parameters of AM: *porosity* = 0.9 and *flow resistivity* = 10000 N·s/m<sup>4</sup>. The material porosity represents the fraction of air space within the material (0 to 1). This will be a function of the packing density of the material. For example, a Material Porosity of 0.9 defines that 10% of the volume is filled with material and 90% is space for the gases.

The described calculation method is compared to experiments in figure 81. For the standard sound pressure measurements, only amplitude calibration is sufficient and the fluctuating pressures measured at each position. Assuming that we have plane waves in the muffler duct, then the sound pressure amplitude will be constant over the duct cross section and the sound pressure is

measured by all microphones. The transmission loss of a muffler mounted with a homogeneous perforated tube has been measured in a quasi-reflection-semi-free terminated measurement tube driven with white noise from loudspeaker in line. The absorber has been mounted with its surface in the wall plane of the muffler shell. The two-load experimental test set up as shown in figure 80.

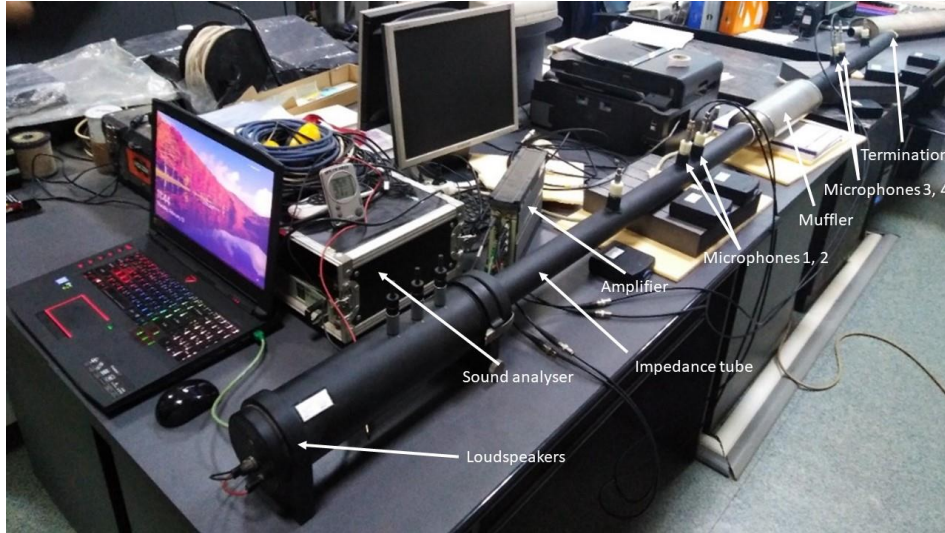


Figure 80 Muffler test rig.

A rigorous two-load approach is adopted to analyze the acoustic performance of a cylindrical muffler whose walls are treated with a locally reacting absorbent liner. The expansion chamber is separated from the central airway which contain a uniform main gas flow by a perforated cylindrical tube. The effect of the perforated center tube is modelled as a partially transmitting surface characterized by the boundary conditions.

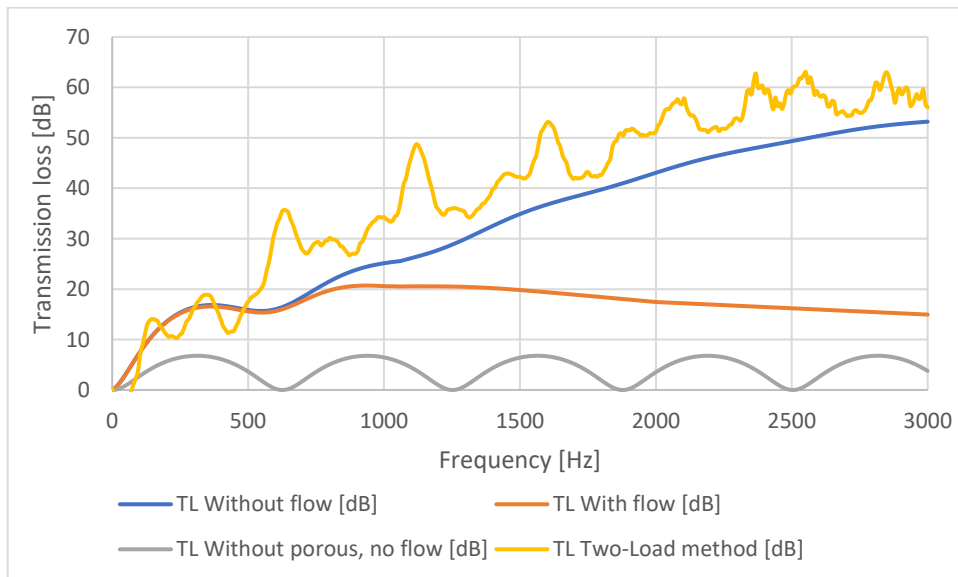


Figure 81 Comparison of Transmission loss calculated for several cases.

Figure 81 presents a comparison of experimental and numerical techniques by concentrating on the transmission loss result of the muffler over frequency. Hybrid mufflers are usually effective in both the low and high frequency ranges. The exhaust flow field was addressed differently using analytical methods, the results include 4 cases:

- Case-1: Indicates the  $TL$  calculated by the analytical approach, based on  $ID$  wave model without flow.
- Case-2: Indicates the  $TL$  calculated by the analytical approach,  $ID$  wave model with flow.
- Case-3: Indicates the  $TL$  calculated by the analytical approach,  $ID$  wave model of the muffler volume (without  $PPiP$ ).
- Case-4: Presents the  $TL$  graph measured by two-load method and performed without the flow.

The effect of adopting  $PPiP$  prior to an experiment was evaluated by estimating the transmission loss using an *ASTM E2611* standard algorithm to post-process the transfer function of the output from the approach of two-load and two types of terminations. To avoid mismatching, the impedance tube must be set to *zero dB* before beginning the experiment. Any termination may theoretically be utilized, but extremely reflect action termination is not advised. If the termination is highly reflective and the signal-to-noise ratio is poor, large random errors may be generated, contaminating the experimental findings. The cut-off frequency in the current expansion chamber muffler is calculated at a frequency of  $3000\text{ Hz}$ , which is obtained by applying the cut-off frequency equation  $F_c = 1,84 \frac{c}{\pi d}$ , where  $d$  is the muffler diameter and  $c$  is the speed of sound. In experimental result the frequency ranges from  $400\text{-}700\text{ Hz}$ , the maximum attenuation was  $35\text{ dB}$  for perforations part ( $PPiP$ ), as well as for the frequency range  $2400\text{-}2600\text{ Hz}$  has reached a maximum  $TL$  of  $61\text{ dB}$ . In fact. However,  $TL$  for the basic (current) hole diameter of the FS muffler at high porosity appears to diminish, which is agree with (Lee and Selamet, 2006). The minor difference between the muffler body geometry with perforated tube (porous) inside and without was revealed in the numerical results.

The difference in geometry between the two, but the geometry without perforated tube of normal mode goes far beyond indicating that this does not improve the transmission loss feature.

Finally, it is to be mentioned that the proposed method (the result related to the case 1 and case 2) are not applicable for porous materials with low flow resistivity and/or small thickness ( $d$ ). The acoustic resistance depends on the flow through the perforate holes. On the other hand, perforates can deteriorate the engine performance, if badly designed, by increasing the flow back pressure.

Figure 82 shows that a muffler with fitted  $PPiP$  and  $AM$  to the outer pipe is the best solution for maintaining power output, although for  $n > 5000\text{ rpm}$ , the power output stays greater than with a volume muffler.

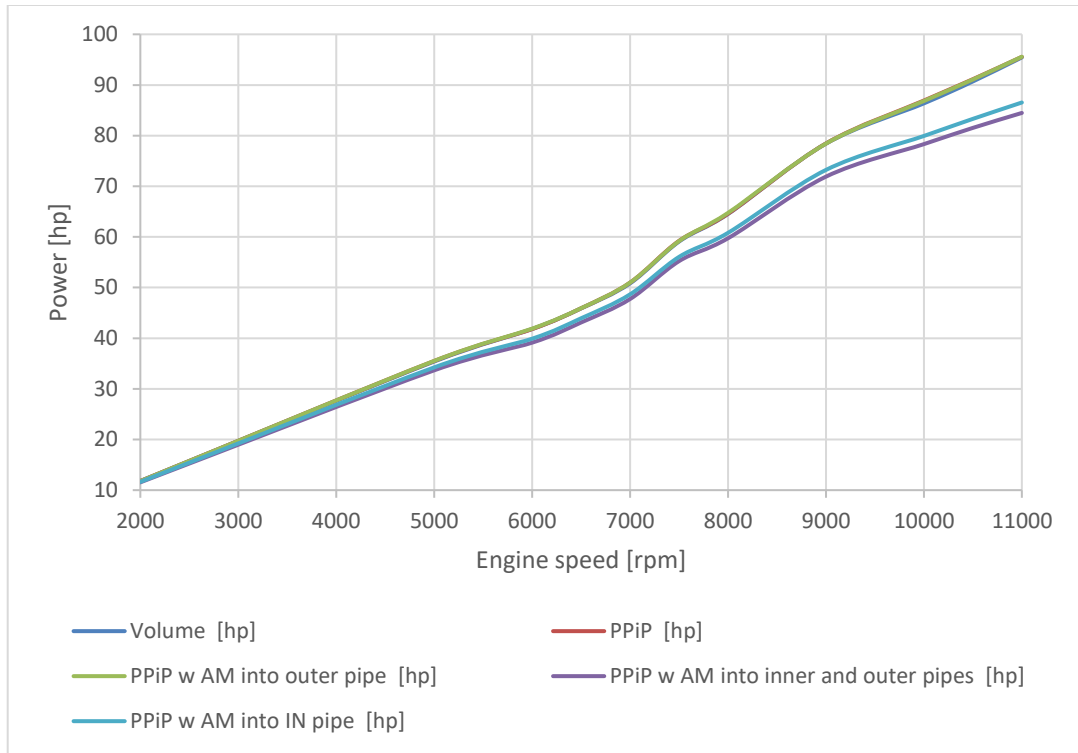


Figure 82 *FS* engine power output with different types of muffler materials

## 6. THESES – NEW SCIENTIFIC RESULTS

- T1. As a result of my investigations, I proposed and utilized a complex simulation technique which connects the advantages both of the *1D* acoustic simulation and *3D CFD* simulation. Based on the combined calculation process I was able to handle the acoustic performance of the intake and exhaust system components of a race car engine and the procedure can be repeated for any other flow related problem.
- T2. An extensive sensitivity analysis based on the proposed technique from *T1* was performed in order to obtain the best muffler geometry for the best acoustic performance. I proved that for the analysed geometry parameters of the muffler with the used parameter ranges of  $L_m$  (length of pipe),  $D_{m\_out}$  (muffler outer diameter)  $D_{m\_in}$  (perforated pipe diameter),  $D_{hole}$  (perforation hole diameter) an optimum solution related to the best acoustic performance (orifice noise) can be selected precisely for the *FS* car.
- T3. As result of my investigations I showed that the proposed combined simulation method is able to optimize engine parameters (such as brake specific fuel consumption, engine power and torque) through muffler geometry modification, despite the main focus is on the orifice noise reduction.
- T4. I proved through my investigations that by using the Johnson–Champoux–Allard (*JCA*) model in case of absorptive material in the muffler, the simulation with the given parameters delivers sufficient results for the transmission loss of a muffler compared to the test rig measurement. With the proposed simulation method incl. *JCA*, I proved that the transmission loss over the frequency of a muffler can be predicted in a good confidence range.



## 7. SUMMARY

An improved method of modelling intake system and hybrid muffler were presented in this research to enhance engine power output, accelerate the  $TL$  prediction using two-load method and software based on finite element method ( $FEM$ ).

- In this research, it has been shown that the gas flow in intake system effects on the  $FS$  engine performance and acoustic behaviour. The proposed calculation methods are tested numerically and by measurements. The team from University of Miskolc improved the car's air intake system using 1D-AVL Boost within the parametric Fire software Workbench environment.  $FS$  regulations limit the minimum diameter of the restrictor to  $20\text{ mm}$ , which regulates the maximum intake mass flow rate. The plenum, downstream of the restrictor, directly influences the amount of fresh air reaching the cylinders. A plenum that is too large causes the motor to react too slowly to the accelerator and, in combination with short suction pipes, triggers the engine to develop sufficient torque only at high rotation speeds. A too small plenum behaves oppositely. Using the equation for the intake runner length, the length of the ideal runner was determined to be approximately  $250\text{ mm}$  and with a diameter of  $32\text{ mm}$ . Hence, design  $II$  of Formula Student Racing is a better choice.
- Several calculation techniques were done to calculate transmission loss in different cases for the muffler, while planewave propagation was applied from generator using two-load method for transmission loss result validation of muffler. These can be considered as an accurate check of the analysis carried out in this work. It is worth pointing out that this work may also serve as a benchmark solution for approximate and numerical techniques used for dealing with hybrid muffler problems.

### ACKNOWLEDGEMENTS

First and foremost, praises and thanks to the God, the Almighty, for His blessings throughout my research work to complete the research successfully.

I would like to express my deep and sincere gratitude to my supervisor, Dr. Jolics Karoly, PhD, Associate Professor in the Faculty of Mechanical Engineering and Informatics, University of Miskolc, for giving me the opportunity to do research and providing invaluable guidance throughout this research. He has taught me the methodology to carry out the research and to present the research works as clearly as possible.

I would like to say thanks to my research colleagues, Dr. Andrei Zelentsov and Dr. Salah Amroune for their scientific contributions.

I am extending my thanks to the Head of Doctoral School Prof. Dr. Gabriella Bognár and Head of Department of Fluid and Heat Engineering Dr. Bencs Peter for their genuine support throughout this research work.

I would like to express my gratitude to the Formula Racing Miskolc team for assistance with design technique.

Finally, I would like to thank my family and my friends for giving me the moral support that helped me to carry out the thesis with the same zeal with which I had started it.

Köszönöm!

## REFERENCE

- [1] Krebber, W., Genuit, K., & Sottek, R. (2002). *Sound quality of vehicle exterior noise*. In *Proceeding of Forum Acusticum*.
- [2] García, A., & Faus, L. (1991). *Statistical analysis of noise levels in urban areas*. *Applied Acoustics*, v. 34, n. 4, 227 – 247.
- [3] Juraga, I., Paviotti, M., & Berger, B. (2015). *The environmental noise directive at a turning point*. In *Proceedings of EuroNoise Conference (2015, Maastricht, The Netherlands)*, pp. 1041–44.
- [4] Mohamad, B., Karoly, J., & Zelentsov, A. (2020). *CFD Modelling of Formula Student Car Intake System*. *Facta Universitatis, Series: Mechanical Engineering*. 18, (1), pp. 153-163. <https://doi.org/10.22190/FUME190509032M>.
- [5] Adámek, L. (2011). *Single cylinder SI engine for Formula Student*. Brno: Vysoké učení technické v Brně, Fakulta strojního inženýrství, 2011. 102 s. Vedoucí diplomové práce Ing. David Svída.
- [6] Blair, G.P. (1998). *Empiricism and Simulation in the Design of the High Performance Four-Stroke Engine*. The Queen's University of Belfast: Society of Automotive Engineers, Inc.
- [7] Institute of Mechanical Engineers. (2019). *Formula SAE rules*. [www.formulastudent.com](http://www.formulastudent.com).
- [8] Ricardo, M. B., Apostolos, P., & Yang, M. Y. (2017). *Overview of boosting options for future downsized engines*. –*Science China Technological Sciences*, 2017, 54, 318-331.
- [9] MAHLE International GmbH. (2017). <http://www.mahle-aftermarket.com>.
- [10] Martyr, A.J., & Rogers, D.R. (2021). *Engine Testing*. Fifth Edition, Butterworth-Heinemann, Oxford. <https://doi.org/10.1016/C2019-0-02809-9>.
- [11] Montenegro, G., Onorati, A., Della Torre, A., & Torregrosa, A. (2011). *The 3D-cell approach for the acoustic modeling of after-treatment devices*. *SAE Int. J. Engines*, 2(4):2519–2530.
- [12] Tiikoja, H., Rämmal, H., Åbom, M., & Bodén, H. (2011). *Investigations of Automotive Turbocharger Acoustics*. *SAE International Journal of Engines*, 4:2531-2542. doi:10.4271/2011-24-0221.
- [13] Montenegro, G., Della Torre, A., Onorati, A., Fairbrother, R., Elnemr, Y., & Dolinar, A. (2012). *Quasi-3D Acoustic Modelling of Common Intake and Exhaust Components*. ICSV19, Vilnius, Lithuania, July 8–12, 2012.
- [14] Eric Brouillard, Brian Burns, Naeem Khan, & John Zalaket. (2011). *The Design and Manufacturing of an Intercooler Assembly with R-134a Integration*. Prestige Worldwide.
- [15] Simon Reifarth. (2010). *EGR-Systems for Diesel Engines*. KTH Industrial Engineering and management. 1400-1179.
- [16] DieselNet Technology Guide. (2006) *Engine Design for Low Emissions*. [www.dieselnets.com](http://www.dieselnets.com). Ecopoint Inc.

- [17] Münz, S., Römuss, C., Schmidt, P., Brune, K.-H., & Schiffer, H.-P. (2008). *Diesel Engines with Low-Pressure Exhaust-Gas Recirculation – Challenges for the Turbocharger*, MTZ.
- [18] Mostafa Ranjbar, Hakan Arslan & Mehmet Orak. (2018) *Effect of Geometry Modification on Sound Transmission Loss in Multi-Chamber Muffler*. The 8th International Conference on Acoustics & Vibration (ISAV2018), Shahid Beheshti University, Iran, 4-5 Dec. 2018.
- [19] Tao, Z. & Seybert, A. F. (2003). *A Review of Current Techniques for Measuring Muffler Transmission Loss*. Society of Automotive Engineers, Inc.
- [20] Mohamad, B., & Zelentsov, A. (2019). *1D and 3D Modeling of Modern Automotive Exhaust Manifold*. Journal of the Serbian Society for Computational Mechanics. 13, (1), pp.80-91. DOI:10.24874/jsscsm.2019.13.01.05.
- [21] Linda Rosencrance. (2019). *Definition of attenuation*. <https://searchnetworking.techtarget.com/definition/attenuation>.
- [22] AVA Consulting. (2018). *Acoustic Transfer Function Measurements*. <https://www.ava-consulting.co.uk/our-services/acoustic-transfer-function-measurements>.
- [23] Ferziger J. H., & Perić, M. (2002). *Computational Methods for Fluid Dynamics*. Springer, third, rev. edition.
- [24] AVL BOOST-SID. (2017). *Linear Acoustics*, user Manual.
- [25] Hyoun-Jin Sim, Sang-Gil Park, Yong-Goo Joe & Jae-Eung Oh. (2008). *Design of the intake system for reducing the noise in the automobile using support vector regression*, Journal of Mechanical Science and Technology, 22, pp. 1121-1131, DOI: 10.1007/s12206-008-0306-z.
- [26] Munjal, M.L. (1987). *Acoustics of Ducts and Muffler*, Wiley, New York.
- [27] Mohamad, B., Karoly, J., & Kermani, M. (2019). *Exhaust System Muffler Volume Optimization of Light Commercial passenger Car Using Transfer Matrix Method*. International Journal of Engineering and Management Sciences. 4, (1). Pp. 132-139. DOI: 10.21791/IJEMS.2019.1.16.
- [28] Kumar S. (2007). *Linear Acoustic Modelling And Testing of Exhaust Mufflers*. Master of Science Thesis, KTH, Sweden.
- [29] Tiikoja, H. (2012). *Acoustic Characterization of Turbochargers and Pipe Terminations*. TRITA-AVE 2012:07. 1651-7660.
- [30] Lavrentjev, J., Åbom, M., & Bodén, H., (1995). *A measurement Method for Determining the Source Data of Acoustic Two-Port Sources*. Journal of Sound and Vibration 183(3): 517-531.
- [31] Dokumaci, E. (2014). *On the effect of viscosity and thermal conductivity on sound propagation in ducts: A re-visit to the classical theory with extensions for higher order modes and presence of mean flow*. Journal of Sound and Vibration, 333, 21, pp. 5583–5599.
- [32] Allam, S, Åbom, M.(2005). *Acoustic modelling and testing of diesel particulate filters*. J Sound Vib. 288: 255–273.
- [33] Hou, X., Du, S., Liu, Z., Guo, J., & Li, Z. (2017). *A transfer matrix approach for structural–acoustic correspondence analysis of diesel particulate filter*. Advances in Mechanical Engineering. <https://doi.org/10.1177/1687814017722495>.
- [34] Simon Reifarth. (2014). *Efficiency and Mixing Analysis of EGR-Systems for Diesel Engines*. ISRN/KTH/MMK/R-14/01-SE.1400-1179.
- [35] Moran, M.J. & Shapiro, H. N. (1998). *Fundamentals of engineering thermodynamics: SI version*, John Wiley.
- [36] Nyerges, A., & Zöldy, M. (2020). *Verification and Comparison of Nine Exhaust Gas*

- Recirculation Mass Flow Rate Estimation Methods*. Sensors. 20, (24):7291. <https://doi.org/10.3390/s20247291>.
- [37] Amares, S., Sujatmika, E., Hong, T. W. Durairaj R., & Hamid. H. S. H. B. (2017). *A Review: Characteristics of Noise Absorption Material*. IOP Conf. Series: Journal of Physics: Conf. Series 908 (2017) 012005.
- [38] MANN-HUMMEL develops innovative solutions. (2010). *Next generation of intake manifolds*. <https://www.mann-hummel.com/en/research-and-development/future-trends/next-generation-of-intake-manifolds/>
- [39] Pricken, F. (2000). *Active Noise Cancellation in Future Air Intake Systems*. SAE Technical Paper 2000-01-0026. <https://doi.org/10.4271/2000-01-0026>.
- [40] Gras sound & vibration. (2020). *Acoustic test types within exhaust noise testing*. <http://www.gras.dk/industries/automotive/exhaust-noise>.
- [41] Braun, M. E. Walsh, S.J., Horner, J.L. & Chuter, R. (2013). *Noise source characteristics in the ISO 362 vehicle pass-by noise test: Literature review*. Applied Acoustics, 74, 1241–1265.
- [42] Gras sound & vibration. (2020). *Vehicle Interior NVH Testing*. <https://www.grasacoustics.com/component/sppagebuilder/?view=page&id=1007>.
- [43] Fleszar, A.R., van der Linden, P.J.G., Johnson, J.R., & Grimmer, M.J. (2001). *Combining vehicle and test-bed diagnosis information to guide vehicle development for pass-by noise*. SAE Technical Paper Series 2001-01-1565; 2001.
- [44] Winterbone, D.E., & Pearson, R.J. (2000). *Theory of engine manifold design: wave action methods for IC engines*. Professional Engineering Publ. London, ISBN:1860582095.
- [45] Vaz, J., Machado, A., Martinuzzi, R., & Martins, M. (2017). *Design and Manufacture of a Formula SAE Variable Intake Manifold*. SAE Technical Paper 2017-36-0181. <https://doi.org/10.4271/2017-36-0181>.
- [46] Kenji, T. (2011). *Engine Intake Control Device*. Patent JP2011064139, Honda Motor.
- [47] Joo, J. Y. (2009). *Variable Intake Manifold*. Patent KR20090065380, Hyundai Motor Company.
- [48] Masahiko, K. (2006). *Variable Intake System*. Patent JP08338252, Mitsubishi Motors Corp.
- [49] Stefan, L. (2006). *Suction System for Supplying an Internal Combustion Engine with Combustion Air*. Patent EP1049859, Volkswagen AG.
- [50] Pascal, C., (2006). *Variable intake system for combustion engines and pipe element for such a device*. Patent EP1083310, Renault.
- [51] Heisler, H. (1995). *Advanced engine technology*. First Edition. Warrendale: SAE International. p. 794. ISBN 1-56091-734-2.
- [52] Mohamad, B., & Amroune, S. (2019). *The analysis and effects of flow acoustic in a commercial automotive exhaust system*. Advances and Trends in Engineering Sciences and Technologies III: Proceedings of the 3rd International Conference on Engineering Sciences and Technologies (ESaT 2018), September 12-14, 2018, High Tatras Mountains, Tatranské Matliare, Slovak Republic. pp. 197-202.
- [53] Mohamad, B., Karoly, J., Zelentsov, A. (2019). *Investigation and optimization of the acoustic performance of formula student race car intake system using coupled modelling techniques*, Design of Machines and Structures, 9, (1), pp.13-23. DOI: 10.32972.dms.2019.002.
- [54] Autozine. (2011). *The First Continuously Variable Intake System in the New Eight-Cylinder Engine from BMW*.

- [55] Mohamad, B. (2019). *Design and Optimization of Vehicle Muffler Using The Ffowcs Williams and Hawkings Model*. Machine Design Journal, 11, (3), pp. 101-106. DOI: 10.24867/MD.11.2019.3.101-106.
- [56] Claywell, M., Horkheimer, D. (2006). *Improvement of Intake Restrictor Performance for a Formula SAE Race Car through 1D & Coupled 1D/3D Analysis Methods*. SAE Motorsports Engineering Conference & Exposition, December 2006. SAE 2006-01-3654.
- [57] Mohamad, B., Karoly, J., Zelentsov, A. (2019). *Hangtompító akusztikai tervezése hibrid módszerrel*. Multidiszciplináris Tudományok, 9, (4), pp. 548-555. DOI: <https://doi.org/10.35925/j.multi.2019.4.58>.
- [58] Мохамед, Б., Кароли, Я., & Зеленцо, А. (2020). *Трёхмерное моделирование течения газа во впускной системе автомобиля «Формулы Студент»* Журн. Сиб. федер. ун-та. Техника и технологии, 13, (5), pp. 597-610. DOI: 10.17516/1999-494X-0249.
- [59] Mohamad, B., Ali, M.Q., Neamah, H.A., Zelentsov, A., Amroune, S. (2020). *Fluid dynamic and acoustic optimization methodology of a formula-student race car engine exhaust system using multilevel numerical CFD models*. Diagnostyka, 21, (3), pp. 103-113. DOI:10.29354/diag/126562.
- [60] AVL List GmbH. (2014). *Guidebook*. Graz, Austria.
- [61] Perry, R. H. (1984). *Perys Chemical Engineers. Handbook*, McGraw-Hill, New York, 6<sup>th</sup> edition. [https://www.autozine.org/technical\\_school/tech\\_index.html](https://www.autozine.org/technical_school/tech_index.html)
- [62] Mohamad, B., (2019). *A review of flow acoustic effects on a commercial automotive exhaust system*. Mobility & Vehicle Mechanics Mobility & Vehicle Mechanics, 45, (2), pp 1-14. DOI:10.24874/mvm.2019.45.02.01.
- [63] Mohamad, B., (2019). *A review of flow acoustic effects on a commercial automotive exhaust system-methods and materials*. Journal of Mechanical and Energy Engineering, 3, (2), pp. 149-156, DOI:10.30464/jmee.2019.3.2.149.
- [64] De Risi, A., Zecca, R., & Laforgia, D. (2000). *Optimization of a Four Stroke Engine by Means of Experimental and 1-D Numerical Analysis*. SAE Technical Paper. 2000-01-0566. <https://doi.org/10.4271/2000-01-0566>.
- [65] How Heoy Geok, Taib Iskandar Mohamad, Shahrir Abdullah, Yusoff Ali, & Azhari Shamsudeen. (2009). *Experimental Investigation of Performance and Emissions of a Sequential Port Injection Compressed Natural Gas Converted Engine*. SAE Technical Papers. 2009-32-0026.
- [66] Mohamad, B., Karoly, J., Zelentsov, A., & Amroune, S. (2020). *A hybrid method technique for design and optimization of Formula race car exhaust muffler*. International Review of Applied Sciences and Engineering, 11, (2), pp. 174–180. <https://doi.org/10.1556/1848.2020.20048>.
- [67] Mohamad, B., Karoly, J., Zelentsov, A., & Amroune, S. (2021). *A Comparison Between Hybrid Method Technique and Transfer Matrix Method for Design Optimization of Vehicle Muffler*. FME Transactions. 49, (2), pp. 494-500. DOI: 10.5937/fme2102494M.
- [68] Tatschl, R. Schneider, J., Basara, D., Brohmer, A., Mehring, A., & Hanjalic, K. (2005). *Progress in the 3D-CFD calculation of the gas and water side heat transfer in engines*. in Verfahren 10 Tagung der Arbeitsprozess des Verbrennungsmotors (Proc. 10th Meeting on the Working Process of the Internal Combustion Engine), Graz.
- [69] Tatschl, R., Basara, B., Schneider, J., Hanjalic, K., Popovac, M., Brohmer, A., & Mehring, J. (2006). *Advanced Turbulent Heat Transfer Modeling for IC-Engine Applications Using AVL FIRE*. Proceedings of International Multidimensional Engine Modeling User's Group Meeting. Detroit, USA.

- 
- [70] Hanjalić, K., Popovać, M., Hadziabdić, M. (2004). *A Robust Near-Wall Elliptic-Relaxation Eddy-Viscosity Turbulence Model for CFD*. Int. J. Heat Fluid Flow, 25, 897-901.
- [71] Popovać, M., & Hanjalić, K. (2005). *Compound Wall Treatment for RANS Computation of Complex Turbulent Flow*. Proc. 3rd M.I.T. Conference, Boston, USA.
- [72] Merker, G., Schwarz, Ch., & Teichmann, R. (2019). *Grundlagen Verbrennungsmotoren: Funktionsweise, Simulation, Messtechnik (Fundamentals of Internal Combustion Engines: Mode of Operation, Simulation, Measurement Technology)*, 9th ed.; Springer: Wiesbaden, 1117 p.
- [73] Basshuysen, R., & Schäfer, F. (2007). (Hrsg.) *Handbuch Verbrennungsmotor*. 4. Auflage. Vieweg und Sohn Verlag. Wiesbaden, 1032 p.
- [74] Kavtaradze, R.Z., Onishchenko, D.O., Zelentsov A.A., & Sergeev S.S. (2009). *The influence of rotational charge motion intensity on nitric oxide formation in gas-engine cylinder*. Int. J. Heat Mass Tran., 52, 4308–4316. DOI: 10.1016/j.ijheatmasstransfer.2009.03.060.
- [75] Prakash Chandra Mishra, Sourav Kumar Kar, & Harshit Mishra. (2018). *Effect of perforation on exhaust performance of a turbo pipe type muffler using methanol and gasoline blended fuel: A step to NO<sub>x</sub> control*. Journal of Cleaner Production (183)869-879.
- [76] Mohamad, B., Szepesi, G., & Bolló, B. (2017). *Combustion Optimization in Spark Ignition Engines*. Multi-Science - XXXI. microCAD Scientific Conference. University of Miskolc-Hungary.
- [77] Mohamad, B., Szepesi, G., & Bolló, B. (2018). *Review Article: Effect of Ethanol-Gasoline Fuel Blends on the Exhaust Emissions and Characteristics of SI Engines*. Lecture Notes in Mechanical Engineering. 29-41.
- [78] Mohamad, B., Szepesi, G., & Bolló, B. (2017). *Review Article: Modelling and Analysis of a Gasoline Engine Exhaust Gas Systems*. International Scientific Conference on Advances in Mechanical Engineering. University of Debrecen-Hungary.
- [79] Ebrahim Taban, Ali Khavanin, Ahmad Jonidi Jafari, Mohammad Faridan & Ali Kazemi Tabrizi. (2019). *Experimental and mathematical survey of sound absorption performance of date palm fibers*. Heliyon, (5). doi: 10.1016/j.heliyon.2019.e01977.
- [80] Allard, J.F., & Champoux, Y. (1992). *New empirical equations for sound propagation in rigid frame fibrous materials*. The Journal of the Acoustical Society of America 91, 3346. doi: 10.1121/1.402824.
- [81] Allard, J.F., & Daigle, G. (1994). *Propagation of Sound in Porous media: Modeling Sound, Absorbing Materials*, ASA.
- [82] Lee I., & Selamet A. (2006). *Impact of perforation impedance on the transmission loss of reactive and dissipative silencers*. The Journal of the Acoustical Society of America. 120, 3706. <https://doi.org/10.1121/1.2359703>.

**LIST OF PUBLICATIONS RELATED TO THE TOPIC OF THE RESEARCH FIELD**

- (1) Mohamad, B., Szepesi, G., & Bolló, B. (2017). *Combustion Optimization in Spark Ignition Engines*. Multi-Science - XXXI. microCAD Scientific Conference. University of Miskolc-Hungary. DOI:10.26649/musci.2017.065.
- (2) Mohamad, B., Szepesi, G., & Bolló, B. (2017). *Review Article: Modelling and Analysis of a Gasoline Engine Exhaust Gas Systems*. International Scientific Conference on Advances in Mechanical Engineering. University of Debrecen-Hungary.
- (3) Mohamad, B., Szepesi, G., & Bolló, B. (2018). *Review Article: Effect of Ethanol-Gasoline Fuel Blends on the Exhaust Emissions and Characteristics of SI Engines*. Lecture Notes in Mechanical Engineering. 29-41. [https://doi.org/10.1007/978-3-319-75677-6\\_3](https://doi.org/10.1007/978-3-319-75677-6_3)
- (4) Mohamad, B., & Amroune, S. (2019). *The analysis and effects of flow acoustic in a commercial automotive exhaust system*. Advances and Trends in Engineering Sciences and Technologies III: Proceedings of the 3rd International Conference on Engineering Sciences and Technologies (ESaT 2018), September 12-14, 2018, High Tatras Mountains, Tatranské Matliare, Slovak Republic. pp. 197-202.
- (5) Mohamad, B., Karoly, J., & Kermani, M. (2019). *Exhaust System Muffler Volume Optimization of Light Commercial passenger Car Using Transfer Matrix Method*. International Journal of Engineering and Management Sciences. 4, (1). Pp. 132-139. DOI: 10.21791/IJEMS.2019.1.16.
- (6) Mohamad, B., Karoly, J., Zelentsov, A. (2019). *Investigation and optimization of the acoustic performance of formula student race car intake system using coupled modelling techniques*, Design of Machines and Structures, 9, (1), pp.13-23. DOI: 10.32972.dms.2019.002.
- (7) Mohamad, B., (2019). *A review of flow acoustic effects on a commercial automotive exhaust system*. Mobility & Vehicle Mechanics Mobility & Vehicle Mechanics, 45, (2), pp 1-14. DOI:10.24874/mvm.2019.45.02.01.
- (8) Mohamad, B., (2019). *A review of flow acoustic effects on a commercial automotive exhaust system-methods and materials*. Journal of Mechanical and Energy Engineering, 3, (2), pp. 149-156, DOI:10.30464/jmee.2019.3.2.149.
- (9) Mohamad, B. (2019). *Design and Optimization of Vehicle Muffler Using The Ffowcs Williams and Hawkings Model*. Machine Design Journal, 11, (3), pp. 101-106. DOI: 10.24867/MD.11.2019.3.101-106.
- (10) Mohamad, B., Zelentsov, A. (2019). *1D and 3D Modeling of Modern Automotive Exhaust Manifold*. Journal of the Serbian Society for Computational Mechanics, 13, (1), pp.80-91. DOI: 10.24874/jsscsm.2019.13.01.05.



---

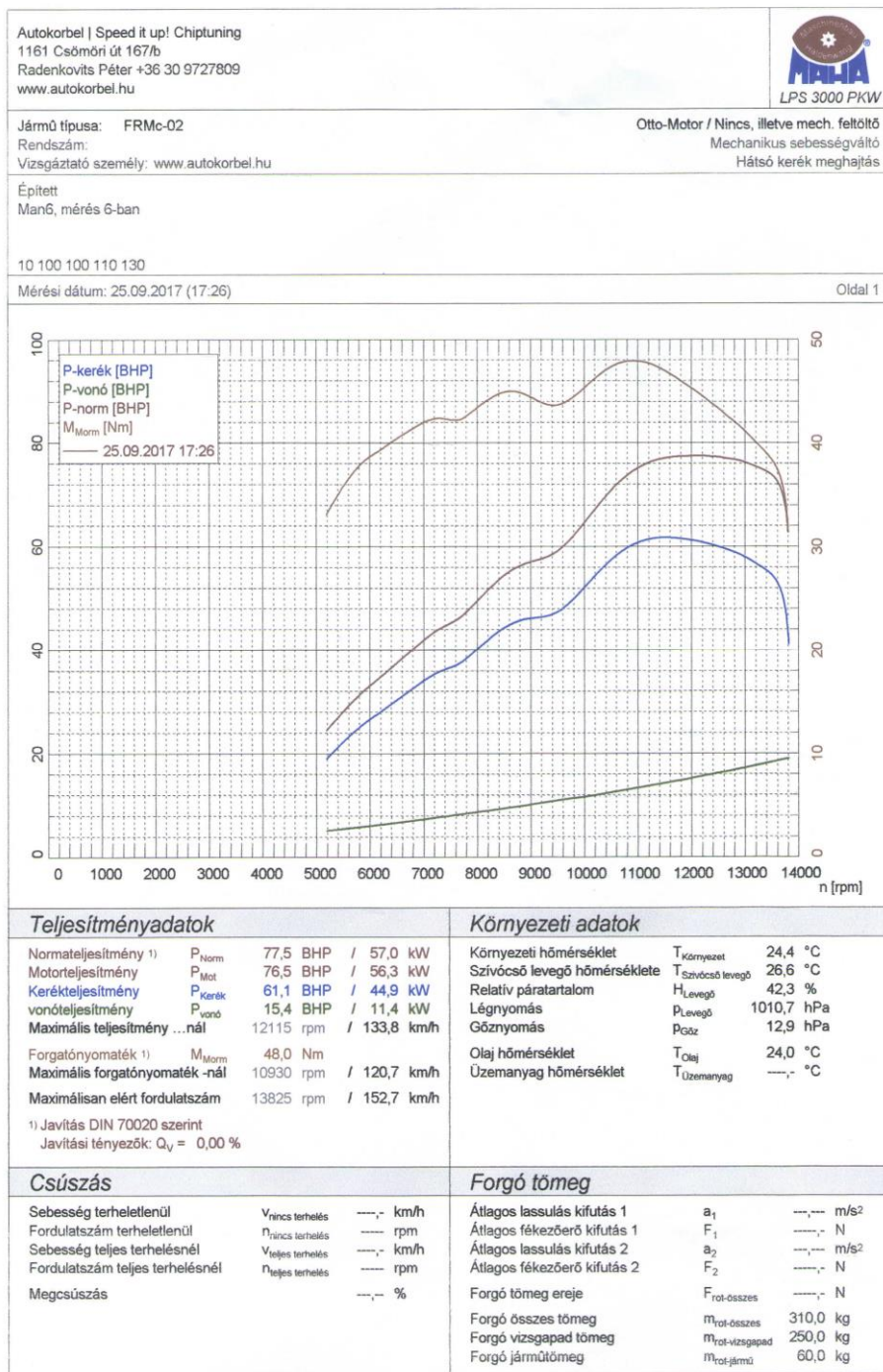
LIST OF PUBLICATIONS RELATED TO THE TOPIC OF THE RESEARCH FIELD

---

- (11) Mohamad, B., Karoly, J., Zelentsov, A. (2019). *Hangtompító akusztikai tervezése hibrid módszerrel*. Multidiszciplináris Tudományok, 9, (4), pp. 548-555. DOI: <https://doi.org/10.35925/j.multi.2019.4.58>.
- (12) Mohamad, B., Karoly, J., & Zelentsov, A. (2020). *CFD Modelling of Formula Student Car Intake System*. Facta Universitatis, Series: Mechanical Engineering, 18, (1), pp. 153-163. <https://doi.org/10.22190/FUME190509032M>.
- (13) Мохамед, Б., Кароли, Я., & Зеленцо, А. (2020). *Трёхмерное моделирование течения газа во впускной системе автомобиля «Формулы Студент»* Журн. Сиб. федер. ун-та. Техника и технологии, 13, (5), pp. 597-610. DOI: 10.17516/1999-494X-0249.
- (14) Mohamad, B., Ali, M.Q., Neamah, H.A., Zelentsov, A., Amroune, S. (2020). *Fluid dynamic and acoustic optimization methodology of a formula-student race car engine exhaust system using multilevel numerical CFD models*. Diagnostyka, 21, (3), pp. 103-113. DOI:10.29354/diag/126562.
- (15) Mohamad, B., Karoly, J., Zelentsov, A., & Amroune, S. (2020). *A hybrid method technique for design and optimization of Formula race car exhaust muffler*. International Review of Applied Sciences and Engineering, 11, (2), pp. 174–180. <https://doi.org/10.1556/1848.2020.20048>.
- (16) Mohamad, B., Karoly, J., Zelentsov, A., & Amroune, S. (2021). *A Comparison Between Hybrid Method Technique and Transfer Matrix Method for Design Optimization of Vehicle Muffler*. FME Transactions. 49, (2), pp. 494-500. DOI: 10.5937/fme2102494M.

## APPENDICES

## A1 Dyno test 1



A2 Dyno test 2

